The gamma rays from celestial objects

Ian W. Kirkman

VHE Gamma Rays from Celestial Objects

by

Ian W. Kirkman, M.Sc.

A Thesis submitted to the University of Durham in accordance with the regulations for admittance to the degree of Doctor of Philosophy

Department of Physics
University of Durham

September 1985

VHE Gamma Rays from Celestial Objects

Abstract

This Thesis describes and discusses the results obtained from observations of the astronomical objects Cygnus X-3 and the Crab Pulsar, made during 1981 and 1982 using the Very High Energy (VHE) Gamma Ray Astronomy Facility of the University of Durham.

Following an introductory chapter, chapter two describes the observational technique used for the work (known as the 'Atmospheric Cerenkov Technique') and chapter three describes in some detail the design, construction and operation of the equipment. Chapter four summarises the data taken during the course of the observations, whilst chapter five describes the analysis techniques used in the examination of this data. Chapter six presents the results derived from these analyses and, finally, chapter seven discusses their implications, both for the objects themselves and for the field of Astrophysics generally.

Unless otherwise stated, the Author has either been principally responsible for, or has played an important part in the production of, all the work reported in this Thesis.

Ian W. Kirkman

September 3rd 1985

Acknowledgements

I wish to thank Professor B.H. Bransden for the provision of facilities in the department of Physics, University of Durham. Thanks are also due to Dr. K.J. Orford and Dr. K.E. Turver for their encouragement throughout the course of the work.

I would especially like to thank my colleagues in the VHE gamma ray astronomy group - Miss P.M. Chadwick, Mr. J.C. Dowthwaite, Mr. A.B. Harrison, Mrs. E.S. Hilton and Mr. M. Walmsley - for their friendship and assistance throughout.

The provision of a Research Studentship by the Science and Engineering Research Council is gratefully acknowledged.

to Alison

Contents

VHE Gamma Rays from Celestial Objects

Contents

Chapter 3 : The Experiment

Chapter 4 : Observations and Data Processing

Chapter One

Introduction

1.1 Introduction

Astronomy is a particularly exciting field for a physicist to work in, enabling him to contribute to the understanding of many of the important properties of the Universe in which we live. This is especially true in the case of Very High Energy (VHE) Gamma Ray Astronomy, in which the processes involved are perhaps some of the most energetic in existence. A study of the subject can shed light on many apparently unconnected topics such as the origin of the cosmic radiation, the physics of pulsar magnetospheres and, at the highest energies, the temperature of the blackbody microwave background. It is therefore hoped that the work reported in this thesis will be found useful both to those directly involved in the field and to those whose main interests lie elsewhere.

1.2 VHE Gamma Rays in the Electromagnetic Spectrum

Figure 1.1 illustrates the Electromagnetic (EM) spectrum from radio up to energies of 10^{16} eV, on which are shown the various observational regions such as radio, visible, X-ray etc. Gamma ray astronomy can be considered to begin at around 10^{6} eV and continue right to the end of the scale where, for reasons which will be explained further, a cut-off in the spectrum exists.

The field therefore covers more than 9 decades in energy, making it easily the widest single field in the EM spectrum. Consequently, the whole field cannot be studied by the use of a single detection technique, but must be broken down into three regions, each requiring a fundamentally different approach. These

Figure 1.1

The electromagnetic spectrum

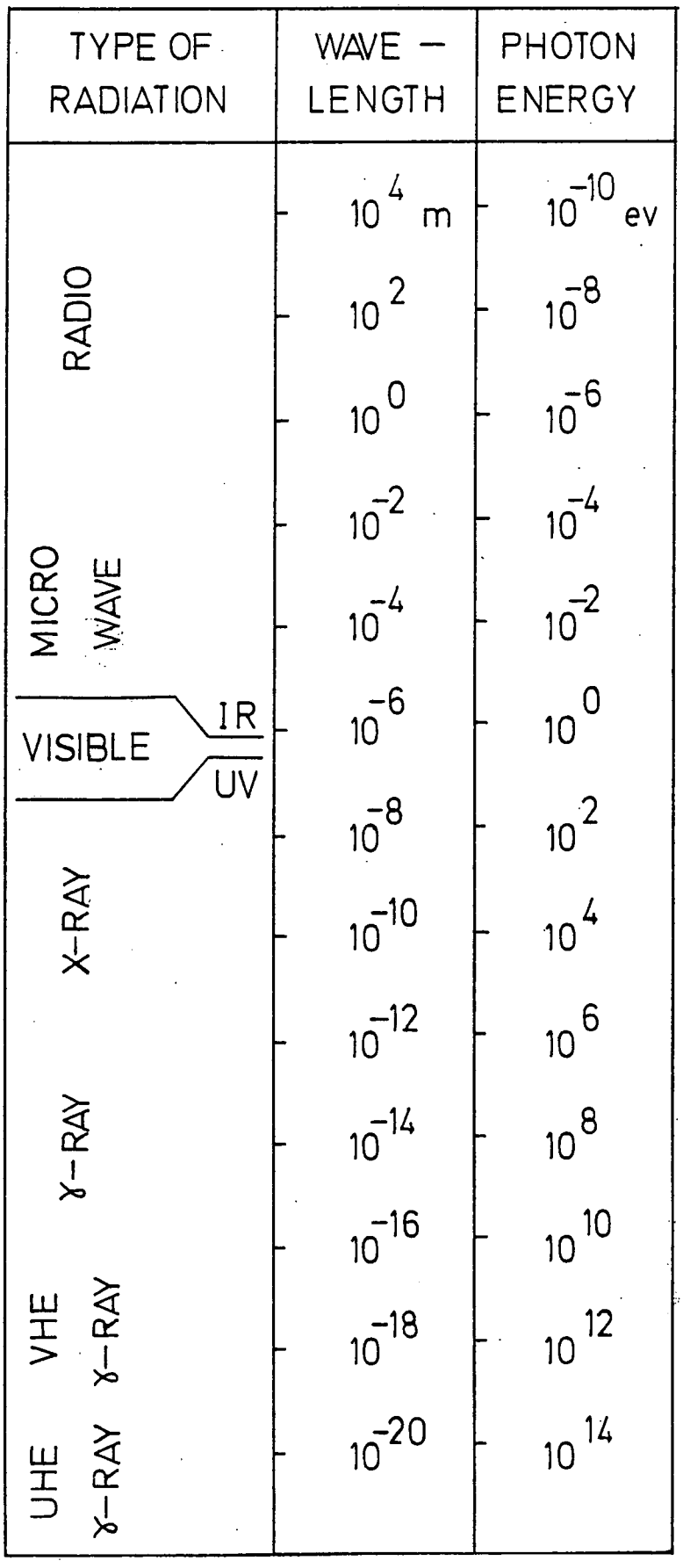
TYPE OF RADIATION
WAVE – LENGTH
PHOTON ENERGY
RADIO
MICRO WAVE
IR
VISIBLE
UV
X-RAY
γ-RAY
VHE γ-RAY
UHE γ-RAY
10^{4} m
10^{2}
10^{0}
10^{-2}
10^{-4}
10^{-6}
10^{-8}
10^{-10}
10^{-12}
10^{-14}
10^{-16}
10^{-18}
10^{-20}
10^{-10} ev
10^{-8}
10^{-6}
10^{-4}
10^{-2}
10^{0}
10^{2}
10^{4}
10^{6}
10^{8}
10^{10}
10^{12}
10^{14}

will be briefly discussed.

1.2a Low-Energy Gamma Ray Astronomy : 10^6 - 10^{10}eV

The atmosphere is opaque to radiation at these energies so observations need to be made from a balloon or satellite based platform. The most common detector used is the spark chamber, within which an incoming gamma ray interacts, causing pair production. Using such a device an estimate can be made of both the primary energy and arrival direction of the gamma ray. Alternatively, at lower energies (1-30 MeV) a scintillation counter incorporating an inorganic compound such as NaI(Tl) may be used.

Although any such satellite technique suffers the disadvantage of having relatively low collecting areas (since the size of detector capable of being carried is limited), the photon fluxes emitted by many celestial objects have been found to be quite sufficient for detection. With the successful operation of the satellites COS-B and SAS-2 (see for example Hermson, 1983, and Kniffen et al., 1977) this has been the region of the gamma ray field which has seen the most activity and, until quite recently, produced most of the positive results.

1.2b The Cerenkov Region : 10^{10} - 10^{13} eV

Gamma rays of such energies are not able to reach the surface of the Earth since they interact with the constituents of the atmosphere in a manner similar to cosmic ray protons, causing a cascade of highly energetic secondary particles. Although at such energies the secondary particles themselves do not penetrate to

ground level in any measurable quantities, they do produce optical Cerenkov radiation which can be detected at the Earth's surface (provided the sky is sufficiently free of cloud) as a tiny flash of predominantly blue light. This method of detection, known as the atmospheric Cerenkov technique, has been used for the observations reported in this work and will be discussed in more detail in Chapter two.

1.2c The Highest Energies : 10^{13} - 10^{15} eV

Primary gamma rays of energy above about 10^{13} eV also interact within the atmosphere and cause the production of a secondary cascade. The secondary particles, however, are produced in such sufficient numbers and with such high energies that they are readily detectable at ground level. Observations of such energetic gamma rays can therefore be made with a ground based array of particle detectors such as those of the Haverah Park or Kiel installations (see for example Lloyd-Evans et al., 1983, and Samorski and Stamm, 1983). This method has the advantage over the atmospheric Cerenkov technique of being able to operate under all climatic conditions though, of course, at a much reduced photon counting rate.

1.3 Gamma Ray Production Mechanisms

A major motivation for the study of VHE gamma ray astronomy is the information that can be deduced about the physical conditions existing in a source which give rise to such energetic emissions.

In order to correctly interpret gamma ray results it is therefore necessary to understand the processes by which VHE gamma ray photons may be produced. The major processes, which are illustrated in Figure 1.2, will be briefly discussed.

(a) Meson Decay : High energy cosmic ray protons, which are considered to permeate the galaxy, interact with the hydrogen gas constituting the interstellar medium, become excited, and subsequently decay to produce π and K mesons. The mesons then decay to electrons, neutrinos and gamma rays, with the gamma rays having energies perhaps 10% of that of the primary cosmic rays. The spectrum of gamma rays produced by this process is dependent upon the interstellar gas density and the cosmic ray energy spectrum, and peaks at around 70 MeV - this being about 50% of the rest mass energy of the π^{o} meson (see Fazio, 1967). It is this process which is thought to be responsible for the diffuse low energy gamma ray emission seen, for example, in the ρ-Ophi cloud (Hermson, 1983).

(b) Inverse Compton Scattering : In this process a low energy photon interacts with a relativistic electron. The electron imparts much of its energy to the photon, raising it to gamma ray energies. The original photon could come from one of several sources :

(1) Starlight

(2) The 3° K microwave background

(3) Synchotron radiation from a discrete source containing relativistic electrons in a magnetic field (in the vicinity of a pulsar, for example).

Figure 1.2

Gamma ray production mechanisms

(a) Meson decay
(b) Inverse Compton scattering
(c) Synchrotron radiation
(d) Curvature radiation

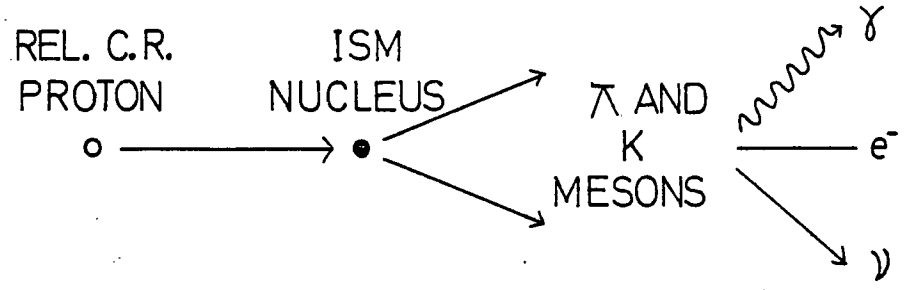
REL. C.R.
PROTON
ISM
NUCLEUS
π AND
K
MESONS
γ
e⁻
ν

(A)

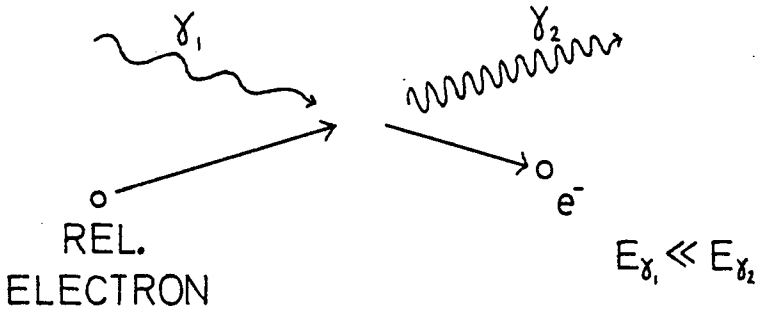
γ1
γ2
e⁻
REL.
ELECTRON
Eγ1 ≪ Eγ2

(B)

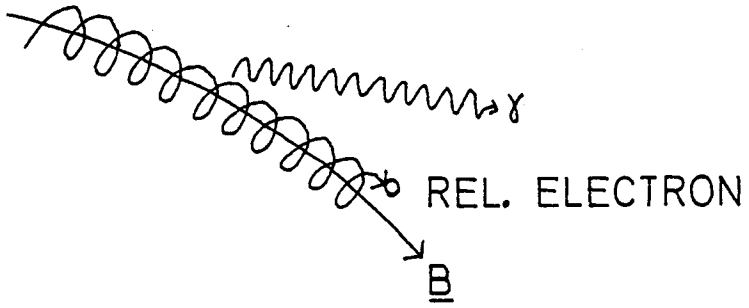
γ
REL. ELECTRON
B

(C)

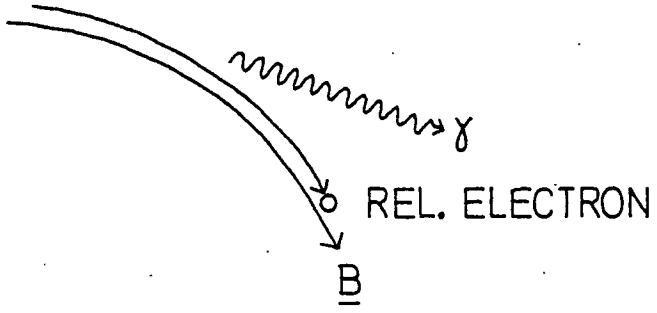
γ
REL. ELECTRON
B

(D)

(c) Synchotron Radiation : Synchotron emission arises whenever relativistic charged particles (especially particles of low mass such as the electron) and magnetic fields occupy the same volume of space. A charged particle moving with a velocity component perpendicular to a magnetic field line feels an accelerating force at right angles to both its direction of motion and the direction of the field. As a result of this acceleration (which is a change of velocity only) the particle emits synchotron radiation.

The energy of the emitted photons is many decades lower than that of the initiating charged particle; this mechanism therefore has implications primarily for low energy gamma ray or X-ray observations. If electrons of energy $> 10^{17}$ eV are the initiating particles (which may be the case in a discrete source) then VHE gamma rays could be produced - though the pair production process, described in Section 1.4c, would cause them to be strongly attenuated.

(d) Curvature Radiation : Relativistic electrons close to the surface of a pulsar are constrained to move almost exactly along the magnetic field lines of the object. Near the poles of the pulsar, where both the strength and curvature of the field is very high, any spiralling of the electrons is strongly damped out and they are accelerated directly along the line of the field. As a result of this acceleration photons may be produced which have energies comparable to that of the primary electrons, though once again pair production absorption would cause them to be relatively short lived.

1.4 Gamma Ray Absorption Mechanisms

In order to deduce the gamma ray flux emitted by an object from the flux received at the Earth, it is necessary to understand the absorption processes that may occur in the space between the two. Three possible processes, illustrated in Figure 1.3, exist :

(a) Absorption by Matter : For photons of energy above about 100 KeV the interaction cross section for pair-production and Compton scattering with the interstellar and intergalactic hydrogen can be considered to be negligible (Fazio, 1967).

(b) Absorption by Photons : A high energy gamma ray, traversing the interstellar or intergalactic medium, may interact with the photons of the 3° K microwave background - a reaction which results in the production of an electron-positron pair and the annihilation of the primary photons. For incident photons of frequency f_1 and f_2 the following energy threshold condition exists :

$$hf_1.hf_2 > (m_e c^2)^2$$

(where m_e = the electron rest mass and h = Planck's constant).

The level of attenuation of a gamma ray beam is clearly dependent upon the distance to the source and the precise temperature of the microwave background. For sources more distant than about 10 Kpc it is expected that the process will become important for photons of energy in excess of about 10^{14} eV (Gould and Schreder, 1966).

(c) Absorption by Magnetic Fields : Energetic gamma rays in strong magnetic fields can decay spontaneously by pair-production (see for example Ogelman et al., 1976). The effect has significant

Figure 1.3

Gamma ray absorption mechanisms

(a) Absorption by matter
(b) Absorption by photons
(c) Absorption by magnetic fields

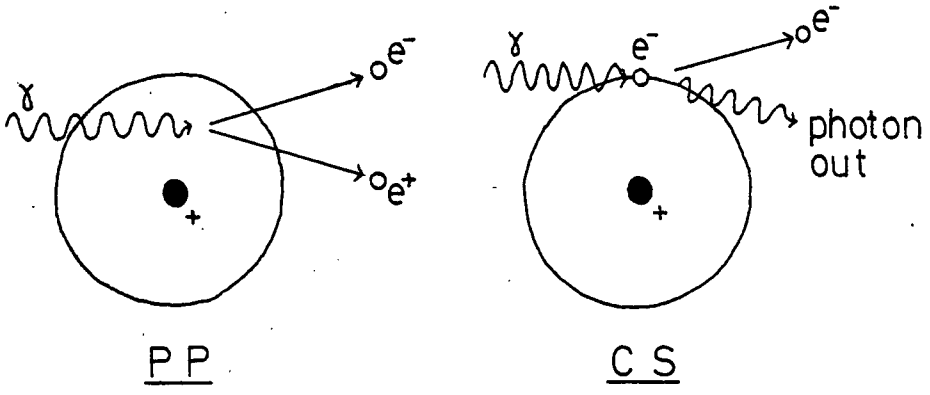

(A)

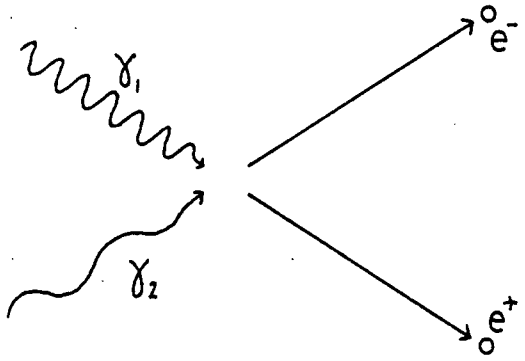

$E_{\gamma_1} \cdot E_{\gamma_2} > (M_e c^2)^2$

(B)

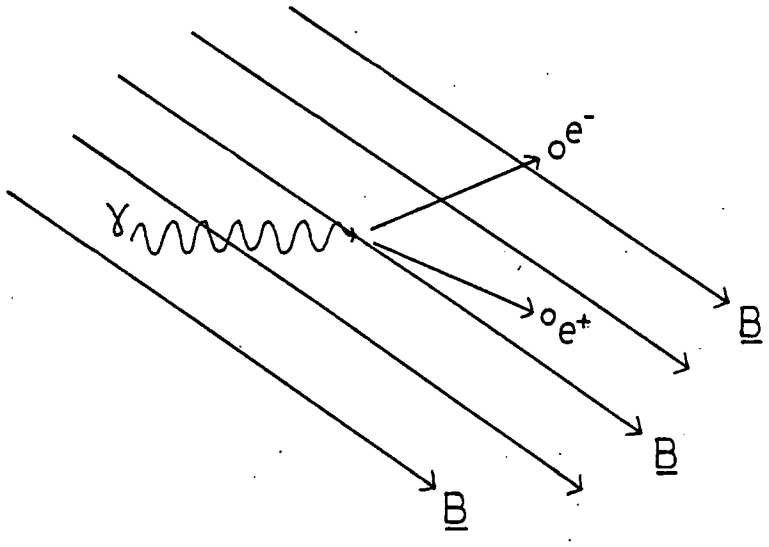

(C)

consequences close to the surface of a pulsar where the field strength is high and any photons produced by a curvature radiation mechanism will be strongly attenuated.

1.5 Brief Summary of the Present State of the Field

There are at present 6 groups active in the VHE gamma ray field, though not all are currently making observations. The facilities operated by these, and 3 other groups in the process of formation, are summarised in Table 1.1. Although all the existing experiments have rather similar energy thresholds (around 1000 GeV) and sensitivities (around 10^{-10} cm^{-2} s^{-1} for a 10 hour observation) the more recent benefit significantly from the use of modern electronics and microprocessors. An example of this is the present experiment which makes use of a microcomputer to control and monitor the equipment, thereby enabling a more thorough record to be kept of its performance than has previously been possible.

Taking the criteria for statistical significance of results of 3-4 standard deviations (SD), suggested by Porter and Weekes (1978) there existed, prior to the present experiment, 4 strong candidate sources for which detections had been claimed at energies in the range 100 - 5000 GeV. These will briefly be discussed :

(1) The Crab Pulsar : A large number of observations of this object have been made by various groups at VHE gamma ray energies with 5 positive detections of pulsed emission having been claimed. For a detailed review of these results see Porter and Weekes (1978) and Grindlay (1982). While there is reasonable agreement that the

LOCATION/ INSTIT.	LAT/ ALT.	TEL. TYPE	THRESHOLD (GEV)	NOTES
Whipple Obs Tucson, USA.	30° N 2700m	60m tesselated collector	500	1983
SAO, UCD		+2m S/Lights	1000	1970-1982
U.of Hawaii		+25m Solar	500	1984
Iowa, Durham		collector		
Crimea, USSR.	30° N	4X1.2m S/Lights	1000	1972-1982
Crimea A.O.	SL	MMT System	500	1983-pres.
Tienshan. CAO+Lebedev	35° N 3000m	2X1.2m S/Lights	1000	1979-pres
Edwards, Cal. U. of Iowa, JPL	40° N SL	2X25m Solar Collectors	500	Aug-Sep 1981-1982
Dugway, Utah. U. of Durham, UK.	40° N 1450m	4Xtriple mirror S/Light tels.	1000	1981-1984
Madison, WI. U. Wisconsin	45° N ?	S/Lights	1000	Dev. Work in 1982
Sutherland, (SA)	30° S	4Xtriple	1000	in dev.
Australia, U. of Durham	30° S	4XTriple mirror	700	in dev.
Australia, U.of Tokio	30° S	?	?	in dev.

Table 1.1

Ground based VHE gamma ray facilities operating at present, or under current developement

spectrum from the object must steepen between the pulsed flux seen at about 1 GeV (McBreen et al., 1973) and that seen at about 1000 GeV, no consensus has emerged about the precise nature of this emission since results reported by different groups have often appeared to be inconsistent.

(2) The Vela Pulsar : Observations in 1972 provided evidence at around the 4 SD level for pulsed VHE gamma ray emission from this object (Grindlay et al., 1975a and 1975b). The indication was that the main pulse of the emission occurred slightly before that seen at radio frequencies.

(3) Cygnus X-3 : This object has been the subject of intensive VHE gamma ray observations since the time of its massive radio outburst in 1972 (Gregory, 1972). The first observations were made by the Crimean group who studied it immediately after the outburst and who have continued to monitor it until the present time. Their results (summarised by Neshpor, et al., 1979) and those of other groups (Danaher et al., 1981; Lamb, et al., 1981) have indicated that the VHE gamma ray emission from the object shows the characteristic 4.8 hour amplitude modulation seen at X-ray (Elsner et al., 1980) and infra-red (Mason et al., 1976) wavelengths, with the peak in the gamma ray emission coinciding with the X-ray maximum. A positive, 4.8 hour modulated signal has also been reported at energies in excess of 10^{15} eV by Samorski and Stamm (1983) and Lloyd-Evans et al., (1983). Doubt still exists, however, about many of the detailed properties of these emissions and further observations are needed.

(4) Cen-A : A detection has been claimed for this object by

Grindlay et al. (1975a and 1975b) from observations made over a total period of 3 years. The overall significance of the detection was about 4.6 SD.

The remarkable diversity of nature of these 4 objects - two known pulsars, an X-ray binary and an active galaxy - leads one to the promising view that many more sources may be discovered in the years to come.

1.6 The Aims of the Present Work

As likely sources for any newly-commissioned northern hemisphere VHE gamma ray observatory two objects are prime candidates: Cygnus X-3 and the Crab Pulsar. Both objects are easily observable at reasonable zenith angles in the late summer and autumn months from Dugway, and both are on the 'strong candidates' list discussed in the previous section. For these reasons most of the available observing time in 1981 and 1982 was devoted to them. This work will report the conclusions drawn from these observations.

At the start of the present experiment Cygnus X-3 was perhaps the best example of a 'standard candle' that existed at energies above 10^{12} eV. It was hoped that observations of the object would contribute to the growing body of information in existence and, in addition, provide a good indication of the performance and sensitivity of the equipment. Observations of the Crab Pulsar, it was hoped, would help to paint a clearer picture of the nature of any pulsed VHE gamma ray emission from the object than existed

previously.

As will be seen, interesting and important results were to be found from observations of both objects.

Chapter Two

The Atmospheric Cerenkov Technique

2.1 Introduction

The sensitivity of satellite-borne detectors to the low fluxes seen at energies above about 10^{10} eV is severely limited by their relatively small collecting areas. For example, a satellite detector of collecting area $1m^2$ would detect only about 1 photon above 10^{12} eV every 100 days from Cygnus X-3 - one of the strongest known sources at such energies. For useful observations to be made a detector of much greater collecting area is required and it is in this respect, as will be explained further, that the atmospheric Cerenkov technique has a major advantage over any other.

The purpose of this chapter is to provide a summary of the production and detection of Cerenkov light in air showers and to give a brief history of the application of the technique to VHE gamma ray astronomy.

2.2 The Theory of Cerenkov Light Production

Given a dielectric medium of refractive index r, the phase velocity of light in the medium, V_{ph}, is given by :

$$V_{ph} = \frac{c}{r} \qquad \text{------ 2.1}$$

where c is the velocity of light in vacuo. It was shown by Cerenkov (1934) that the passage of a charged particle through the medium with a velocity, V_p, in excess of V_{ph} results in the emission of coherent electromagnetic radiation. The simplest way to represent the effect is through a Huygens constructon - as shown

in Figure 2.1. Considering radiation to be continuously emitted from the vicinity of the particle as it traverses the path from A to B, it can be shown that constructive interference will occur for those photons emitted at an angle A_c to the direction of motion of the charged particle, where A_c is given by :

$$\cos(A_c) = \frac{V_{ph}}{V_p} = \frac{1}{\beta . r} \qquad \text{----- 2.2}$$

where $$\beta = \frac{V_p}{c} \qquad \text{----- 2.3}$$

The symmetry of emission of the Cerenkov photons about the direction of motion of the charged particle results in the formation of a Cerenkov cone of radiation, as shown in Figure 2.2.

It follows from the above relations that for a given value of refractive index there exists a particle threshold velocity, V_{min}, given by :

$$V_{min} = \frac{c}{r} \qquad \text{----- 2.4}$$

below which no radiation will take place, and for which $A_c = 0$. In the case of an ultra-relativistic particle, for which β approaches unity, a maximum angle of emission, A_{max}, exists, given by :

$$A_{max} = \cos^{-1}(1/r) \qquad \text{----- 2.5}$$

Since the refractive index of a medium is not constant, being dependent upon photon wavelength, neither is A_{max}. Furthermore,

Figure 2.1

A Huygens representation of the Cerenkov effect

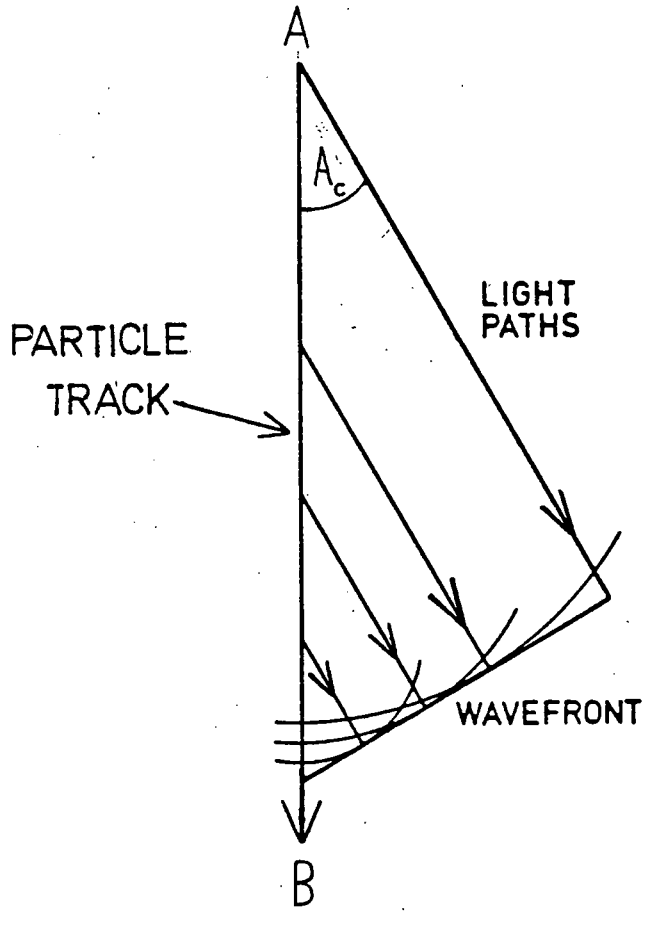
A
A_c
LIGHT
PATHS
PARTICLE
TRACK
WAVEFRONT
B

Figure 2.2

The formation of a Cerenkov cone of emission

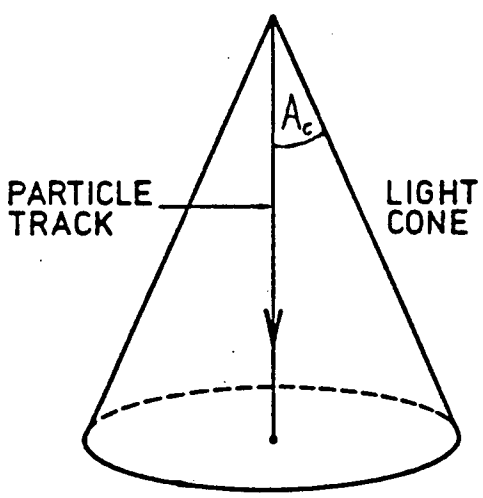
A_c
PARTICLE TRACK
LIGHT CONE

no emission can take place at those frequencies for which the refractive index of the medium is less than unity, since the requirement is that the charged particle has a velocity in excess of V_{ph}, which would in this case be greater than c. This limits the Cerenkov yield to the microwave, infrared, visible and ultra-violet parts of the spectrum and prohibits the emission of X-ray or gamma ray Cerenkov photons.

The variation of the Cerenkov yield with wavelength has been discussed by Frank and Tamm (1937) and by Jelley (1958). It has been shown that the number of photons emitted per unit path length, by a charged particle of velocity β, between the wavelengths λ_1 and λ_2 is given by :

$$\frac{dN}{dl} = \left(\frac{2\pi}{137}\right).\left(\frac{1}{\lambda_1} - \frac{1}{\lambda_2}\right).\sin^2(A_c) \qquad \text{----- 2.6}$$

where A_c is given in equation 2.2.

An example of the use of this equation is that of a relativistic electron of energy above 1 MeV passing through air of refractive index 1.00029. Under these circumstances about 28 photons per metre of path length would be emitted between the wavelengths 350 and 550 nm.

2.3 Cerenkov Light in Air Showers

When either a VHE gamma ray or a high energy cosmic ray particle enters the atmosphere it is faced with at least 1030 g cm^{-2} of matter through which to pass in order to reach ground level. In

either case, interaction between the primary photon or particle and the atmospheric nuclei occurs at a relatively early stage resulting in the formation of relativistic daughter products such as pions, strange particles and heavy mesons. Charged pions in the shower either interact catastrophically with air nuclei producing other pions, or they decay to produce muons and neutrinos. The muonic component of the shower, formed in this way, is highly penetrating and the majority of muons survive without further interaction to ground level. Neutral pions produced in the shower have a very short lifetime (about 10^{-16} s) and decay almost immediately into 2 gamma rays which pair produce to form energetic electrons and positrons. These in turn give rise, via the bremsstrahlung process, to energetic gamma rays which once again pair produce back to electron-positron pairs. In this way an electron-photon (e - γ) cascade developes with the number of electrons first increasing rapidly until the so-called 'height of maximum' is reached (at a height of about 12 km), and then decreasing (as the energy of the Bremsstrahlung produced gamma rays becomes too low for them to pair-produce) to die away completely at a height well above sea level. The process is shown schematically in Figure 2.3 (Jelley, 1983). For a more detailed description see, for example, Protheroe (1977), or Macrae (Ph.D. thesis, in preparation).

Although the energetic particles in a shower do not penetrate to ground level in any measurable quantities (at least for primary energies of around 1000 GeV), the relativistic electrons produce optical Cerenkov light (by the process described in Section 2.2) which does - and which may be detected using a relatively simple

Figure 2.3

A schematic representation of the development of a gamma ray induced air shower

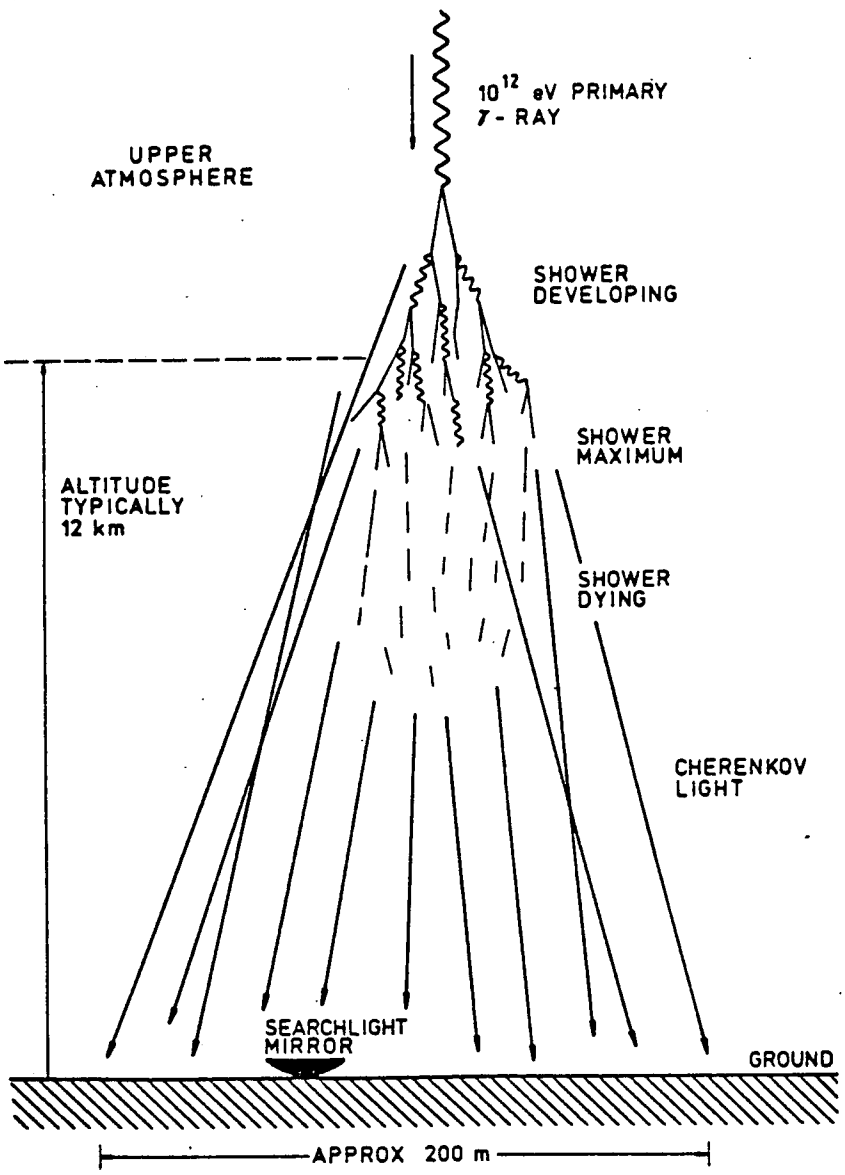
10^{12} eV PRIMARY
γ - RAY
UPPER
ATMOSPHERE
SHOWER
DEVELOPING
SHOWER
MAXIMUM
ALTITUDE
TYPICALLY
12 km
SHOWER
DYING
CHERENKOV
LIGHT
SEARCHLIGHT
MIRROR
GROUND
APPROX 200 m

optical system. The precise amount of Cerenkov light produced in an air shower depends upon the type of initiating primary. At energies of around 1000 GeV a cosmic ray particle imparts relatively more of its energy into the muon component of the shower and, as a result, gives rise to only about half the number of Cerenkov photons produced by a primary gamma ray of the same energy (Weekes and Turver, 1977). Because of this the energy threshold of a system using the technique is about 30% higher for primary cosmic rays than for primary gamma rays.

Let us now review some of the important characteristics of the Cerenkov light produced in a gamma ray initiated air shower.

Spectral Shape : For the reasons discussed in Section 2.2 it is evident that much of the Cerenkov light in an air shower will be produced in the visible - ultra-violet region of the EM spectrum. A simulation of the expected development of a 100 GeV gamma ray induced air shower (Browning and Turver, 1977) leads to the spectrum, shown in Figure 2.4, of those photons having directions of motion parallel to that of the incident gamma ray. As can be seen, the Cerenkov light is emitted predominantly at the blue end of the visible spectrum. The 'cut-off' apparent at wavelengths below about 320 nm arises because of absorption in the several km of atmosphere the light passes through on its way to ground level.

Typical Photon Density : This is a factor which depends strongly upon the primary energy of the shower. At primary gamma ray energies of 1000 GeV it has been shown (Macrae, Ph.D. thesis, in preparation) that typical photon densities of 50-100 m^{-2} may be expected at sea level.

Figure 2.4

The spectral composition of Cerenkov photons at sea level, near the centre of the light pool produced by a vertically arriving 100 GeV gamma ray

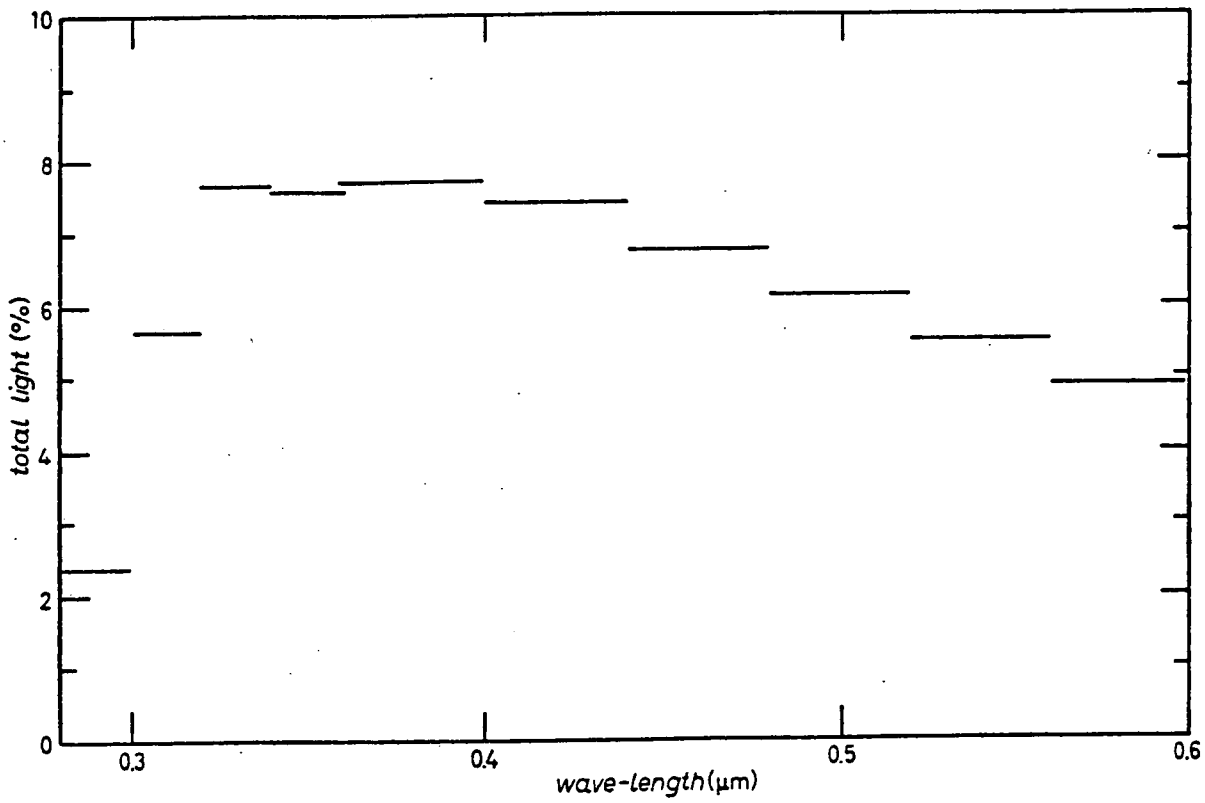
10
8
6
4
2
0
total light (%)
0.3
0.4
0.5
0.6
wave-length (μm)

The Angular Distribution : The refractive index of air at sea level is 1.00029 giving rise, as can be shown from equation 2.2, to a Cerenkov cone angle for relativistic electrons of about 1.3°. The extent of the light pool produced at ground level, however, is influenced to a greater degree by the multiple Coulomb scattering of the electrons in the e - Y cascade - which can be as high as 10°.

Lateral Distribution : Detailed computer simulations have been performed which predict the shape and size of the light pool produced at ground level by a gamma ray initiated air shower. An example of such a 'lateral distribution' is given in Figure 2.5 (Macrae, Ph.D. thesis, in preparation), which shows the variation of photon density expected from a vertically arriving primary gamma ray of energy 1000 GeV, as seen by a Dugway telescope with field of view 1.7° (see Section 2.4). It is the large extent of this light pool which gives the technique the very large effective collecting areas ($> 10^3$ m^2) necessary for work at these energies.

Duration of Light Flash : Direct measurements show that the Cerenkov light pulse produced at sea level by a proton or gamma ray of primary energy 1000 GeV has a typical duration of about 10 ns - corresponding to a physical thickness of the light front of about 3m. The risetime of the pulse, which is considerably less than this, dictates that fast photomultiplier tubes with short response times need to be used.

Zenith Angle Dependence : The rate of detection of proton or gamma ray induced air showers shows a strong zenith angle dependence, with those showers arriving away from the zenith occuring much less

Figure 2.5

The 'lateral distribution' of Cerenkov light produced by a vertically arriving 1000 GeV gamma ray induced air shower

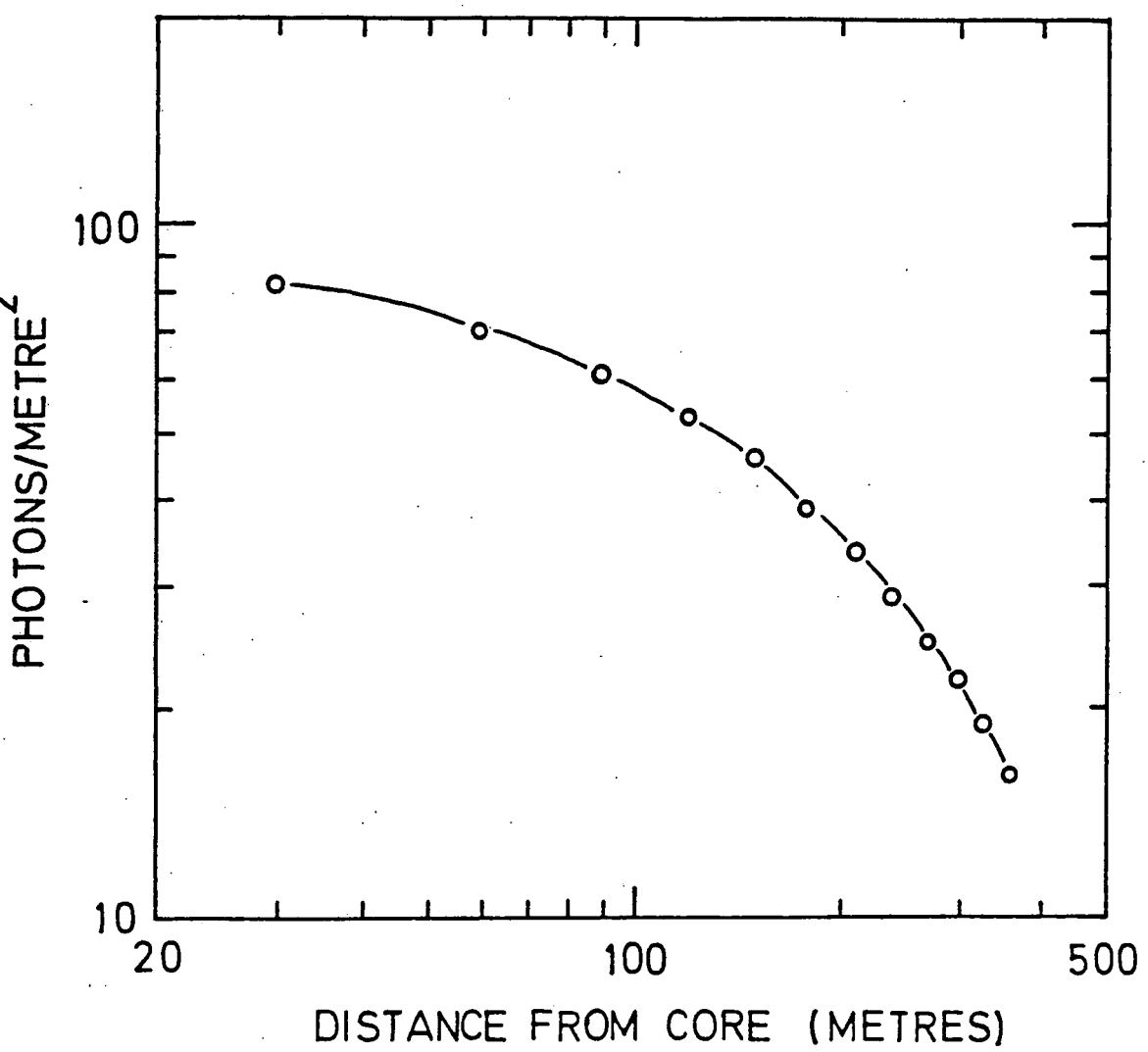
100
10
PHOTONS/METRE^2
20
100
500
DISTANCE FROM CORE (METRES)

frequently than those arriving vertically. This can be understood in terms of the greater atmospheric depth faced by those primaries arriving obliqely - with the resultant increase in the level of photon absorption occuring before the Cerenkov light reaches ground level. Galbraith and Jelley (1955) have shown that the count rate is roughly proportional to $\cos^{2.5}(\theta)$ - where θ is the zenith angle - and this is borne out by the present experiment (see Section 3.7b).

Having summarised the main properties of the Cerenkov radiation produced in an air shower let us now consider the ways in which it may be detected.

2.4 The Principles of Design of a VHE Gamma Ray Telescope

The essential components of a system able to detect the weak Cerenkov light produced by cosmic or gamma ray induced air showers are shown in Figure 2.6. The Cerenkov light is reflected from the face of a concave mirror onto the photocathode of a fast photomultiplier tube which translates the light flash into an electronic pulse whose height and width are related to the strength and duration of the optical flash. A system as simple as this, however, would respond mainly to the fluctuations in night-sky brightness occurring at the observing site and would not be of very much use as a detector of air showers.

To overcome this problem several such mirror combinations are pointed at the same part of the sky and the light flashes recorded by each tube (at typical rates of several Khz, depending upon the

Figure 2.6

The essential components of a ground based
VHE gamma ray telescope

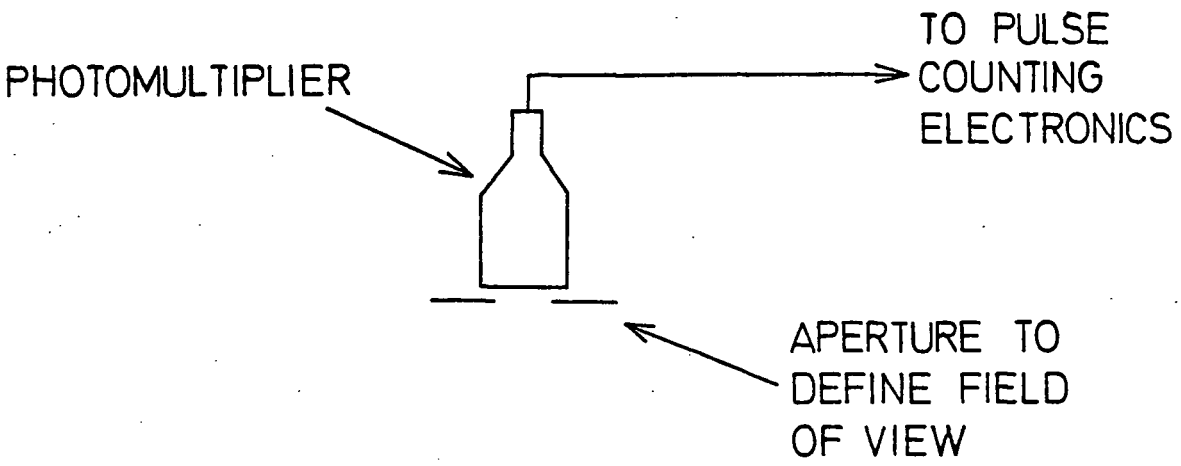
PHOTOMULTIPLIER
TO PULSE COUNTING ELECTRONICS
APERTURE TO DEFINE FIELD OF VIEW

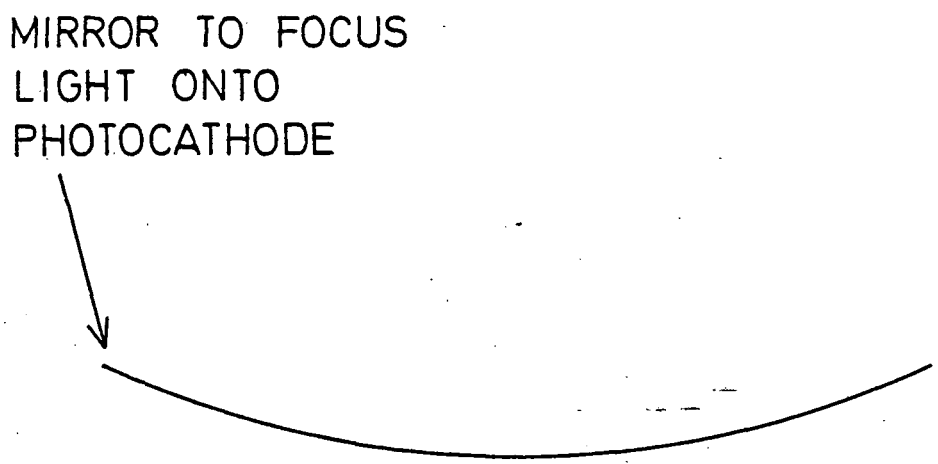
MIRROR TO FOCUS LIGHT ONTO PHOTOCATHODE

sky brightness and the EHT supplied to the tubes) are fed into a coincidence unit which requires a signal to occur in each of the channels within a given time-gate (of the order of 100ns) to register an event. Using such a method the system becomes sensitive only to the extremely short flashes of light produced by an air shower. For example, the Dugway equipment requires a 3-fold coincidence between paraxial mirror-phototube systems for detection, and under typical observing conditions the accidental rate (the rate at which the random sky noise produces a pulse in each tube within the duration of the time-gate) is less than about 1 event per 10 hours.

The basic response characteristics of such a coincidence system are dependent upon several parameters :

The Phototube Sensitivity : This parameter specifies the minimum number of photons which need to be deposited on the photocathode for the tube to produce a voltage pulse higher than the discrimination level adopted (see Section 3.5). In order to minimise the energy threshold of a telescope phototubes should be used which are particularly sensitive to the blue end of the optical range where much of the Cerenkov light is produced.

The Mirror Area : This is another factor which affects the energy threshold of the system since the larger the mirror collecting area the greater the number of photons deposited on the tube face for a given shower energy.

The Field of View : This is defined by the focal length of the mirror and the effective cathode diameter of the photomultiplier tube. Typically it is set to be about 1.7° (as defined by the full

width at half maximum (FWHM)), though in practice the finite width of the Cerenkov cone has the effect of increasing this value to about 2.2° (see Section 3.7c). Ideally, the field of view of the telescope should be matched as closely as possible with the beam width of the Cerenkov flash; if it is any wider then the system unnecessarily counts cosmic ray protons arising from near the edge of the field of view, and if it is too narrow then gamma ray induced showers coming from the source may not always be detected.

The details of design of a ground based VHE gamma ray telescope will be discussed further in Chapter 3.

2.5 A Brief History of Ground Based Cerenkov Observations

It was Blackett (1948) who first suggested that the Cerenkov radiation produced by relativistic particles in cosmic ray induced air showers may contribute significantly to the night sky brightness. He showed that perhaps 0.01% of the total night sky brightness may arise in this way - a fraction it was not considered feasible to attempt to detect.

In 1953 Galbraith and Jelley suggested that since the optical Cerenkov flash produced by an air shower would only last for perhaps 10 ns, during which time the Cerenkov photon density may considerably exceed that of the night sky, it might indeed be detectable. This they demonstrated to be the case using relatively simple equipment consisting of the fastest available photomultiplier tube mounted at the focus of an ex-army 25 cm f/0.5 parabolic signalling mirror. They observed large single pulses

from the night sky which had the expected pulse height spectrum and which they showed to occur simultaneously with the pulses from a nearby shower particle detector (Galbraith and Jelley, 1953).

It was soon realised that the technique had great value for the study of the cosmic ray background and the subject was taken up in a number of other countries, most notably the Soviet Union (Nesterova and Chudakov, 1955) where the first independent confirmation of the work was obtained. The suggestion that the technique could be applied to the study of energetic gamma rays was made soon after by Morrison (1958). For a summary of this early work see Jelley (1967), and Jelley and Porter (1963).

In the years since then the application of the technique to VHE gamma ray astronomy has been taken up by a number of groups most notably in the USSR, Ireland, the USA, India and the UK, and a total of 20 experiments have been performed. For a detailed description of these experiments see Porter and Weekes (1978). For a summary of those experiments presently being performed see Table 1.1. Although many developments have been made in the field, especially with the improvement in electronics over the past 2 decades, the basic principles of the detection technique have remained the same.

2.6 Observational Techniques used in this Work

The vast majority of showers detected by a ground based gamma ray telescope are initiated by the primary cosmic ray background. As a result, except in cases of unusually strong gamma ray

emission, the 'signal/noise' in the data recorded by the system is very low. The 'saving grace' is the fact that the cosmic ray proton background is found to be highly isotropic in both a spatial and a temporal sense.

The simplest and earliest used observational method takes advantage of the spatial anisotropy of gamma ray events from a discrete source and is known as the 'drift scan' technique. In this the telescope is pointed at a particular part of the sky and kept stationary; as the Earth rotates the telescope sweeps across a line of constant declination and the source is allowed to pass through its field of view. Since the zenith angle of the telescope remains constant, a constant background counting rate is expected. Thus, a gamma ray emitting source would be expected to increase the overall rate of the system while in the field of view.

A single drift scan usually takes the form of three distinct sections; an 'ON' period during which time the source is in the field of view, and two 'OFF' periods before and after the ON period when the source is out of the field of view and only a background counting rate is expected. The duration of scan necessary depends upon the declination of the source as this is the factor which determines the time taken by the source to drift across the physical aperture of the telescope. The technique is relatively simple to use but has the disadvantage that due to the necessity of determining an accurate background counting rate the source is only in the field of view of the system for about 30% of the total observing time.

An alternative to the drift scan method is to continuously track

the source, keeping it in the centre of the field of view at all times. While this method would not be successful in detecting emission from an object producing a continuous unpulsed flux of gamma rays - since the incoming gamma ray events would simply increase the apparent background rate of the system - it is particularly sensitive to transient or periodic gamma ray emission, either of which would show up as a temporal anisotropy in the data. The principal advantage of the technique lies in the fact that the object is monitored 100% of the time. A disadvantage lies in the increase in complexity of analysis techniques necessary to recover any signal existing in the data.

The data analysis techniques applicable to observations taken in both the above modes will be discussed in detail in Chapter 5.

Chapter Three

The Experiment

3.1 Introduction

It is not the purpose of this chapter to present a full and detailed description of every aspect of the Dugway array - such a task would be beyond the scope of this work and would indeed constitute a whole thesis of its own. Rather, it is intended to summarise the basic design and construction characteristics of the equipment and to provide details of its calibration and performance. In addition, the various problems encountered in its operation, and some of the ways in which they were overcome, will be described.

3.2 Geographical Description of the Site

The array is situated at a height of about 1450 metres above sea level on the plains of the Utah desert, about 100 miles south west of Salt Lake City, USA, at geographic 40.20° N and 112.82° W. The geocentric coordinates of the site are :

$$\sin(i) = 0.64219786 \qquad \text{and}$$

$$\cos(i) = 0.76502095$$

As can be seen in Plate 3.1 the site is open and flat and due to its relative isolation from city lights (the nearest small town, Toele, is about 40 miles away) has very good atmospheric 'seeing'. In addition, its location within the confines of the US army's Dugway Proving Ground provides important and necessary facilities such as accomodation and security during the periods when the site

Plate 3.1

An elevated view of the Dugway array

is unmanned. The geographical parameters of the site make it ideal for studying a wide variety of important northern hemisphere objects such as the Crab Pulsar, Cygnus X-3 (which passes almost directly overhead) and 4C21 - the recently discovered millisecond pulsar. The reasonably high elevation of the site (almost a mile above sea level) is also advantageous for optical Cerenkov work.

The weather patterns experienced at the site help to make it favourable for atmospheric Cerenkov observations. The relative cloud cover throughout the year (obtained from the Global Atlas of Relative Cloud Cover, 1967-1970, published by the US Department of Commerce and the USAF), when combined with the total night sky time, gives the expected number of hours of data available in each month shown in Table 3.1.

The array itself consists of four independently operable gamma ray telescopes located at the centre and apices of an equilateral triangle of approximate side 100 metres - see Figure 3.1. Each telescope (which will be described in detail in the next section) is controlled and monitored from a house trailer located inside the array, within which is contained the control and data recording systems.

3.3 The Telescope Design

Each telescope (one of which is illustrated in Plate 3.2) consists of a computer steerable alt-azimuth platform upon which are mounted three 1.5 metre diameter 'searchlight' mirrors. The platform is stabilised by being set into a 10" thick concrete

Month	Max Hours	% clear	% scat.cloud	Total
Jan	170	23.9	18.8	73
Feb	160	18.9	20.9	64
Mar	150	23.7	20.8	67
Apr	130	23.6	23.1	61
May	100	20.4	26.8	47
Jun	95	38.3	28.8	64
Jul	100	37.2	35.1	72
Aug	110	40.5	32.3	80
Sep	130	52.8	24.5	100
Oct	150	45.5	22.4	102
Nov	165	33.7	21.7	91
Dec	185	30.0	20.0	93

Table 3.1

The expected number of available hours in each month for observations from Dugway

Figure 3.1

The geometrical arrangement of the array

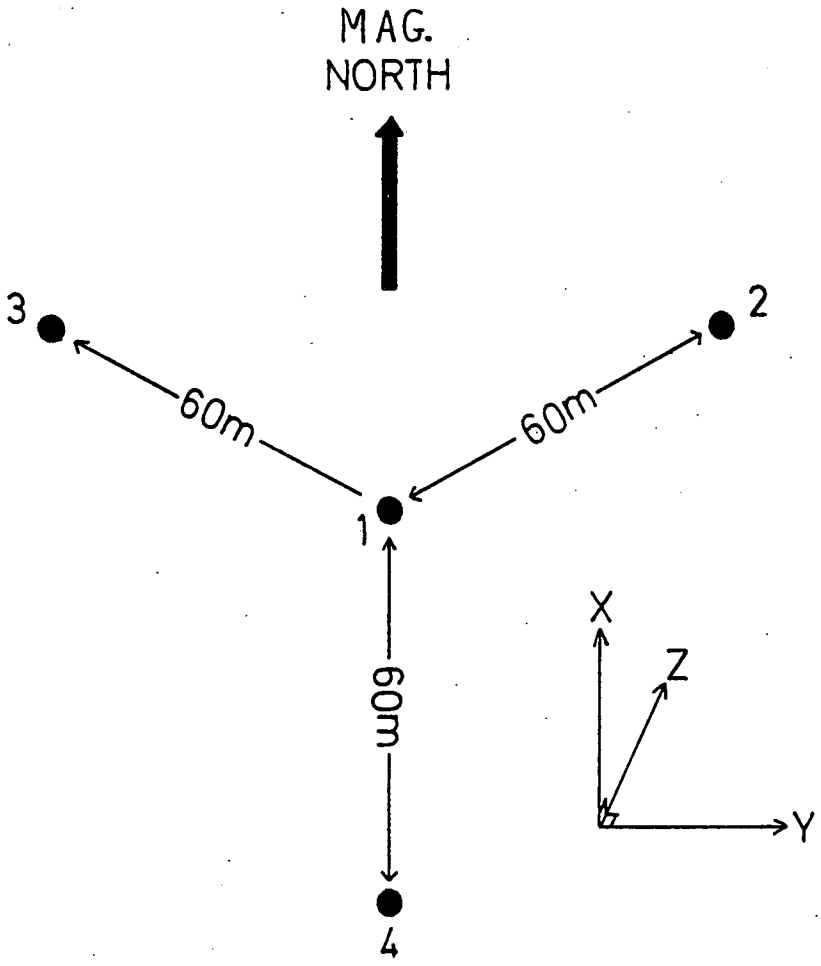
MAG.
NORTH
3
2
60m
60m
1
60m
4
X
Z
Y

Plate 3.2

A Dugway VHE gamma ray telescope

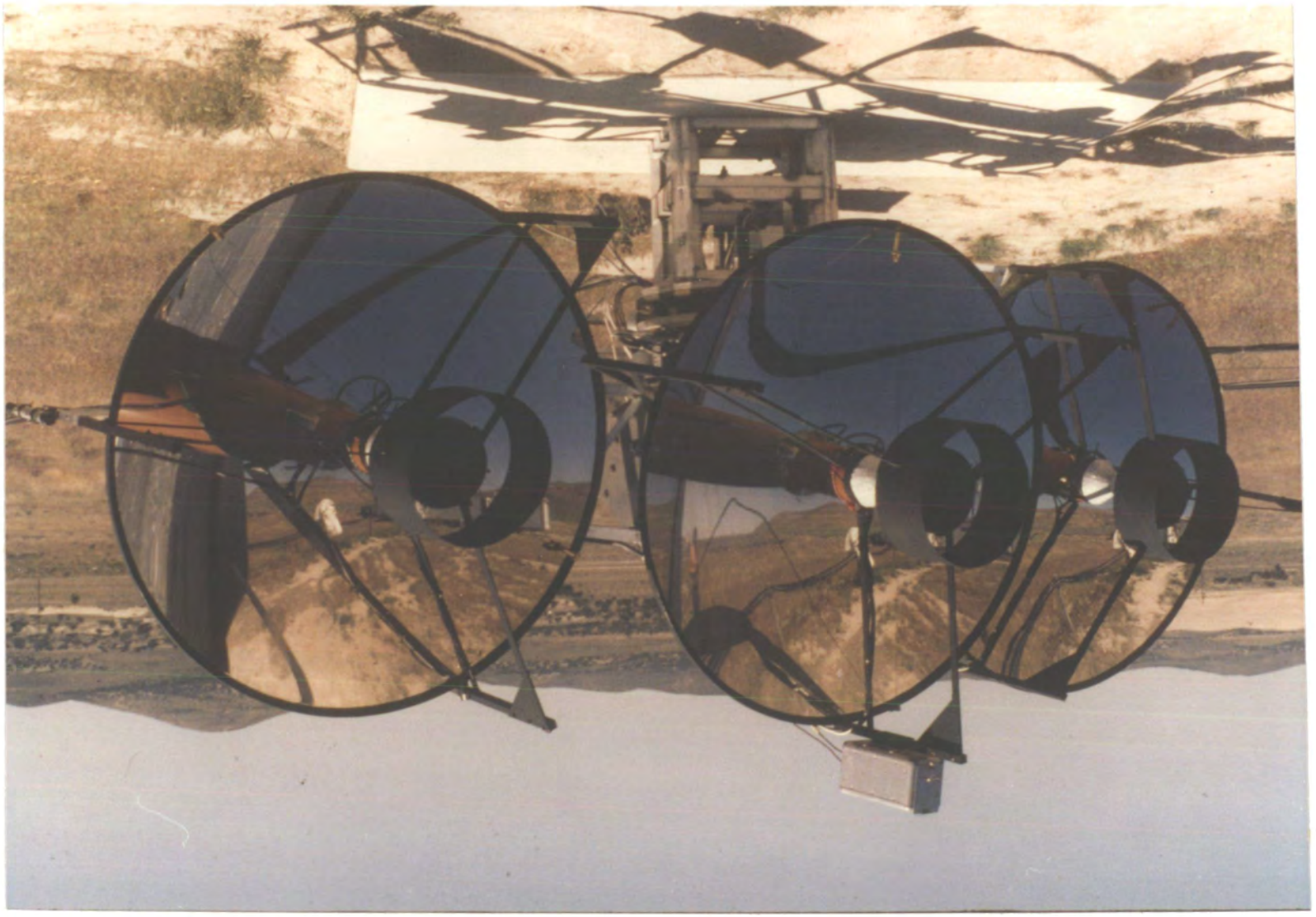

plinth which provides the telescope with the necessary firm base. The three primary mirrors are attached to this platform by means of rigid aluminium wings and are accurately aligned (to a typical tolerance of about 0.1°) so as to have parallel optical axes.

The field of view of a ground based telescope designed to detect VHE gamma rays from discrete sources is a critical factor in determining its sensitivity. Given the requirements discussed in Section 2.4, the optics of the Dugway telescopes was designed, as illustrated in Figure 3.2, to give the system a point source aperture function response of about 1.7°, as defined by the FWHM. In order to achieve this a Cassegrain system was employed in which a secondary mirror of diameter 12", placed about 0.5 m in front of the primary, reflects the image onto a roughly 3" diameter circular aperture placed in the focal plane. A fast 5" photomultiplier tube is placed about 8 cm behind this aperture, thus ensuring that the shower image is not focussed, but is spread evenly over the cathode surface of the tube. This is done to help prevent the changes in phototube gain which occur if a focussed image is allowed to fall upon different parts of the cathode. To reduce the amount of stray light reflecting into the phototube the secondary mirror is surrounded by a matt black cylindrical baffle.

The superstructure of the telescope is supported on three metal bearings which run on the horizontal platform and allow the telescope to be rotated in the azimuthal plane under the control of a geared DC motor. The telescope can be driven in altitude by means of a semi-circular geared rack acted on by the gear of a second motor attached to this platform. A pair of shaft encoders

Figure 3.2

A plan of the telescope optics

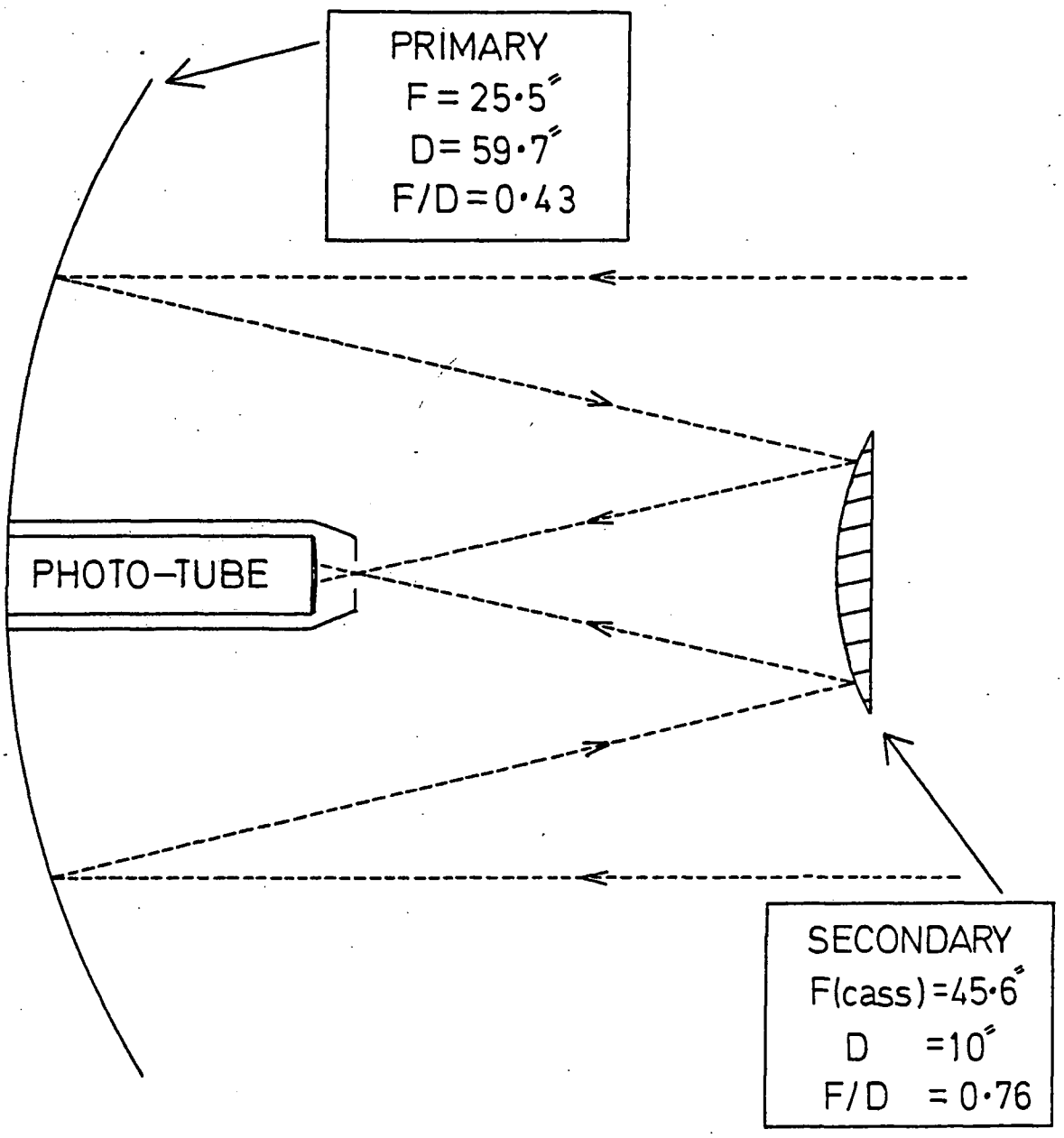
PRIMARY
F = 25·5″
D = 59·7″
F/D = 0·43
PHOTO–TUBE
SECONDARY
F(cass) = 45·6″
D = 10″
F/D = 0·76

linked to the azimuthal and altitudinal gear wheels provide information on the pointing direction of the telescope, and allow it to be steered around the sky under computer control with a sensitivity of better than 0.2°. Attached to an arm of the telescope is a highly sensitive television camera which is aligned optically with the focal axis of the mirrors and, with a field of view of about 10° and an ability to record stellar magnitudes as small as 6-7, enables a continuous check to be kept of both the approximate pointing direction of the telescope and the clarity of the sky.

Each telescope is controlled and monitored from a house trailer located near the centre of the array. The two are connected by several groups of cables which initially pass underground from the telescope, through metal tubing, to the 'mother-box' - a weather proofed aluminium box situated about 3 metres from the telescope. From here the cables are carried on posts to the control room where they are fanned out to their relevant destinations. In detail the various groups of cables are :

Phototube cables : There are 3 cables connected to each phototube; an EHT supply cable, a high quality signal cable and a cable carrying the digitised temperature inside the casing of the tube. The EHT cables run only as far as the mother-box where the EHT supply units are housed. The temperature and signal cables run all the way back to the trailer.

Position Sensor cables : A lead from each shaft encoder carries digital information which enables the computer to deduce the pointing direction of the telescope.

Motor Cables : A cable to each motor enables the pointing direction of the telescopes to be varied.

AGC Cables : Laboratory tests have demonstrated (Orford, private communication) that the gain of a phototube (the factor by which the dynode chain amplifies the initial number of photocathode electrons) is a function of the tube anode current. Since gain changes affect the response rate of a telescope to the cosmic ray background (by changing the number of photons required to trigger a phototube) it therefore becomes necessary to stabilise the anode currents when observations requiring a constant background count rate (such as drift scans) are made. To achieve this a small servo-controlled light emitting diode (LED), placed in the field of view of each mirror, is used to maintain a constant level of anode current in the phototubes.

Camera Leads : As mentioned, a highly sensitive night sky camera, mounted paraxial with the focal axis of the telescope, is used to help monitor the pointing direction of the system.

In addition to the EHT units the mother box also holds the general power supply for the telescope and a switching unit which allows it to be steered under manual control.

3.4 The Control and Monitoring of the Equipment

The essential component of the system is a 'Tektronix 4051' microcomputer which both controls and monitors almost every aspect of the array performance. This is achieved by placing both the 4051 microcomputer and a Mostek 'F8' microprocessor controller,

together with all the units they control, on an IEEE-488 databus which acts as a parallel interface between the various components. A plan of the databus is shown in Figure 3.3.

For the majority of the time the F8 microprocessor is engaged in recording incoming events; when a coincidence unit (see the next section) reports that an air shower has been detected the processor 'consults' various units sitting on the databus for such information as the exact time of the event, the 'TAC' values, the 'QT' values and the anode currents - this information is then sent to the 9-track tape deck which writes it to tape. Various other types of information recorded on tape under the control of the 4051 microcomputer are described in Section 4.4b. The 4051 computer also regularly calculates the position in the sky of the source being studied and, through the motor driver units, steers the telescopes accordingly.

A unit connected to the IEEE-488 databus continuously servo-controls the illumination level of an LED placed in the field of view of each phototube to maintain the current at a fixed level.

3.5 Summary of the Fast Electronics System

A block diagram of the fast electronics system (Orford, private communication) is given in Figure 3.4. Let us discuss each section in turn :

(a) The Coincidence System : The signal received from each of the three phototubes comprising a telescope is fed into a high quality Lecroy 'VV100' amplifier which amplifies it by a factor of 10. The choice of amplifier is important since it is necessary for it to be

Figure 3.3

A plan of the IEEE-488 databus

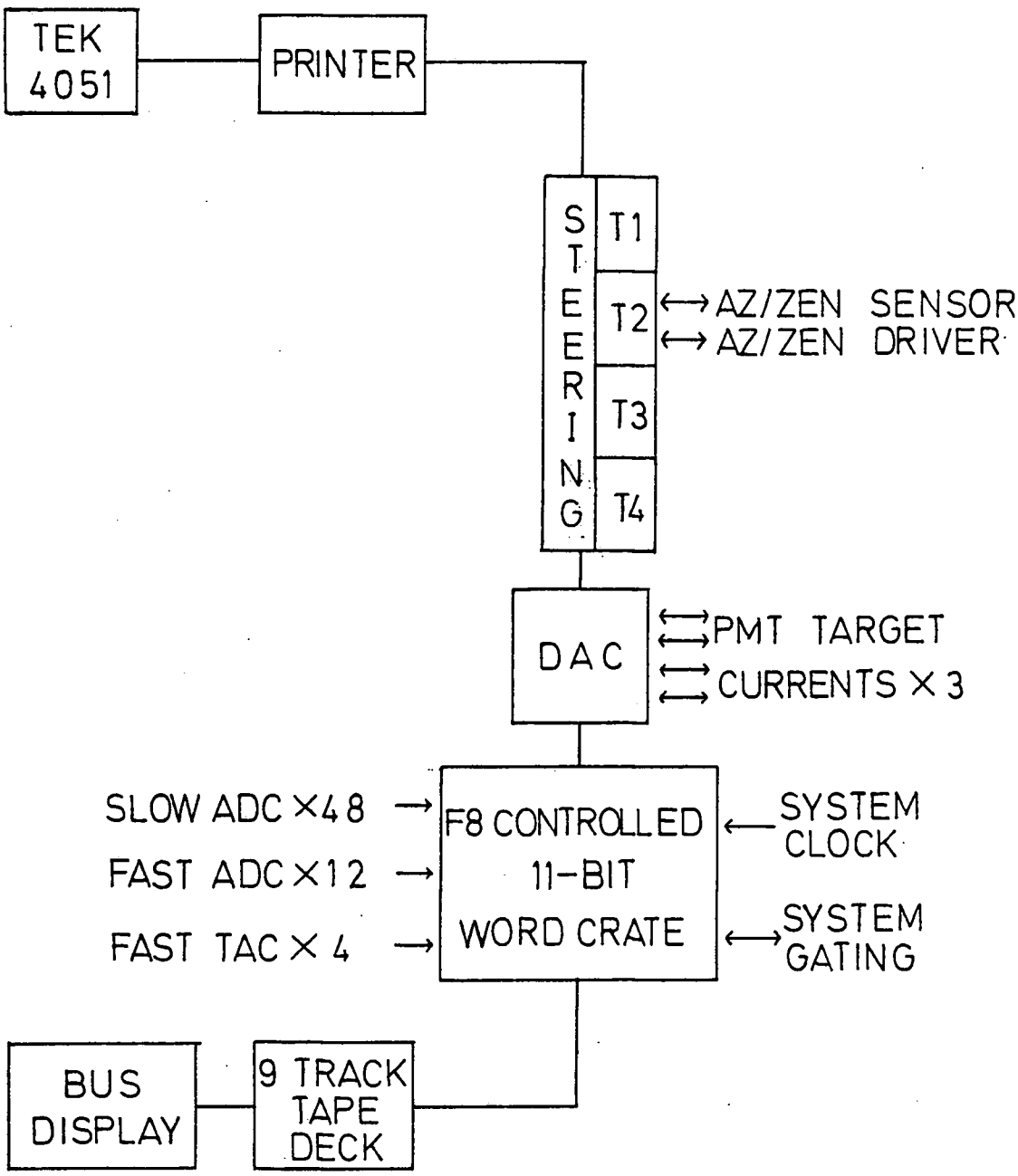
TEK 4051
PRINTER
STEERING
T1
T2
T3
T4
↔AZ/ZEN SENSOR
↔AZ/ZEN DRIVER
DAC
PMT TARGET
CURRENTS X 3
SLOW ADC X48
FAST ADC X12
FAST TAC X 4
F8 CONTROLLED
11-BIT
WORD CRATE
SYSTEM CLOCK
SYSTEM GATING
BUS DISPLAY
9 TRACK TAPE DECK

Figure 3.4

The fast electronics system

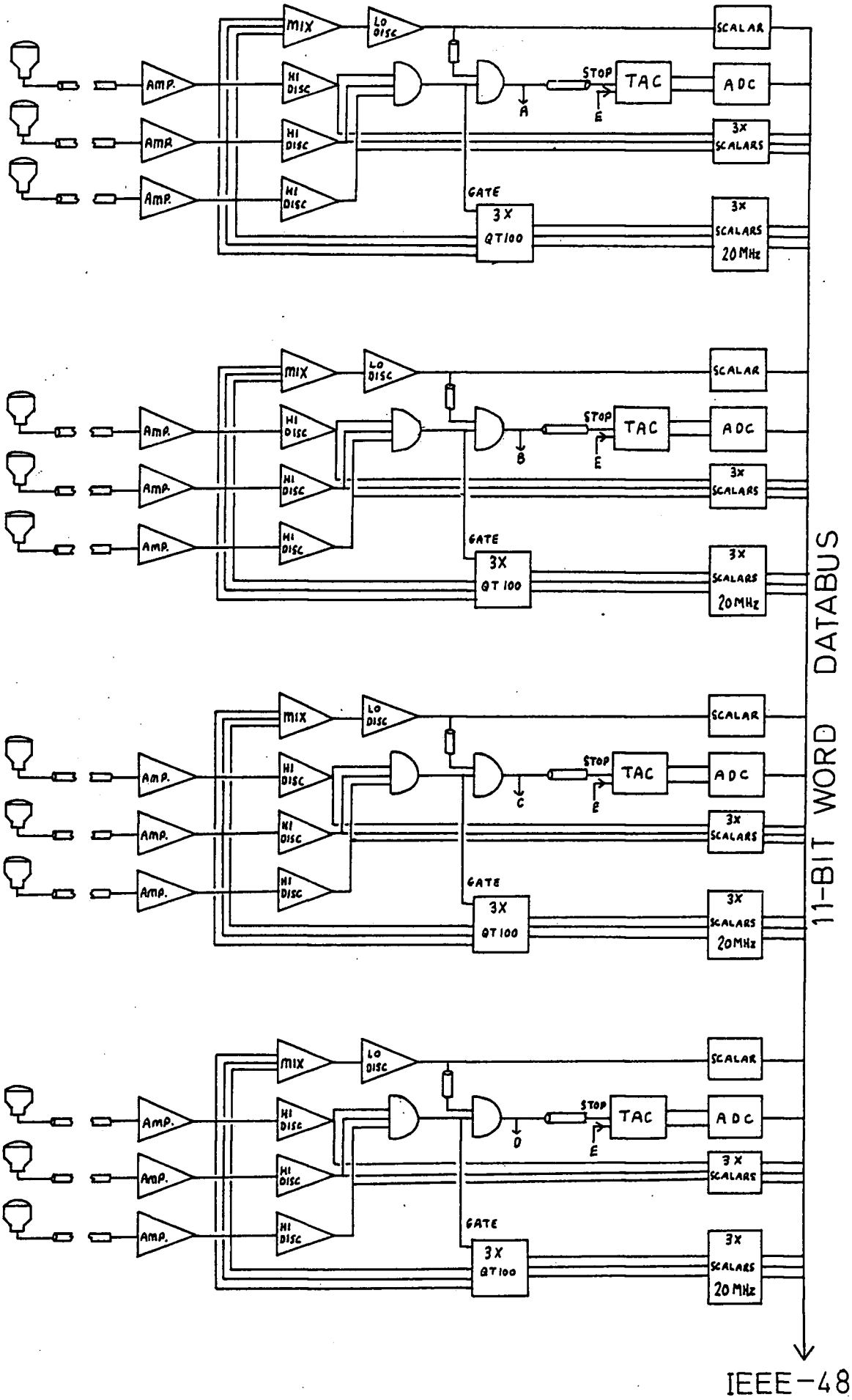
MIX
LO DISC
SCALAR
AMP.
HI DISC
STOP
TAC
ADC
A
E
3X SCALARS
GATE
3X QT100
3X SCALARS 20MHz
B
C
D
11-BIT WORD DATABUS
IEEE-488 DATABUS

able to respond to the extremely short duration pulses (risetimes of the order of a few ns) produced by the passage of an air shower. Each amplified signal is then passed into a discriminator unit which rejects any pulse having a peak voltage of less than about 100 mV (this varies slightly with each phototube), thereby reducing much of the low-level noise produced in the tubes. The three amplified and discriminated signals are then fed into a coincidence unit which requires a signal to arrive from each of the channels within a specifiable time interval (of the order of 100 ns) in order to produce an output. This output is then required to arrive in coincidence with the delayed output from a 4th discriminator unit into which has been fed the total mixed and amplified signal from the 3 phototubes. An output from this second unit is then used as a signal to both the TEK 4051 and the TAC units that an air shower has been detected.

(b) The 'Fast-Timing' System : Associated with each telescope is a time-to-analogue converter unit (TAC) which converts measured time delays into an analogue signal. When a coincidence signal is received from any one of the telescopes (signals A, B, C and D - as discussed in the previous section) a signal 'E' is used to start each TAC unit counting the time delay until its own telescope also detects the passage of the shower. If a telescope is not triggered by the shower its TAC unit automatically stops counting after about 200 ns has elapsed. In this way the output from the TAC units (which is digitised and recorded whenever a Cerenkov flash is detected) provides a measure of the relative arrival time of the shower front at each of the telescopes - from which an accurate

determination of its arrival direction can be deduced. The calibration and analysis of the information provided by the TAC units is discussed further in Sections 3.6c and 5.4.

(c) The 'QT' System : The signal produced when a coincident pulse is received from each of the 3 photomultiplier tubes comprising a telescope is used as a 'gate' to direct a 'charge-to-time' converter unit to read the charge contained in each of the 3 pulses. These charge values are then digitised and put onto the 11-bit word databus for eventual recording onto 9-track tape.

3.6 Calibration Procedures

3.6a The Array Survey

In order to accurately deduce the arrival direction of a shower triggering three or more of the telescopes from the relative times of arrival of the shower at each it is necessary to know their relative positions. This was deduced by measuring the ground distance and orientation from magnetic north of each telescope from a datum point located close to the centre of the array. From this information a simple trigonometrical analysis yields the relative positions of telescopes 2,3 and 4 from telescope 1.

Defining an x,y,z, cartesian frame in which 'x' and 'y' lie in the azimuthal plane, 'x' points to magnetic north and 'z' points to the zenith (as indicated in Figure 3.1), we deduce the information given in Table 3.2. The estimated uncertainty in each of the given measurements is of the order of $\pm$ 0.1m which, in itself, gives rise to an uncertainty in deduced arrival directions for III-fold

Telescope	'x'	'y'	'z'
1	0.00	0.00	0.00
2	30.88	51.45	-1.83
3	28.43	-52.66	0.46
4	-60.13	0.66	1.82

Table 3.2

The relative position (in metres) of telescopes 2,3 and 4 from telescope 1. A cartesian coordinate system is used with 'z' pointing to the zenith and 'x' pointing to magnetic north

initiating showers of about 0.1° (depending upon the precise orientation of the shower with respect to the array).

3.6b The Energy Threshold

The approximate energy threshold of a telescope can be deduced from the rate at which it records events initiated by the cosmic ray background (which constitute the vast majority of events detected). To perform this calibration it is necessary to convert the count rate of the telescope (in events s^{-1}) to a flux value (in events cm^{-2} s^{-1} str^{-1}). Thus, both the field of view and the effective collecting area of the telescope need to be accurately known. Let us consider each in turn for telescope 3.

Count Rate at the Zenith : The average count rate of telescope 3 at the zenith during the 1981 season of drift scan observations of Cygnus X-3 was found to be :

$$\text{average zenith rate} = 16.9 \text{ min}^{-1}$$
$$= .282 \text{ s}^{-1}$$

Field of View : Considering the aperture function of telescope 3 to be approximated by a Gaussian function of FWHM 2.2° $\pm$ 0.2° (see Section 3.7c), a standard spherical integration may be performed (Orford, private communication) which implies that :

$$\text{field of view} = (1.67 \pm 8{:}\tfrac{33}{29}).10^{-3} \text{ str}$$

Collecting Area : This is a parameter difficult to define precisely because of the nature of the detection technique. In contrast to satellite-borne detectors which respond directly to the primary cosmic or gamma ray flux an array such as the present one detects only the secondary Cerenkov radiation produced in the interaction of the primary and its daughter products with the atmosphere. Consequently the area within which the core of a shower can fall and still trigger a telescope response is a function of the primary energy of the shower. An estimate of this area can be made by considering the fact that the majority of showers which trigger telescope 3 do not also trigger telescope 1. This would indicate that most showers detected by the telescope fall well within about 60 metres of it. As a reasonable estimate let us therefore take the effective collecting area as being the circle, centred on telescope 3, of radius 40 $\pm$ 10 m. This implies :

effective collecting area of tel. 3 = (5027 $\pm$ 2513) m^2

From the above values we therefore deduce that the average integral cosmic ray flux seen at the zenith by telescope 3 is about (3.4 $\pm$ 1.8).10^{-2} m^{-2} s^{-1} str^{-1}. Assuming the integral cosmic ray flux at 1000 GeV to be 1.14 10^{-1} m^{-2} s^{-1} str^{-1}, and an integral spectral slope of -1.6 (Craig, 1984) we therefore deduce :

energy threshold of telescope
3 to cosmic ray induced showers = (2130 ± 132) GeV.

Since telescope 3 has the highest individual counting rate of any of the telescopes this value corresponds to the absolute energy threshold of the array to cosmic ray induced showers. Computer simulations have indicated that gamma rays are more efficient in producing Cerenkov photons at ground level than are cosmic rays of the same energy (see Section 2.3), and thus the absolute threshold of the array to gamma ray induced showers is expected to be a factor of about 0.7 of this value. We therefore deduce :

absolute energy threshold of the
array for gamma ray induced showers = (1491 ± 92) GeV.

It is clear from this analysis that the estimated energy threshold of the system is likely to be uncertain by about a factor of two. For the purpose of evaluating source luminosities (see Section 5.5) the absolute threshold to gamma ray induced showers (for the low energy channel) was taken to be 1000 GeV, while the overall threshold (for all Cerenkov events detected) was taken to be 1300 GeV.

3.6c The Calibration of the TAC Units

The output from the TAC unit of a telescope gives the relative time of arrival of a shower at the telescope in a digital form which, to be meaningful, needs to be converted into nanoseconds of

time. Each unit was electronically calibrated by feeding it with pairs of pulses separated by known time intervals (one of which started, and one of which stopped the unit) and recording the digitised output. This method clearly demonstrated the output from the units to be a strictly linear function of the input delay time.

It was not found practicable to attempt to perform absolute calibrations of this system since various delays existed between the telescopes and their TAC units, such as in the phototubes and the cables, which were not the same for each telescope. Because of this a 'relative calibration' was performed in which the response of the system to real air showers of known average arrival directions was examined. This procedure was employed for each telescope and the results found to be satisfactorily consistent. A more detailed discussion of the technique will be reported separately (Walmsley, Ph.D. thesis, in preparation).

3.6d The Calibration of the QT Units

Little work has been done, as yet, in decalibrating and interpreting the data produced by the QT units. As with the TACS, the output from a QT unit is in digital form with the number of bits directly proportional to the charge contained in the photomultiplier pulse initiated by a shower. A detailed discussion of the information which can be extracted from the QT values will be reported separately (Dowthwaite, Ph.D. thesis, in preparation).

3.6e The Clock Calibration

As will be become clearer in Chapters 5 and 6, it is important to accurately monitor the clock rate at all times in order to perform meaningful periodicity analyses of the data. The timing in the experiment was based on the 5, 10 and 15 Mhz radio signals provided by the WWV station at Denver, Co., which, once per minute, produces 5 cycles of a 1 Khz modulation - the front edge of which is synchronised to Coordinated Universal Time (UTC). The oven-controlled crystal-based clock is initialised on this tick to an absolute accuracy of about $\pm$ 0.5 ms (depending upon the quality of the received signal at the time), but from this moment on drifts slowly out of phase with UTC at a rate proportional to the error in its own vibrational frequency.

At any time the amount by which the clock is in error can be measured using an oscilloscope which is set to trigger on the front edge of the clock pulse (provided once per second) and display the incoming WWV pulse. This calibration was performed at regular intervals and it was found that the crystal clock ran at a highly stable (though incorrect) rate. This is demonstrated in Figure 3.5 which shows the clock drift from UTC over the period in November 1982 when a positive periodic signal was observed from the Crab pulsar (see Chapter 6). The drift of the clock from UTC during this interval was +15.94 $\pm$ .02 ms per day (ie the clock ran fast) requiring a correction to be made to the subsequent event times which changed by about 50% of a Crab pulsar cycle each day.

Figure 3.5

The timing error of the clock unit over
the interval Nov 12 to Nov 22 1982

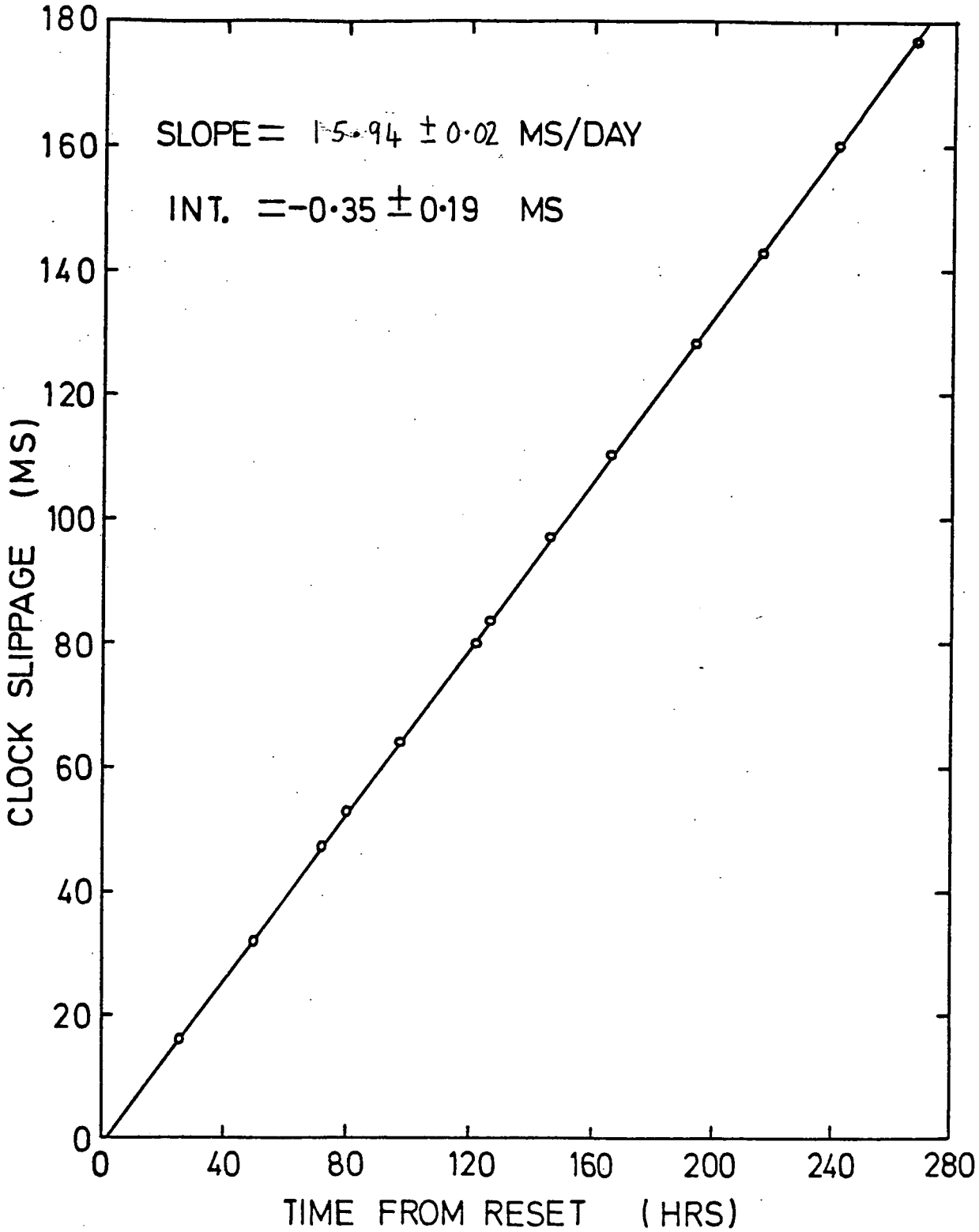
SLOPE = 1·5·94 ± 0·02 MS/DAY
INT. = −0·35 ± 0·19 MS
CLOCK SLIPPAGE (MS)
TIME FROM RESET (HRS)
0
20
40
60
80
100
120
140
160
180
0
40
80
120
160
200
240
280

3.7 The General performance of the Equipment

3.7a Steering Accuracy

The accuracy with which a telescope was able to be steered to a specified target was checked by performing a raster scan about a bright star such as Polaris and recording the level of anode current induced in the phototubes with the AGC system switched off. It was routinely found that the anode currents maximised within about $\pm$ 0.2° of the position desired - indicating the presence of the star close to the centre of the field of view.

Steering errors did occur occasionally and were usually caused by a fault in a sensor cable - perhaps due to a solder joint cracking in very cold weather. In this respect the monitors were found to be invaluable as a means of identifying steering errors quickly, therefore enabling the fault to be promptly corrected with minimal loss of observing time.

3.7b Counting Rate

As expected, the array counting rate was found to be strongly zenith angle dependent. In addition, it was found to vary significantly from telescope to telescope. Examination of the count rates observed during the Cygnus X-3 drift scans in 1981 reveals the following information :

Average overall count rate = 20.5 min^{-1}

Average rate at the zenith = 29.3 min^{-1}

Average rate at θ = 35° = 17.9 min^{-1}

Overall average value of n = 2.47

where 'n' is the exponent in the equation :

$$C = A.\cos^{n}(\theta)$$

which approximately relates the count rate, C, to the zenith angle θ (n being deduced from a simple fit to the count rate at the two zenith angles quoted). A good example of the C/θ relation is the night of the 31st August 1981, on which 10 scans of Cygnus X-3 were made under a good clear sky, with all the telescopes functioning correctly. The average count rate recorded by the array during each scan is plotted against zenith angle in Figure 3.6.

The highest counting instrument in 1981 was telescope 3 which counted at a rate of about 16.9 min^{-1} at the zenith, and about 11.3 min^{-1} at θ = 35° , having an 'n-value' of about 2.02. In contrast, telescope 4 counted at a rate of only 7.8 and 2.3 min^{-1} at θ = 0° and θ = 35° respectively, and had an 'n-value' of about 6.1. This relationship between the steepness of the count rate fall-off with zenith angle and the apparent energy threshold is equally evident when the counting rate for showers triggering different numbers of telescopes is examined. Shown in Figure 3.7 is the average count rate during each scan on the night of August 31 1981 for the independent groups of events triggering I-fold, II-fold, III-fold and IV-fold telescope responses from the array. Of interest is the very rapid fall off with zenith angle of the II, III and IV-fold response rate with the subsequent consequences for the array timing analysis.

Figure 3.6

The number of counts recorded by the array (in 36 minute scans of Cygnus X-3) as a function of the zenith angle on the night of Aug 31 1981

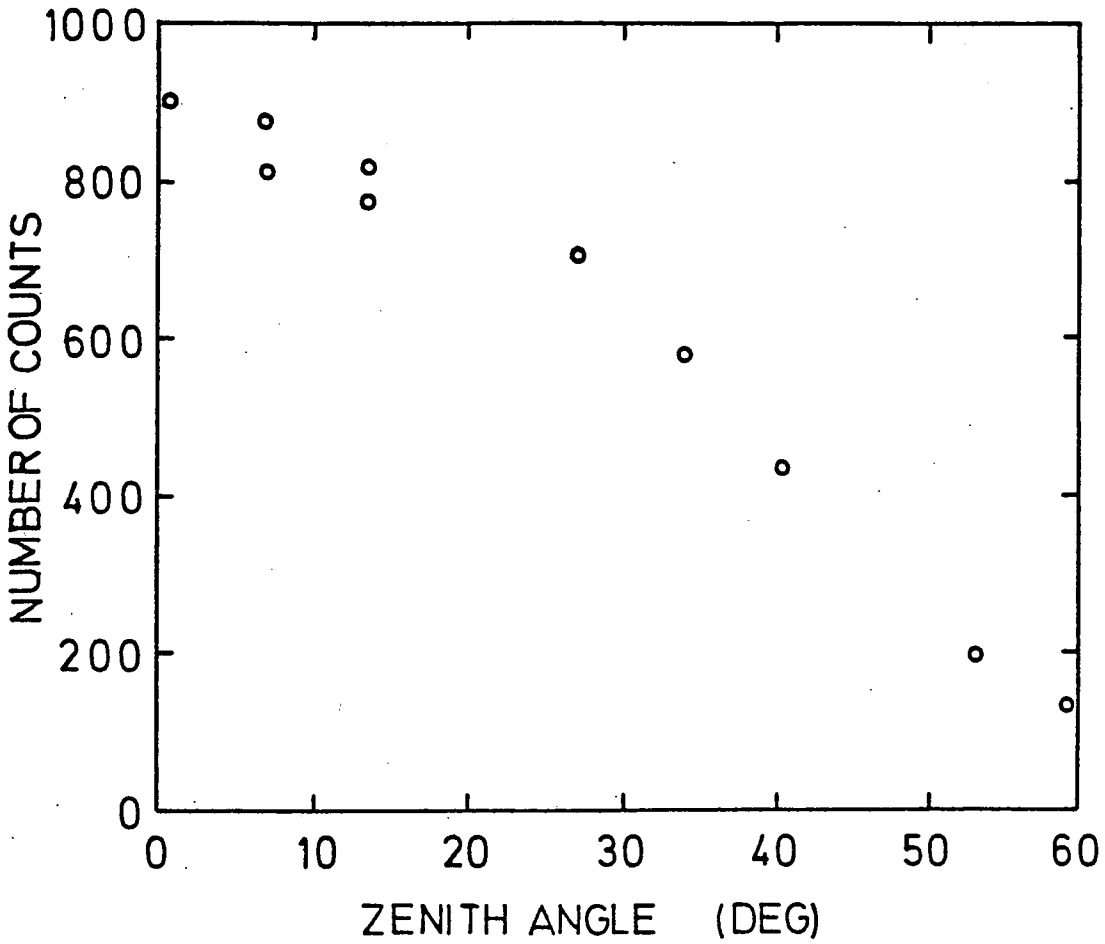
1000
800
600
400
200
0
NUMBER OF COUNTS
0
10
20
30
40
50
60
ZENITH ANGLE (DEG)

Figure 3.7

The number of counts recorded by the array (in 36 minute scans of Cygnus X-3), for showers triggering different numbers of telescope responses, as a function of the zenith angle on the night of Aug 31 1981

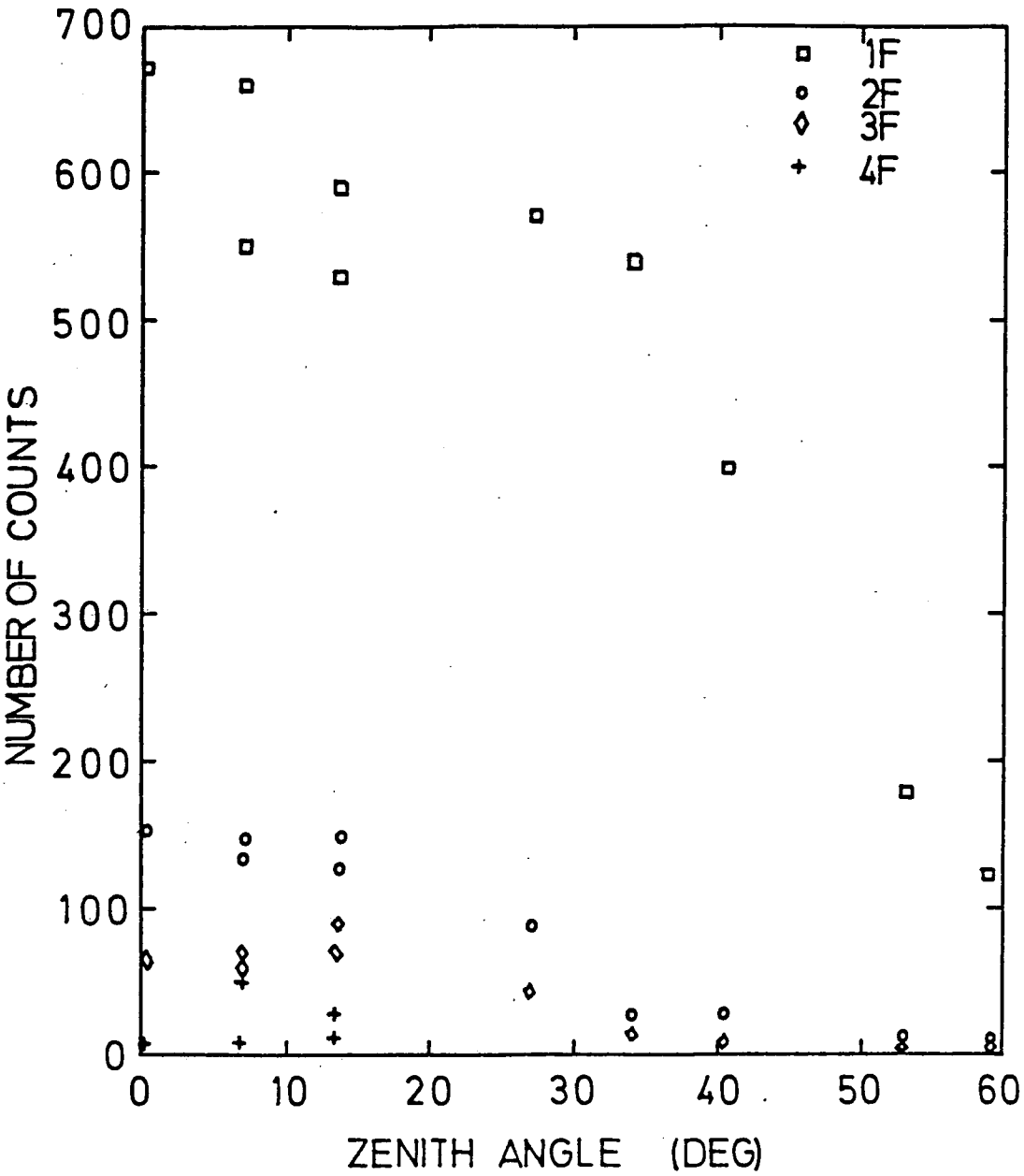
700
600
500
400
300
200
100
0
NUMBER OF COUNTS
0
10
20
30
40
50
60
ZENITH ANGLE (DEG)
1F
2F
3F
4F

The contrast between the counting rates of the individual telescopes was to a large extent unexpected. Careful examination revealed that the probable cause was a combination of the differences in surface quality and optical alignment of the mirror systems.

In early 1982 the optics of each telescope was carefully readjusted to give the highest possible coincidence rate. As a result, although telescopes 1, 3 and 4 showed only a slight improvement, the count rate of telescope 2 increased to roughly equal that of telescope 3. This not only improved the overall count rate of the array but also meant that II and III-fold responses were more numerous at the higher values of zenith angle than had been the case in 1981.

The accidental counting rate was carefully monitored and found to be virtually zero (less than 1 count per night) at all times.

3.7c The Aperture Function

As was discussed in Section 3.3, the mirror optics were designed to give a field of view of about 1.7 degrees, as defined by the FWHM. The technique used for determining the pointing accuracy of a telescope (described in Section 3.7a) was also found to be useful in checking that this value had been achieved. If we take the anode current as being a reasonable indicator of the position of the star relative to the optic axis of the telescope we can effectively map out the two dimensional point source aperture function of each mirror. This was done for each mirror of each telescope in turn and cross sections taken through the point of

maximum value indeed indicated the FWHM to be about 1.7°. Example raster scans for the three mirrors of telescope 1 are shown in Figure 3.8.

The method outlined above suffers one major drawback in that it assumes that the physical aperture function of the mirrors is the same as the acceptance function of the system to real air showers. In fact, due to the > 1° beam width of a typical shower the FWHM of the acceptance function is likely to be greater than 1.7°. Evidence for this hypothesis was forthcoming from computer simulations of the response of the Dugway array to simulated air showers (Macrae, private communication), which indicated a FWHM for 1000 GeV showers in the region of 2.0° - 2.4°.

3.7d General Problems

Operating the Dugway array over long hours and in the extreme conditions of Utah was bound to lead to a variety of problems - some anticipated, others completely unexpected.

Most of the problems encountered were of a relatively trivial nature and often simply necessitated replacing a blown transistor or fuse. A more serious problem was caused by the repeated damage done to underground cables by rodents - a problem only eliminated by running all such cables through metal tubing. Other problems were caused by the extremes of temperature encountered on the site. In summer it was necessary to cool the control room in order to maintain the TEK 4051 and the electronics at a low enough temperature to function. Even so, at midnight in July and August the trailer temperature could still be as high as 85° - 90° F. In

Figure 3.8

Anode current cross sections obtained from raster scans of Polaris for the three mirror systems of telescope 1

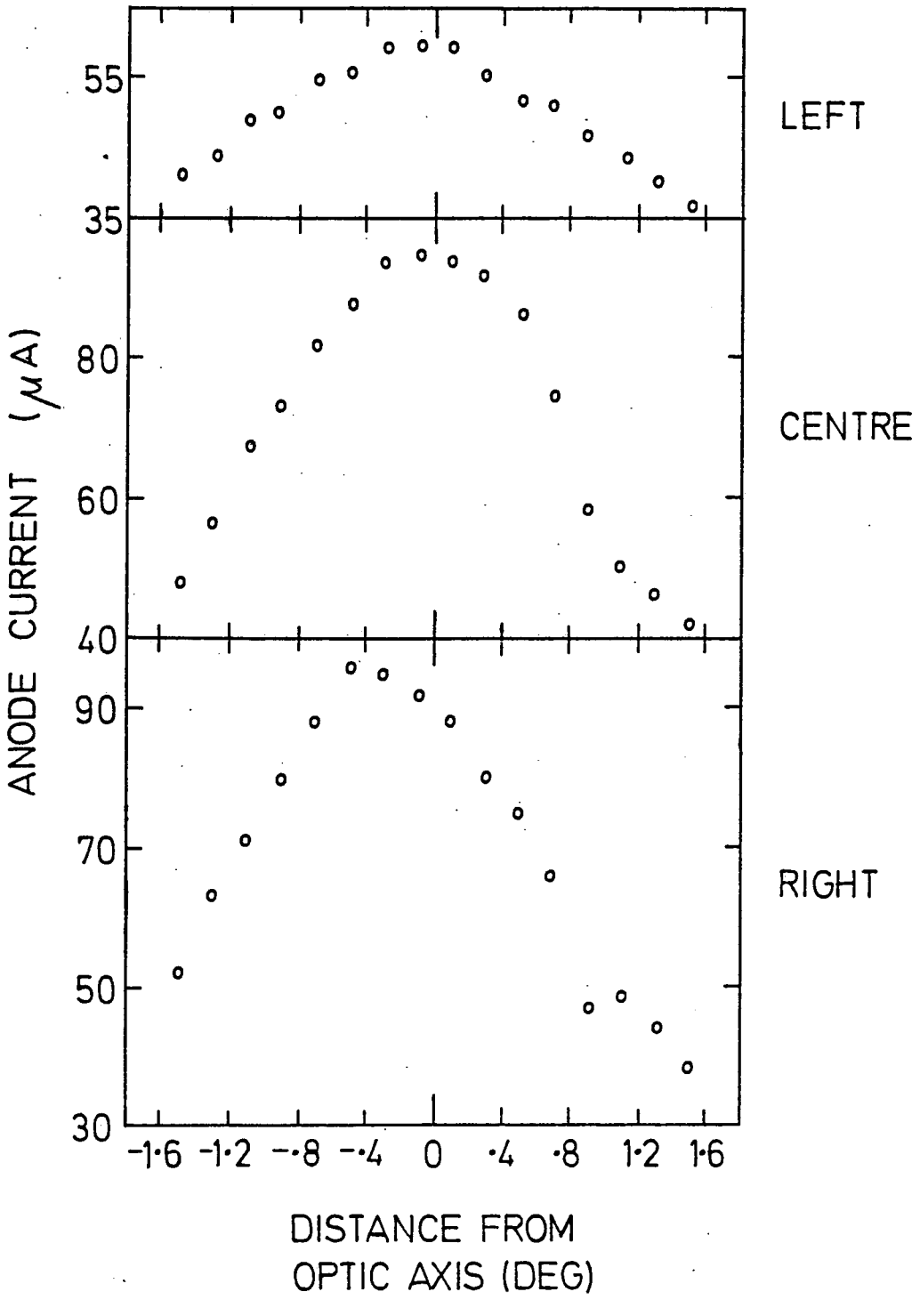
55
35
80
60
40
90
70
50
30
ANODE CURRENT (μA)
LEFT
CENTRE
RIGHT
-1·6 -1·2 -·8 -·4 0 ·4 ·8 1·2 1·6
DISTANCE FROM
OPTIC AXIS (DEG)

contrast, in late October and November the extreme nightime cold caused ice to form on the bearings which tended to inhibit their smooth rotation - this problem was solved by fixing a protective cover around the plinth to prevent moisture collecting. In addition, ice formed on the mirror surfaces, affecting their reflective properties and reducing the count rate of the system almost to zero. This was difficult to overcome and limited the conditions under which the array could be operated.

Only one 'major disaster' occurred during the 1981 and 1982 seasons of observations, when a lightning strike hit the radio aerial and caused extensive damage to the central electronics. As a result all electronics units were subsequently disconnected from both the radio/TV aerials and the external sensor cables whenever the array was left unmanned.

Chapter Four

Observations and Data Processing

4.1 Introduction

Work began on the installation of the Dugway array in late April 1981 and continued through to early July when the facility became fully operational. Between late July and early November 1981, and mid July and late November 1982, an intensive programme of observations was carried out, with over 525 hours of data being recorded from a total of 9 celestial objects.

The two principal sources of interest (which will be reported on in this work) were the Crab Pulsar (PSR 0531+21), and the highly variable X-Ray source Cygnus X-3, both of which were felt to be reasonable VHE gamma ray candidates. Tables 4.1a and 4.1b give the number of hours of data taken in each of the observational windows available, in 1981 and 1982 respectively, for each of the two objects.

4.2 Details of Observations

4.2a Cygnus X-3

Drift Scan Mode : Between late July and early November 1981 a total of 142 individual 36 minute drift scans of Cygnus X-3 were made, all with the AGC system employed. Of these, 76 had been made under stable enough sky conditions (see Section 4.3) as to allow a search for an excess of 'ON-source' counts (see Section 5.2) to be made. Two distinct phases of observations existed:

(1) From the start of observations on July 30 1981 until September 3, 48 acceptable scans were made, centred on phases 0.0, 0.125, 0.25, 0.375, 0.5, 0.625, 0.75 and 0.875 of the 4.8 hour cycle, as defined using the ephemeris of Van der Klis and

Source	July/Aug	Aug/Sept	Sept/Oct	Oct/Nov
Cyg X-3 (DS mode)	16.2	46.2	19.2	3.6
Cyg X-3 (TR mode)	-	2	2.5	23
PSR 0531+21 (TR mode)	-	-	6.3	27.5

Table 4.1a

The number of hours spent on PSR0531 and Cygnus X-3 in 1981

Source	June	July	Aug	Sept	Oct	Nov
Cyg X-3 (DS mode)	4	-	-	-	5	-
Cyg X-3 (TR mode)	-	22	32	45	28	14
PSR 0531+21 (TR mode)	-	-	7	16	45	70

Table 4.1b

The number of hours spent on PSR0531 and Cygnus X-3 in 1982

Bonnet-Bidaut (Van der Klis et al., 1981)

(2) From September 25 until October 3 a further 28 acceptable scans were made, centred on phases 0.03, 0.155, 0.28, 0.405, 0.53, 0.655, 0.78 and 0.905 of the 4.8 hour cycle. This phase slippage of 0.03, corresponding to the 10 minute 'ON-time', was made in order to widen the coverage of the 4.8 hour cycle.

The number of scans made at each of the 16 observed phases is given in Table 4.2, along with the number of events recorded in the 30 minutes of each scan used in the analysis.

Tracking Mode : Observations of Cygnus X-3 in the tracking mode were made between September 30 and November 2, 1981, during which time 27 hours of data were taken. Unfortunately, this data was found to be of only limited value since the coverage of the object at around phase 0.625 had been minimal. In addition, the AGC system had not been employed thus rendering unreliable a count rate analysis of the data.

In 1982 a total of 141 hours of data were taken from Cygnus X-3 with the telescopes, operating in the tracking mode, resteering onto the object every minute. Since the AGC system was employed throughout the observations an analysis of the observed count rates could be made in the search for transient effects at phase 0.625. As is discussed in Section 5.2b, this data was analysed by splitting it up into 36 minute segments centred on phases 0.0, 0.125, 0.25 etc. of the 4.8 hour cycle, and examining these segments as if they were drift scan data. A total of 106 acceptable 'pseudo drift scans' were obtained totalling some 64 hours of data. The reason for the large fraction of data not

Phase	No.scans	No.events
0.0	5	2670
0.03	5	3377
0.125	5	3474
0.155	3	1940
0.25	6	4305
0.28	4	2163
0.375	7	4769
0.405	4	1690
0.5	5	3457
0.53	2	615
0.625	7	3714
0.655	4	1347
0.75	7	3684
0.78	4	1690
0.875	6	3636
0.905	2	1390

Table 4.2

Cygnus X-3 drift scan data 1981 : The number of acceptable scans and events at each 4.8 hour phase

analysed was that the observations made in September 1982, totalling some 45 hours, consisted mostly of nights of variable weather which were not found to be acceptable for this analysis. Table 4.3 gives the number of 'pseudo drift scans' obtained from the object under acceptable conditions at each of the 8 phases 0.0, 0.125, 0.25, 0.375 etc. of the 4.8 hour cycle.

4.2b The Crab Pulsar

In 1981 observations of the Crab Pulsar were made in the tracking mode on 13 nights between September 25 and November 2. In total, almost 34 hours of data were taken, during which time 20032 events were recorded. Typically, the data were taken for about 2-3 hours each night, with the object rising from a zenith angle of about 40°. The AGC system was not employed for the observations.

The observations in 1982 were much more extensive, as can be seen in Table 4.1b. More than 137 hours of data were taken on 37 nights between August 18 and November 23 producing a total of 140435 events. Once again the observations were made with the system operating in the tracking mode and, as in 1981, the AGC system was not employed. Unfortunately, in the subsequent review of the data it was realised that during the observations made in October 1982 the system had not been correctly tracking the object. An error of one day in the assumed Julian date had led to the system tracking the wrong point in the sky. Since this resulted in the object being perhaps a degree from the centre of the field of view it was felt preferable to reject this data rather than

Phase	No.'scans'	No.events
0.0	13	8481
0.125	15	10277
0.25	11	6923
0.375	4	2110
0.5	8	4778
0.625	19	15810
0.75	18	16448
0.875	18	13693

Table 4.3

Cygnus X-3 Tracking Data 1982 : The number of acceptable 'scans' and events at each 4.8 hour phase

prejudice any results which may arise from the remainder.

4.2c Other Objects

As was mentioned in Section 4.1 extensive observations, totalling over 92 hours, were made on 7 other objects during the 1981 - 1982 operating seasons. Shown in Table 4.4 is the amount of time spent on each of these objects during the above period; it is clear that none received the same high priority given to the Crab Pulsar or Cygnus X-3. As a result further observations of these and other objects were undertaken in 1983 and 1984. Pending a full analysis the results from these objects will be reported separately (Walmsley, Ph.D. thesis, in preparation, and Dowthwaite, Ph.D. thesis, in preparation).

4.3 The Suitability of Data for Analysis

When a sample of data is initially examined a decision is necessary as to whether or not it is suitable for analysis. Since a variety of reasons exist for rejecting data let us discuss each in turn :

Variable sky conditions : When observations are made in the drift scan mode it is important that the cosmic ray induced background count rate is constant during a scan. For this reason clear and stable sky conditions are required, since the passage of a cloud through the field of view of a telescope significantly affects its count rate. The observer is therefore required to keep a very detailed record of both the sky clarity and the cloud content, and

Object	No.hours
PSR 0355+54	24
PSR 0655+64	3
PSR 1913+16	16
PSR 1929+10	8
PSR 2223+65	19
2CG 135	19
2CG 195	4

Table 4.4

The number of hours of data taken on other objects observed in 1981 and 1982

to state at the time of the observation whether or not the data is suitable for a count rate analysis.

AGC problems : If the anode gain control (AGC) unit of a telescope was not functioning correctly during an observation there can be no guarantee that the energy threshold (and therefore the background count rate) of the telescope was constant. Under these circumstances (which would be noted in the observation log) the data from the telescope would not be acceptable for a count rate analysis.

Pointing direction : The approximate pointing direction of each telescope is continuously monitored throughout an observation through the use of the sensitive television cameras discussed in Section 3.3. In addition, the housekeeping records (which will be discussed in Section 4.4b) provide an accurate measure of the steering error of each telescope once per minute. Data taken during a period when the system was not steering correctly would obviously not be acceptable for analysis.

4.4 The Database

4.4a Treatment of the Data prior to Analysis

The data recorded by the array is stored on magnetic tape in a densely packed format thereby minimizing the number of tapes necessary. These raw tapes in themselves cannot be used as the prime database at Durham since they are not compatible with the existing mainframe computer system. In addition, it would be unwise to regularly access such 'master' tapes since the risk of

contaminating them would be high with constant use. For these reasons the master tapes are stored as 'primary back-up' tapes and an independent mainframe database is created which can be immediately accessed and which would be easily recoverable in the event of accidental erasure. Several stages exist in the production of this database :

(1) Raw Dugway Tapes : There usually exists one 1600' tape per observing trip containing data stored in a densely packed binary format. Each file on the tape corresponds to a single night's observation and may therefore hold data taken on several objects.

(2) Starlink Compatible Raw Tapes : The raw Dugway tape is mounted as a foreign tape on the VAX 11/750 computer of the 'Starlink' system, and is copied to a second tape with a file format compatible to the machine.

(3) Unpacked Tapes : The Starlink compatible raw tape is mounted, read, converted to 'ASCI' format and copied to an 'unpacked' tape which contains the data in a standard expanded format which is more easily read and understood. At this stage a file on the tape still contains all the data recorded on a particular night.

(4) Source Tapes : A night's data in unpacked format is edited into 'source' files. The source file, containing one night's data on one object, is then copied onto the relevant source tape which holds all the data on the object in question.

A total of 9 source tapes were created for the 1981 and 1982 seasons of observation - one tape for each object observed. Each tape holds all the data available on a particular object and, as a result, is the only tape which needs to be regularly accessed.

4.4b The Data Format

The various types of data stored in a source file take the form of 'data records' which have varying lengths and formats depending upon the type of information contained. These records are :

Start of night record. Precedes all other data in a file and specifies the date of the observation (in local time), the mountain standard time (MST) and correponding clock microsecond time of the record, the initials of the observer, the observing technique and AGC level adopted for the first object, and a summary of the existing and expected weather conditions for the night.

Change of source record. This record is written to tape whenever observations are about to begin on a new source. Given is the source name, the source right ascension and declination, the microsecond time of the start of observations, and the observing technique and AGC level adopted on the source.

Drive record. This is recorded whenever the telescopes are given a command to change their pointing direction. The information given is the microsecond time of the drive command and the zenith and azimuthal angles to be adopted by the telescopes.

Event record. This contains the information which is recorded when an air shower triggers one or more of the telescopes. The data recorded are the microsecond time of the event, the number of telescopes participating in the event, the TAC value and 3 QT values (for the left, centre and right phototubes respectively) for each of the telescopes and the anode current in each of the photomultiplier tubes (in order 1L, 1C, 1R, 2L, 2C etc). A further

specification is made as to whether or not the telescopes were being steered when the event was recorded.

Message record. Contains any message entered by the observer at any point in the night.

Housekeeping record. This is written to tape once every minute and contains useful information about the state of the system. Included are the microsecond time of the record, the single fold rates, anode currents, temperatures and atmospheric pressures of, or at, each of the phototubes, and the instantaneous steering error of each telescope (how accurately each telescope was pointing to the required point in the sky at the time of the record).

4.4c Structure of the Database

In addition to the source tapes (which form the primary database and hold about 200 Mbytes of data) a certain amount of data can be stored on the disk memory of the VAX 11/750 computer. Two types of disk storage are available : a permanent storage 'COSMOS' disk on which the group allocation is about 20 Mbytes, and a temporary storage 'SCRATCH' disk which can hold, for periods of up to about a week, about 30 Mbytes of data.

In practice, the only information that it is necessary to keep on disk is that which is produced by the barycentring routine (see Section 5.3a); namely, the barycentric arrival time of each event and the combination of telescopes which responded to it.

A typical line from a data file would be of the form '152445270.12345678901', which indicates that the event had a trigger code of 15 (which means that all the telescopes were

triggered), and gives the Barycentred Julian Ephemeris time of the event to an accuracy of about 1 μs. The trigger code is evaluated using the following simple equation :

$$\text{trigger code} = 1.T1 + 2.T2 + 4.T3 + 8.T4$$

where T1 = 1 if telescope 1 participated in the event

T1 = 0 if telescope 1 did not participate in the event

etc

Thus, for example, a shower triggering telescopes 1,2 and 4 only would have a trigger code of 11. By limiting the type of information stored in this way it is possible to maintain virtually the whole of the essential data in an immediately accessible form on the COSMOS disk.

These standard datafiles contain all the information necessary for either a count rate or periodicity analysis of the data (see Chapter 5). If a particular sample of data needs to be investigated in more detail then reference can be made to the data stored on the source tapes, the relevant part of which can be temporarily copied to the SCRATCH disk. In addition to the general database there also exists a large suite of Fortran-77 formulated analysis programs which have been developed over a period of time and which perform the types of data analyses discussed in Chapter 5.

Chapter Five

Data Analysis Techniques

5.1 Introduction

In this chapter it is intended to summarise the data analysis techniques which have been used in the course of this work. The major problem connected with ground based VHE gamma ray astronomy is the high 'noise' level caused by the isotropic cosmic ray background, and the main aim is one of distinguishing between gamma ray and cosmic ray induced showers. It is not possible at present to directly distinguish between individual showers of the two types using the type of detector employed in either this or past experiments. As a result most techniques take advantage of either the spatial or temporal anisotropy of the arriving gamma ray events.

5.2 Count Rate Analysis of the Cygnus X-3 Data

5.2a Drift Scan Data

As has been described in Chapter 2, a single drift scan of a celestial object consists of 3 distinct sections; the first and last thirds of the scan during which the object is outside of the field of view of the telescopes ('OFF' periods), and the middle third during which it transits through the field of view ('ON' period). Since Cygnus X-3 has a declination angle of around 40° and consequently requires about 10 minutes to pass through the field of view of the telescopes (FWHM 1.7°) the minimum possible drift scan duration (if two OFF periods are desired) is 30 minutes.

In the 1981 series of observations drift scans were of 36 minutes duration thus enabling 8 complete scans to be made in each 4.8 hour

cycle. The first two and last two minutes of each scan are ignored in the analysis as they contain substantial 'dead time' due to the telescopes being re-pointed ready for the next scan. The two OFF periods are taken as minutes 3 to 12 and 25 to 34, while the ON period is taken from minutes 14 to 23, a one minute gap being left between the OFF and ON periods.

If gamma rays are received from an object during the period in which it is in the field of view then on average an excess of counts would be expected in the ON period when compared with the OFF (background) periods. In the simplest analysis, therefore, the number of counts in the ON period is statistically compared with the expected number (as derived from the OFF periods) and a probability of gamma ray detection ascribed to the scan. This simple but effective technique (known as a 'top-hat' analysis) thus assumes that the aperture function of the system is a square wave of duration 10 minutes instead of the more complex unimodal function which would more closely approximate to the truth. Although this simple approach has been the one principally used in the routine analysis of the data a more sensitive method (based on the correlation analysis of the COS-B team) has been investigated and shown to be effective, and may be the better method for analysing future data. The two techniques will now be discussed in more detail.

(1) Top-Hat Analysis : Let us suppose that 'b' events occur in the first OFF period, 'a' events occur in the second OFF period and 'd' events occur in the ON period (the notation used here stands for before, during and after transit). The number of gamma rays that

appear to have been received in the ON period, N_o, can be deduced to be :

$$N_o = d - (b+a)/2 \qquad \text{----- 5.1}$$

It is now necessary to ascribe a statistical uncertainty to this value.

Several different approaches have been made to this problem by past workers and no common method appears to have been used. We therefore decided to adopt the Maximum Likelihood method which applies itself specifically to the statistical analysis of data samples containing relatively small numbers of events.

For this treatment of the data (due to Orford, private communication) let us make the following assumptions :

(1) N counts are recorded during the ON source period.

(2) A total of B counts are recorded during the total OFF source period.

(3) The ratio of the total OFF source time to the ON source time is α.

(4) The true number of source counts in the ON period (which is unknown and may be zero) is S.

(5) The true number of background counts expected in the ON source period (which is also unknown) is T.

We now consider the possibility of occurance of two mutually exclusive hypotheses :

(a) Suppose that S=0, ie that N and B are simply statistical fluctuations from T. The probability of this situation occurring is given by :

$$L(N,B|S=0,T) = L_0(T) = L(N|T).L(B|T)$$

$$= \frac{e^{-T} . T^N}{N!} . \frac{e^{-\alpha T} . (\alpha T)^B}{B!}$$

$$= \frac{e^{-(1+\alpha)T} . T^{(N+B)} . (\alpha)^B}{N!\ B!}$$

(b) Suppose that S is not zero, ie that N is not simply a statistical fluctuation from T. The probability of this situation occurring is given by :

$$L(N,B|S,T) = L_S(S,T) = L (N|(T+S)).L (B|T)$$

$$= \frac{e^{-(T+S)} . (T+S)^N}{N!} . \frac{e^{-\alpha T} . (\alpha T)^B}{B!}$$

$$= \frac{e^{-((1+\alpha).T+S)} . (T+S)^N . (\alpha T)^B}{N!\ B!}$$

If the true background rate is not known exactly then the two hypotheses are said to 'composite' and no 'most powerful' test exists for determining the relative likelihood of one or the other being true. In this case a reasonable test statistic to use (Eadie et al., 1971) is the Maximum Likelihood ratio :

$$\lambda = \frac{\text{Max}\ (\ L(\ N,B \mid S=0,T\ ))}{\text{Max}\ (\ L(\ N,B \mid S,T\ ))}$$

$$\lambda = \frac{\text{Max}\ (\ L_o(T))}{\text{Max}\ (\ L_s(S,T))}$$

The expression $\text{Max}(L_o(T))$ is found by setting :

$$\frac{\delta(L_o(T))}{\delta(T)} = 0$$

Whilst the expression $\text{Max}(L_s(S,T))$ is found from :

$$\frac{\delta(L_s(S,T))}{\delta(S)\,\delta(T)} = 0$$

It can be shown that :

$$\lambda = \frac{(N+B)^N .\ (\alpha(N+B))^B}{((1+\alpha)N)^N((1+\alpha)B)^B} \qquad \text{----- 5.2}$$

for drift scans $\alpha = 2$ and therefore :

$$\lambda = \frac{(N+B)^N .\ (2(N+B))^B}{(3N)^N\ \ (3B)^B} \qquad \text{----- 5.3}$$

which gives the relative likelihood of N being a statistical fluctuation of T. In the process of evaluating the derivative of $\text{Max}\ (L_s(S,T))$ it is shown that $\hat{T}$, the most likely value of T is given by :

$$\hat{T} = B/\alpha$$

and thus that:

$$\hat{S} = N - \hat{T} \qquad \text{----- 5.4}$$

where $\hat{S}$ is the most likely value of the source strength. The upper and lower limits on S are obtained by relaxing the value of λ to S_+ and S_-, which include the 68% confidence region for $\hat{S}$.

(2) Cross-Correlation Analysis : The method outlined below is that discussed and developed by Hermson (1980) and was used in a two dimensional form in the search for point sources in the gamma ray data from the COS-B satellite. In the treatment of drift scan data a one dimensional approach is taken.

The drift scan is first divided into 36 one minute bins into which the events fall. A search is then made for a signal existing over and above the background level, having a shape consistent with the Point Spread Function (PSF) of the telescopes. Let us denote the number of events in each bin j as N_j, and the PSF as $F_{r,j}$ the predicted contribution of a source at bin r to bin j. At each bin r a correlation value C_r is evaluated as follows :

$$C_r = \frac{A}{m} \cdot \sum_j (N_j - N).(F_{r,j} - F) \qquad \text{----- 5.5}$$

with A : a normalisation constant

m : number of bins (36 in this example)

N : the average of N_j

F : the average of $F_{r,j}$ over the m bins

Following Hermson the distribution of C_r over the scan is called the correlation map; if at a bin r the correlation between the PSF and the binned data is high then C_r will be significantly positive. If no signal exists in the data and the background is either flat or has a constant gradient with r then C_r is on average zero. The constant A can be normalised so that the maximum value of the correlation function C_r is equal to the source strength (in counts). If this is done and Equation 5.5 is rearranged the following expression for C_r is obtained :

$$C_r = \frac{(m.\Sigma(FN) - (\Sigma F.\Sigma N)).\Sigma F}{(m.\Sigma(F^2) - (\Sigma F)^2)}$$

(where all subscripts have been omitted)

From a statistical consideration of the distribution of values of the correlation function, C_r, for a scan both without a source and with a flat background, it can be shown that the parent mean of such a distribution is zero. In addition, an expression can be obtained for the parent standard deviation of the distribution, S_r. The ratio of C_r to S_r expresses the correlation value in terms of parent standard deviations of the function for a random distribution of counts in a scan. This ratio can be shown to be :

$$\frac{C_r}{S_r} = \frac{(m.(\Sigma(FN) - (\Sigma F).(\Sigma N))}{((m.\Sigma(F^2) - (\Sigma F)^2).\Sigma(N))^{1/2}} \quad \text{--- 5.6}$$

The larger the value of C_r/S_r the less probable it is that any observed excess can be ascribed to a random background variation.

Clearly it is necessary to define F to be a good approximation to the PSF of the system and in this analysis it is taken to be a gaussian of FWHM 2.2°. Practical application of the technique has shown it able to pick out excesses in the data which are not immediately obvious to the eye and which do not necessarily occur in the centre of the scan.

5.2b Tracking Data

Our main aim in observing Cygnus X-3 in 1982 was to verify results which had been obtained in 1981. Unfortunately, while the majority of the data from Cygnus X-3 in 1981 had been taken in the drift scan mode, the tracking mode had been used throughout the whole of 1982. We therefore required a technique for examining the tracking data in such a way as to allow the use of the Maximum Likelihood method discussed earlier. This we did by identifying the phase at which emission seemed to occur (from 1981), taking three 10 minute sections about this phase (before, during and after), and comparing the number of counts in the middle sample with the predicted number from the two adjacent samples.

Several objections to this method immediately spring to mind. For example, the count rate is not constant if the zenith angle of the telescopes is changing, and so the number of counts expected in the before and after periods will not be equal. It can be shown, however, that the error in the value of the number of events

predicted in the ON period from the non-linear change of count rate with zenith angle θ is less than 0.3% for all values of θ. Considering the size of the excesses seen at phase 0.625 during the 1981 season of drift scans (see Section 6.2b) we considered this effect to be negligible. A second objection which arises is the fact that the peak emission may not occur at precisely the assumed phase. This is a valid criticism which led us to examine the tracking data in more detail in an attempt to discover the exact time structure of the emission (see Section 6.2c).

5.3 Periodicity Analysis of Data

5.3a Reduction of the Data to the Barycentre

In an experiment such as the present one it is important before performing a periodicity analysis of a data sample to have corrected the event times for the quite significant effects arising from both the motion of the Earth about the Sun, and the spin of the Earth about its own axis. This is done by correcting each individual event time (measured in the moving laboratory frame) to the time at which the event would have been recorded at the barycentre of the Solar System.

A program was developed to perform this function which operated as follows :

(1) The raw event time was corrected for both the drifting of the crystal clock and the time of transit between the WWV station in Denver and Dugway (about 3 ms), and then converted to Coordinated Universal Time (UTC).

(2) From the relative position of the object observed and the Dugway site, in the Earth's geocentric reference frame, the event time was corrected to the centre of the Earth.

(3) Using information provided by the MIT barycentre ephemeris (Ash et al., 1967) specifying the position of the geocentre of the Earth relative to the Solar System barycentre, the event time was corrected to the time at which it would have reached the barycentre.

(4) A relativistic correction was further applied to the event time to take into account the small changes in rate of Earth-based clocks due to the varying speed of the Earth in its orbit about the Sun.

Spot values of the absolute correction, (which can be as high as 500 seconds depending upon the declination of the object and the time of year), when compared with values obtained by a variety of other astronomical research groups, have been found to be satisfactorily consistent. An example is given in Table 5.1 which compares values of the barycentric correction obtained from the Durham program with those obtained from the program used by the Mount Hopkins Observatory group (Weekes, private communication). The correction is for the Crab Pulsar and is appropriate to the site of the MHO. Thus use of the program enables us to keep reasonable absolute phase in observations of all pulsars except perhaps the recently discovered millisecond pulsar 4C21.

Date	UTC	Delay (MHO)	Delay (Dur)	Diff.(μs)
06-12-83	0920	488.498123	488.498117	6
06-12-83	0950	488.527847	488.527832	15
06-12-83	1020	488.557251	488.557226	25
08-12-83	0730	491.050908	491.050931	23
08-12-83	0800	491.075545	491.075559	14
08-12-83	0830	491.099828	491.099832	4

Table 5.1

A Comparison of the Barycentric Corrections Evaluated by the MHO and the Durham Algorithms

5.3b Orbital Correction for Binary Pulsars

The previous section dealt with the corrections necessary to account for the orbital motions of the observing site; if the source is itself in a binary orbit (eg PSR 1913+16) a further correction needs to be made. The parameters specifying the size of the correction are the diameter of the orbit (in light seconds), the orbital period, the orbital ellipticity and the orbital phase; given that these are sufficiently well known from observations at other wavelengths the size of the correction can be deduced to a high degree of accuracy.

5.3c Analysis with a Known Ephemeris

If the parameters specifying the period and phase of a pulsar are well defined from observations at other wavelengths then only one hypothesis need be tested in the analysis. This is in contrast to the more general case in which a precise ephemeris is not available and the analysis has to be repeated at the large number of different periods possible, thereby greatly increasing the number of degrees of freedom expended in the test.

In order to assist in the analysis of the present Crab Pulsar data contemporary radio measurements were undertaken from Jodrell Bank which provided a very accurate month-by-month ephemeris for the whole of 1982. This ephemeris, given in Table 5.2 (Lyne, private communication), specifies the exact period, period first derivative and phase of the Pulsar at an epoch in each month during the one year interval. Using this information the precise phase of the object, relative to the radio main pulse, can be deduced for

DATE	ARRIVAL TIME (JD)	PERIOD (SECS)	PDOT (MICS/DAY)
Feb 82	5015.500000167454	.033267658429	.036433118
Mar	5043.500000145266	.033268678512	.036430497
Apr	5074.500000244988	.033269807879	.036430519
May	5104.500000038866	.033270900773	.036431357
June	5135.500000205150	.033272030095	.036426127
July	5165.500000077662	.033273122926	.036426786
Aug	5196.500000266609	.033274252156	.036427217
Sept	5226.500000362315	.033275381396	.036427151
Oct	5257.500000091713	.033276474180	.036427415
Nov	5288.500000120266	.033277603411	.036426514
Dec	5318.500000270764	.033278696195	.036426046

Table 5.2

The arrival time, period and period first derivative of the Main radio pulse of the Crab Pulsar at each month in 1982. (Lyne, private communication)

any time in 1982.

Given that the following parameters are known :

t_o : the epoch of the ephemeris

ϕ_o : the phase of the pulsar at time t_o

P_o : The period of the pulsar at time t_o

P_1 : The time derivative of the period at t_o

it is usual to evaluate the corresponding frequency terms f_o and f_1 using the following formulas :

$$f_o = 1/P_o \qquad \text{and}$$

$$f_1 = -P_1/(P_o)^2$$

From these parameters the phase ϕ_i of the pulsar at any time t_i can be evaluated using :

$$\phi_i = \phi_o + f_o.(t_i - t_o) + f_1.(t_i - t_o)^2/2 \quad \text{--- 5.7}$$

Once the phase of each event in the data sample has been determined the uniformity of the resultant phase distribution can be tested for evidence of pulsed gamma ray content using one or other of the statistical tests discussed in Section 5.3f.

5.3d Search for an Undefined Period

An object such as Cygnus X-3, which although known to emit VHE gamma rays has never been identified as a pulsar, clearly lends

itself to this form of analysis. It is advantageous to identify a data section which it is hoped contains a significant number of gamma rays and with Cygnus X-3 this is done by analysing only the 'ON' time of those scans showing a statistically significant excess.

We take the lower period limit for a gamma ray emitting pulsar to be 1ms (the newly discovered pulsar 4C21 has a period of about 1.5 ms for example), and the upper limit to be about 10 seconds; the data being analysed at a number of trial periods between these two limits. The particular number of trial periods is related to the time duration of the data sample being tested since it is only necessary to use periods which are harmonics of the data interval. Thus, when unfolded with two adjacent and independent trial periods the relative phase of the first and the last events in the series changes by exactly one cycle.

Suppose the time duration of the sample is T and the lower and upper period limits are P_l and P_u respectively. The minimum number of trial periods which need to be tested, N_t, is given by :

$$N_t = \frac{T}{P_l} - \frac{T}{P_u} \qquad \text{----- 5.8}$$

The separation between two adjacent trial periods is not constant, being less at the lower periods. For example, just as many trial periods need to be tested between 20 ms and 25 ms, as between 100 ms and 100 s. In practical applications of the method trial periods separated by 1/3rd of a harmonic interval are used.

A second application of this technique is the case in which the ephemeris of a pulsar is known, but is sufficiently uncertain (due perhaps to a lack of recent measurements) as to require a small amount of sweeping about the predicted period. This would also apply in the case of a binary Pulsar whose orbital parameters are not sufficiently well defined.

Given that a particular value of period is being tested, the relative phase of each event in the data sample can be determined and the resultant phase distribution tested for uniformity using one or other of the techniques discussed in Section 5.3f.

5.3e Search for Transient Pulsed Emission

Another variable in the periodicity analysis technique is the data segment used; the data sample can be analysed as a whole if continuous pulsed emission is thought to occur, or the data can be split into sections of variable trial lengths if bursts of pulsed emission are thought to occur with a duration less than the period of observation. The second method can often be an essential part of the analysis for two principal reasons :

(1) If the duration of pulsed emission from the pulsar is shorter than the duration of the whole time series then inclusion of the whole data sample in the analysis reduces the percentage of pulsed events and weakens the effectiveness of the test.

(2) It can be shown from the analysis of randomly generated periodic data that if the pulsed events are concentrated together within the data sample (ie are not spread evenly throughout the data), then the best period recovered by a sweeping technique can

be significantly offset from the true period of the pulsed events (Orford, private communication).

5.3f Statistical Analysis of Phase Information

In the specialised case in which the expected shape of the phase distribution is well known from other measurements the usual procedure followed, known as 'epoch folding', is to bin the phases in the series to produce the 'light curve' of the object. The resulting histogram can then be tested for uniformity in two ways :

(1) Pearson's chi-squared test - a general test of the 'flatness' of a histogram, and the amount of deviation from expectation of the individual bin values.

(2) Binomial comparison - in the special case in which a definite prediction exists as to the position in the light curve of any excess of events, the number of events in the bin or bins in question can be compared with the expected number as derived from the rest of the light curve.

In many cases this sort of test suffers some disadvantages - principally those arising from the arbitrary choices made in the binning procedure.

In the more general case in which the shape of the expected light curve is totally unknown the 'uniformly most powerful' test (Mardia, 1972) for the uniformity of a circular phase distribution, which also avoids the problem of arbitrary choice, is the Rayleigh test. In this, a vector of modulus R is formed as the resultant of a series of unit vectors at the phases of the events in the time series. In essence the test correlates the event time series with

a sine wave at the trial period, and is analagous to a test in continuous data for the amplitude of a particular frequency existing in a power spectrum. Given that each event in the series has an assigned phase ϕ_i we calculate the two terms :

$$C = (\Sigma(\cos(\phi_i)))/N \qquad \text{and}$$

$$S = (\Sigma(\sin(\phi_i)))/N$$

from which R is then evaluated as :

$$R = (C^2 + S^2)^{1/2}$$

The probability of the term NR^2 is evaluated accurately from :

$$\text{Prob}(NR^2>K) = e^{-K}.\left(1+\frac{(2K-K^2)}{4N}\right.$$

$$\left.-\frac{(24K-132K^2+76K^3-9K^4))}{228N}\right. \quad \text{----- 5.9}$$

An approximation to this series is the first term $\exp(-NR^2)$, which corresponds to the probability of the term $2NR^2$ arising from a X^2 distribution with 2 degrees of freedom.

Two main problems connected with the use of this test exist :

(1) The test assumes that only a single directionality exists in the distribution, and a problem arises when it is applied to the analysis of data taken from a pulsar emitting a light curve with both a main and inter-pulse. In this case when the data is unfolded with the pulsar period the two pulses are assigned almost

exactly opposite phases and R, the modulus of the resultant vector, will not have a significantly large value. In other words a complicated light curve will not correlate with a sine wave. If we assume, however, that the main and inter-pulse are approximately 180° apart (which is often the case) the pulsar light curve will correlate with a sine wave of twice the pulsar frequency. The data is therefore unfolded with both P and P/2.

(2) The test is most efficient in detecting pulsed emission having a broad peaked light curve. When the whole of the excess occurs in a narrow peak the effectiveness of the test in identifying the pulsed emission is much reduced. As has been pointed out (Leahy, et al., 1983) the Rayleigh Test in this case becomes less sensitive in finding pulsed emission than the standard epoch folding technique discussed earlier.

5.4 The Array Timing Analysis of the Data

From the information recorded about each event triggering a response from the system it is possible to determine the relative time of arrival of the shower front at each of the telescopes. If three or more telescopes are involved in the event then the approximate arrival direction of the shower can be deduced. Let us consider the following parameters :

t_i, t_j : The time of arrival of the shower front at telescopes i and j respectively, relative to the time of arrival at telescope 1

x_i, y_i, z_i : The x,y,z coordinates of telescope i relative to telescope 1.

x_j, y_j, z_j : The x,y,z coordinates of telescope j relative to telescope 1.

(where we take a cartesian coordinate frame with 'x' pointing due north, and 'z' pointing to the zenith.)

Assuming a flat shower front it can be shown that :

$$\begin{aligned}
&\mathrm{Cos}^2(\theta).((y_1 z_2 - y_2 z_1)^2 + (x_2 y_1 - x_1 y_2)^2 + (x_1 z_2 - x_2 z_1)^2) \\
&\quad + 2.c.\mathrm{Cos}(\theta).((x_2 t_1 - x_1 t_2).(x_1 z_2 - x_2 z_1) \\
&\quad + (y_2 t_1 - y_1 t_2).(y_1 z_2 - y_2 z_1)) \\
&\quad + (c^2.((y_1 t_2 - y_2 t_1)^2 + (x_2 t_1 - x_1 t_2)^2) \\
&\quad - (x_2 y_1 - x_1 y_2)^2) \\
&\quad = 0 \qquad \text{----- 5.10}
\end{aligned}$$

Solving the quadratic leads to two values of the zenith angle θ; one being the true zenith angle of the shower, the other being its mirror image in the azimuthal plane. The azimuth angle of the shower can now be determined from the equation :

$$\mathrm{Cos}(\phi) = \frac{(c.(x_2 t_1 - x_1 t_2) + \mathrm{Cos}(\theta).(x_1 z_2 - x_2 z_1))}{\mathrm{Sin}(\theta).(x_2 y_1 - x_1 y_2)} \qquad \text{----- 5.11}$$

Thus the arrival direction of the shower is determined in the 'alt-azimuth' system. It is usually more useful to convert the values into α, δ, the right ascension and declination of the shower and, since the time of arrival of the shower is known to a

high degree of precision, this can be done using the standard conversion procedures. The factors which introduce uncertainty into the method are :

(1) The assumption of a flat shower front.

(2) Uncertainty in the relative position of the telescopes.

(3) Uncertainty in the values t_i and t_j, principally due to jitter in the TAC units.

It was initially hoped that arrival directions would be determined to within about $\pm$ 0.2°, thus enabling around 80% - 90% of the 3-fold telescope responses to be rejected as coming from OFF-source. Unfortunately, due to a combination of all three problems listed above it appears that a resolution of only about $\pm$ 0.5° has been achieved (Walmsley, private communication). In addition, the rate at which the system recorded 3-fold events was not as high as had been expected, as discussed in Section 3.7b. Consequently the method has not been found to be as useful as was originally hoped when the experiment was designed. However, work is continuing in an attempt to further develop the technique and it is hoped that it will have some part to play in future VHE gamma ray experiments.

5.5 The Derivation of Flux and Luminosity

It is common practise in ground based Cerenkov astronomy to express the flux of gamma rays observed from an object, whether

derived from drift scan data or through a periodicity search, in terms of its ratio to the cosmic ray background flux seen during the observation. It is more useful to convert this figure (usually given in percentage terms) to a flux expressed, for a discrete source, in photons cm^{-2} s^{-1}.

Let us suppose that in a given data sample, taken at a gamma ray energy threshold of 1300 GeV (corresponding to a cosmic ray threshold of about 2000 GeV), a count excess of 10% is seen. The integral cosmic ray flux at this threshold is known to be about 3.8 10^{-6} cm^{-2} s^{-1} str^{-1} (see Section 3.6b). Thus, since the field of view of the array is about 1.67 10^{-3} str. we deduce the expected cosmic ray flux at $E_{cr} > 2000$ GeV to be 6.3 10^{-9} cm^{-2} s^{-1}. The excess of gamma rays is therefore deduced to correspond to a flux of about 6.3 10^{-10} cm^{-2} s^{-1} at $E_\gamma > 1300$ GeV. For energy thresholds other than the one given above the background cosmic ray flux may be evaluated by assuming an integral spectral slope of -1.6 (Craig, 1984).

Once the gamma ray flux is known it is also informative to deduce the luminosity of the source. Assuming that the source emits isotropically this parameter is evaluated using the following equation :

$$L = 4\pi F d^2 E_\bullet \qquad \text{----- 5.12}$$

where L : luminosity in ergs s^{-1}

F : flux in cm^{-2} s^{-1}

d : distance to source in cm

E_a : average photon energy detected from source

The only uncertain parameter in this equation is E_a, the average energy of the initiating gamma rays emitted by the source. Let us suppose that the source has a differential spectrum given by :

$$S(E) = A.E^{-\gamma}$$

where $S(E)dE$: number of gamma rays of energy between E and E+dE

E : energy of gamma rays

γ : differential spectral slope

The integral spectrum is therefore given by :

$$N(>E_t) = \frac{(A.E_t^{1-\gamma})}{(1-\gamma)}$$

where $N(>E_t)$: total number of gamma rays above threshold energy

E_t : energy threshold

Now the total energy contained in the spectrum above an energy E_t, $E(>E_t)$, is given by :

$$E(>E_t) = \int_t^\infty S(E)EdE$$

$$= \int A.E^{(1-\gamma)}dE$$

$$= \frac{(A.E_t^{2-\gamma})}{(2-\gamma)}$$

$$E(>E_t) = N(>E_t).E_t.\frac{(1-\gamma)}{(2-\gamma)}$$

Equation 5.12 now becomes :

$$L = 4\pi F d^2 E_t \frac{(1-\gamma)}{(2-\gamma)} \qquad \text{----- 5.13}$$

The factor $(1-\gamma)/(2-\gamma)$, which in practice is always greater than 1, corrects for the fact that most gamma rays detected at a particular threshold energy have an energy in excess of the threshold value.

This equation also illustrates the fact that the differential slope of a spectrum must be less than -2, otherwise the spectrum will contain an infinite amount of energy.

Chapter Six

Results

6.1 Introduction

When it came to examining the data taken on the various objects observed in 1981 and 1982 a clear order of priority was necessary. The two principal sources observed, the Crab Pulsar and Cygnus X-3, have received the most attention and will be reported on in this work. The analysis of the other objects observed is continuing, and will be reported seperately (Walmsley, Ph.d. thesis, in preparation and Dowthwaite, Ph.D. thesis, in preparation).

6.2 Cygnus X-3

6.2a Aims of the Analysis

As was discussed in Section 1.5, extensive observations of Cygnus X-3 have been made in the years since its radio outburst in 1972 (Gregory, 1972), with positive detections having been reported at all wavelengths from radio up to energies in excess of 10^{15} eV.

The most distinguishing feature of the object is the characteristic near-sinusoidal 4.8 hour amplitude modulation of its infra-red (Mason et al., 1976) and X-ray (Elsner et al., 1980) emission, not yet seen in either the radio or the optical. At gamma ray energies of around 100 MeV some doubt exists, with the SAS-2 observation in 1973 (Lamb et al., 1977) showing an apparently 4.8 hour modulated positive signal, which was not confirmed by the later COS-B measurements (Strong et al., 1982). At energies in excess of 1000 GeV results from 3 observatories suggest that a 4.8

hour periodic signal exists with the phase of the gamma ray maximum coinciding with that seen in X-rays (Neshpor et al., 1979; Danaher et al., 1981; Lamb et al., 1981). Recent claims of a positive 4.8 hour modulated signal have also been made at energies in excess of 10^{15} eV (Samorski and Stamm, 1983, and Lloyd-Evans et al., 1983).

In addition to this accepted short term variation, a further 34.1 day amplitude modulation of the object's X-ray emission has also been reported (Molteni et al.,1980).

The principal aims of our observations of Cygnus X-3 have therefore been to confirm the 4.8 hour modulation of gamma rays above 1000 GeV, to ascertain the time structure of any emission found, and to search for the reported 34.1 day modulation.

6.2b The 4.8 Hour Periodicity

Considering first the 1981 data, drift scans were summed with others having identical phases, as defined by the ephemeris of Van der Klis and Bonnet-Bidaut (Van der Klis et al., 1981), and analysed for count rate excesses using the Maximum Likelihood method described in Section 5.2a. Table 6.1 gives the number of events recorded before, during and after the transit of Cygnus X-3, together with the observed excess number of counts and the upper and lower limits of this excess, for each of the observed phases. The excess, expressed as a percentage of the cosmic ray background, is plotted against phase in Figure 6.1. It is noted that the only significantly positive excess occurs at phase 0.625/0.655 for which the ON/OFF ratio is 1.076 ± 0.031 (based upon 1770 counts ON source and 3291 counts OFF source). We had thus

Phase	B	D	A	S	S_+	S_-
0.0	931	862	877	-42.0	36.4	36.1
0.03	1114	1127	1136	2.0	41.3	40.9
0.125	1115	1154	1205	-6.0	41.8	41.5
0.155	593	665	682	27.5	31.5	31.2
0.25	1476	1434	1395	-1.5	46.6	46.2
0.28	708	723	732	3.0	33.1	32.7
0.375	1617	1583	1569	-10.0	48.9	48.6
0.405	567	520	603	-65.0	28.7	28.4
0.5	1191	1150	1116	-3.5	41.7	41.4
0.53	201	208	206	4.5	17.8	17.4
0.625	1152	1293	1268	83.0	43.7	43.4
0.655	423	477	448	41.5	26.5	26.2
0.75	1237	1207	1240	-31.5	42.9	42.6
0.78	561	566	563	4.0	29.3	28.9
0.875	1231	1198	1207	-21.0	42.7	42.4
0.905	451	468	471	7.0	26.6	26.3

Table 6.1

The number of Cerenkov events recorded in 1981 before, during and after the transit of Cygnus X-3 at each phase of the 4.8 hour cycle. Also shown are the excess number of events with the associated positive and negative uncertainties

Figure 6.1

The % excess of Cerenkov events recorded from Cygnus X-3 in 1981 at various phases of the 4.8 hour cycle

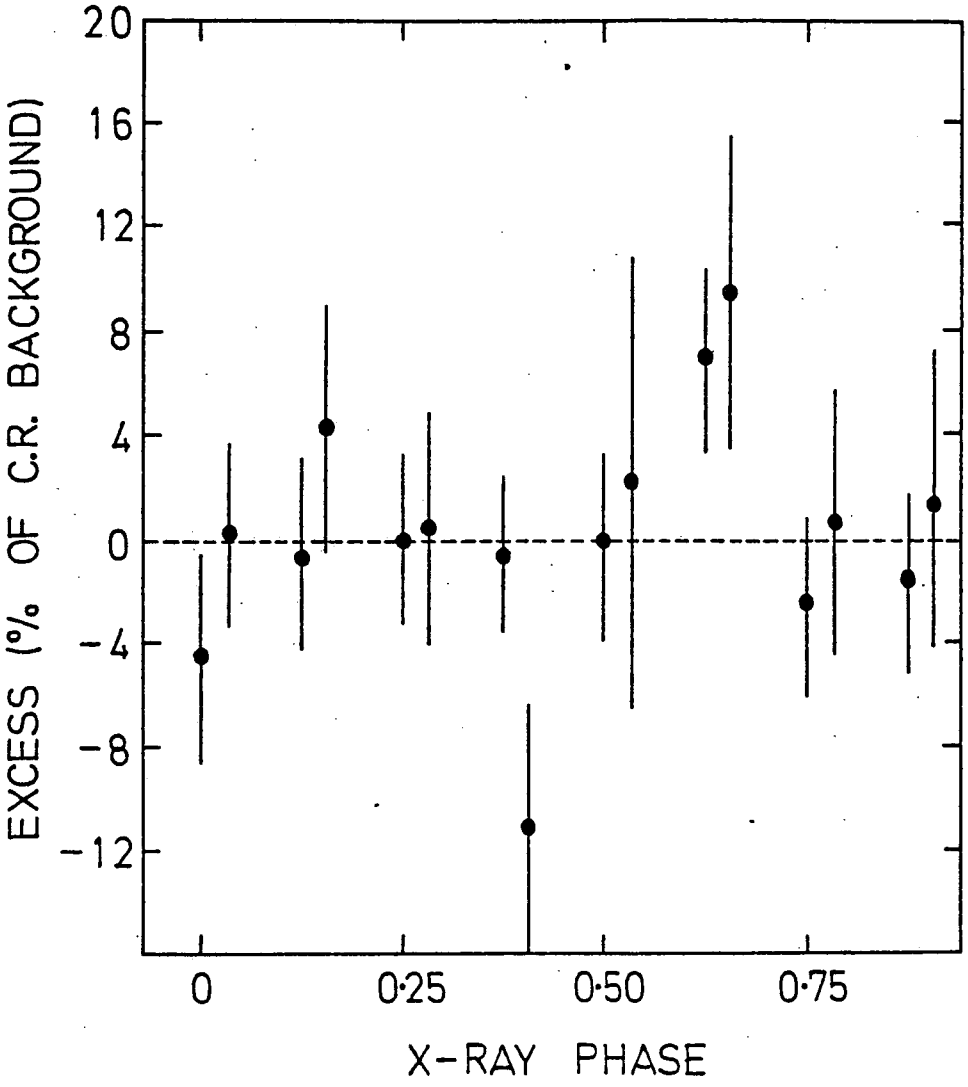
20
16
12
8
4
0
-4
-8
-12
EXCESS (% OF C.R. BACKGROUND)
0
0·25
0·50
0·75
X-RAY PHASE

obtained evidence at the 2.4 standard deviation level for gamma ray emission at phase 0.625/0.655, constituting 7.6% of the cosmic ray background and corresponding to an integral peak flux of at least $4.8\ 10^{-10}$ cm^{-2} s^{-1} at E > 1300 GeV.

In view of earlier results which suggested that the spectral slope of Cygnus X-3 at VHE gamma ray energies may be steeper than that of the cosmic ray background (Vladimirsky et al., 1973), we investigated whether the observed excess at phase 0.625/0.655 occurred more strongly in the response of any particular telescope. We found that telescope 3, which had a significantly lower energy threshold than the others, indeed contributed most of the excess counts. Table 6.2 lists, by phase, the observed excesses for showers which triggered telescope 3, while Figure 6.2 shows these excesses expressed as a percentage of the cosmic ray background. It is seen that this telescope alone showed an excess of 14% at phase 0.625/0.655, at the 3.35 standard deviation level (1079 counts ON and 1893 counts OFF), corresponding to an integral peak flux of about $1.4\ 10^{-9}$ cm^{-2} s^{-1} for E > 1000 GeV. A more detailed discussion of the implications of this effect is given in Section 6.2e.

The tracking data taken in 1982 yielded a total of 106 acceptable 'pseudo drift scans' (as discussed in Section 4.2a), which were analysed in the same manner as the 1981 drift scan data. Table 6.3 lists, by 4.8 hour phase, the observed excesses for all events recorded in 1982, and these excesses expressed as a percentage of the cosmic ray background are shown in Figure 6.3. The effect at phase 0.625 is seen to be reduced from the value

Phase	B	D	A	S	S_+	S_-
0.0	424	400	394	-9.0	24.8	24.4
0.03	569	539	548	-19.5	28.8	28.4
0.125	513	572	545	43.0	29.1	28.8
0.155	347	391	410	12.5	24.3	23.9
0.25	759	718	693	-8.0	33.0	32.7
0.28	457	431	469	-32.0	25.9	25.6
0.375	805	783	773	-6.0	34.5	34.2
0.405	365	348	381	-25.0	23.3	23.0
0.5	725	720	669	23.0	32.9	32.5
0.53	129	120	115	-2.0	13.6	13.3
0.625	651	770	723	83.0	33.6	33.2
0.655	260	309	259	49.5	21.1	20.8
0.75	509	508	502	2.5	27.8	27.4
0.78	346	338	359	-14.5	22.8	22.5
0.875	688	648	629	-10.5	31.4	31.1
0.905	272	267	295	-16.5	20.4	20.1

Table 6.2

The number of Cerenkov events recorded on the low energy channel in 1981 before, during and after the transit of Cygnus X-3 at each phase of the 4.8 hour cycle. Also shown are the excess number of events with the associated positive and negative uncertainties

Figure 6.2

The % excess of Cerenkov events recorded in the low energy channel from Cygnus X-3 in 1981 at various phases of the 4.8 hour cycle

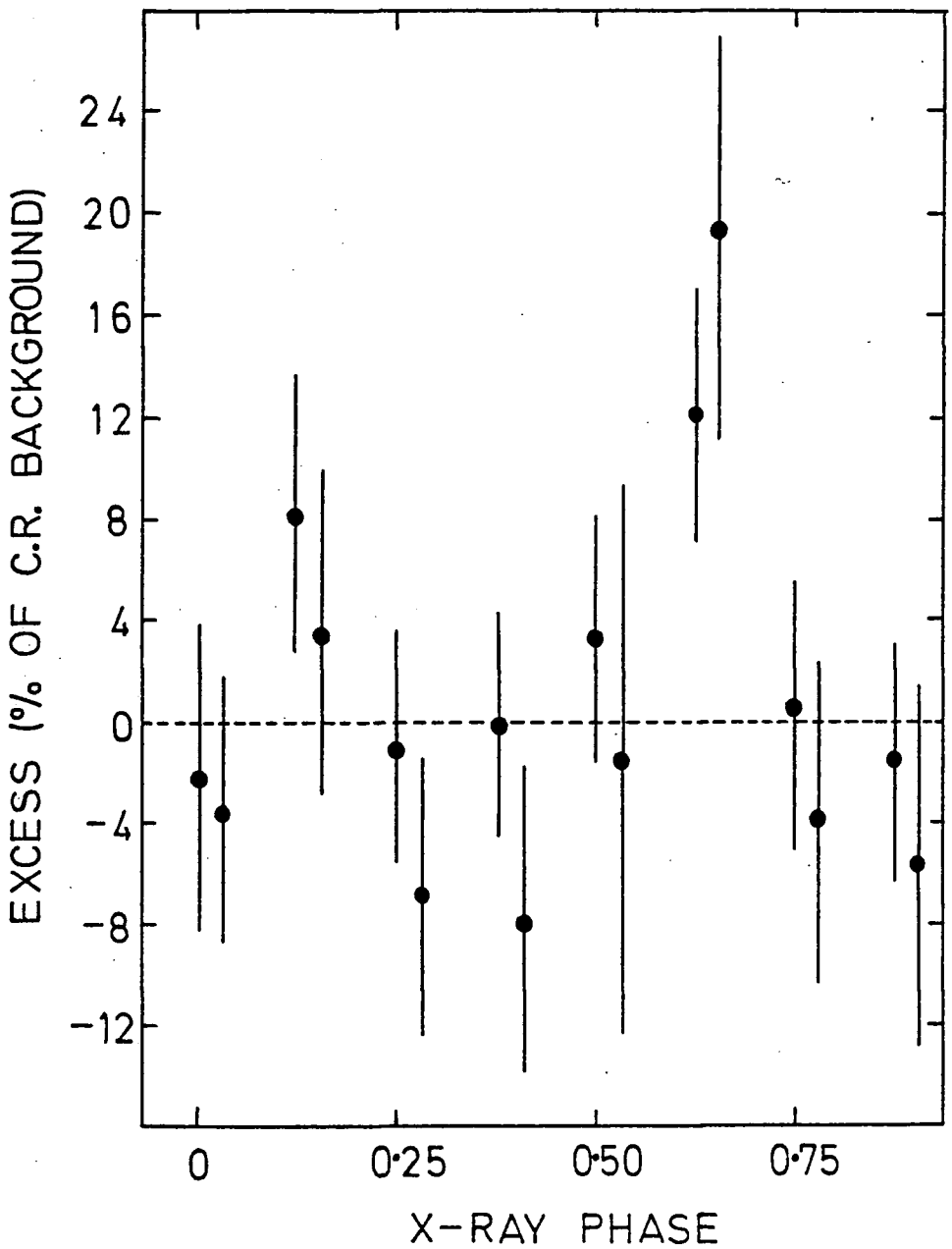
EXCESS (% OF C.R. BACKGROUND)
24
20
16
12
8
4
0
-4
-8
-12
0
0·25
0·50
0·75
X-RAY PHASE

Phase	B	D	A	S	S_+	S_-
0.0	2844	2812	2825	-22.5	65.2	64.6
0.125	3605	3380	3292	-68.5	71.4	71.4
0.25	2414	2283	2226	-37.0	58.9	58.4
0.375	755	692	663	-17.0	32.5	32.2
0.5	1619	1552	1607	-61.0	48.6	48.3
0.625	5261	5359	5190	133.5	89.2	88.8
0.75	5442	5549	5457	99.5	89.8	89.8
0.875	4693	4604	4396	59.5	83.5	83.4

Table 6.3

The number of Cerenkov events recorded in 1982 before, during and after the transit of Cygnus X-3 at each phase of the 4.8 hour cycle. Also shown are the excess number of events with the associated positive and negative uncertainties

Figure 6.3

The % excess of Cerenkov events recorded from Cygnus X-3 in 1982 at various phases of the 4.8 hour cycle

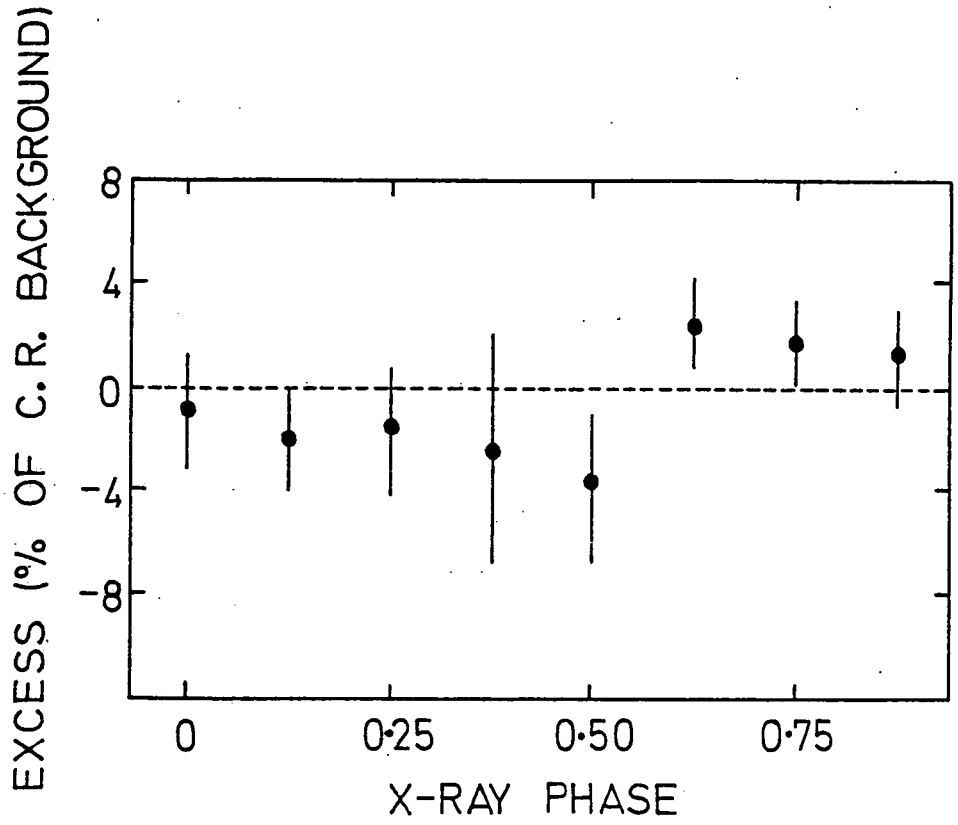
EXCESS (% OF C.R. BACKGROUND)
8
4
0
-4
-8
0
0·25
0·50
0·75
X-RAY PHASE

observed in 1981; an excess of 2.6% at only the 1.5 standard deviation level. However, taking the low energy channel (in 1982 redefined as those showers triggering telescopes 2 or 3), the effect is larger, as detailed in Table 6.4 and Figure 6.4. At phase 0.625 an excess of 6.8% is observed at the 2.7 standard deviation level, corresponding to an integral peak flux of about $6.8\ 10^{-10}$ cm^{-2} s^{-1} for E > 1000 GeV.

Taking the 1981 and 1982 data together and considering just the low energy channel we find an excess of 8.8% of the cosmic ray background at the 4.1 standard deviation level (3686 counts ON and 6774 counts OFF), corresponding to an integral peak flux of about $(8.76 \pm 2.13).10^{-10}$ cm^{-2} s^{-1} at E > 1000 GeV. As is shown in Figure 6.5 no significant excess is seen at any other phase. Assuming the ON-time to be the 10 minutes about phase 0.625 we therefore deduce the average flux from Cygnus X-3, over the whole of the 4.8 hour cycle, to be $(3.0 \pm 0.76)\ 10^{-11}$ cm^{-2} s^{-1}. Taking the object to be at a distance of 10 Kpc, this implies an average power output of about $3.5\ 10^{36}$ ergs s^{-1} above 1000 GeV, assuming a differential gamma ray spectral slope of -2.2.

The average flux seen in the low energy channel at around phase 0.625/0.655, and the flux averaged over the whole of the 4.8 hour cycle are shown in Figure 6.6, which compares our results with those at other wavelengths. Further discussion of this figure will be given in Chapter 7.

6.2c The Time-Structure of the Emission at Phase 0.625

A problem connected with the simple 'top-hat' type treatment of

Phase	B	D	A	S	S_+	S_-
0.0	1294	1361	1316	56.0	45.0	44.7
0.125	1789	1661	1505	14.0	49.8	49.7
0.25	1191	1073	1032	-38.5	40.6	40.3
0.375	321	307	286	3.5	21.6	21.3
0.5	589	610	587	22.0	30.2	29.9
0.625	2502	2607	2379	166.5	61.9	61.4
0.75	2653	2626	2640	-20.5	63.0	62.5
0.875	2312	2302	2203	44.5	58.6	58.2

Table 6.4

The number of Cerenkov events recorded on the low energy channel in 1982 before, during and after the transit of Cygnus X-3 at each phase of the 4.8 hour cycle. Also shown are the excess number of events with the associated positive and negative uncertainties

Figure 6.4

The % excess of Cerenkov events recorded in the low energy channel from Cygnus X-3 in 1982 at various phases of the 4.8 hour cycle

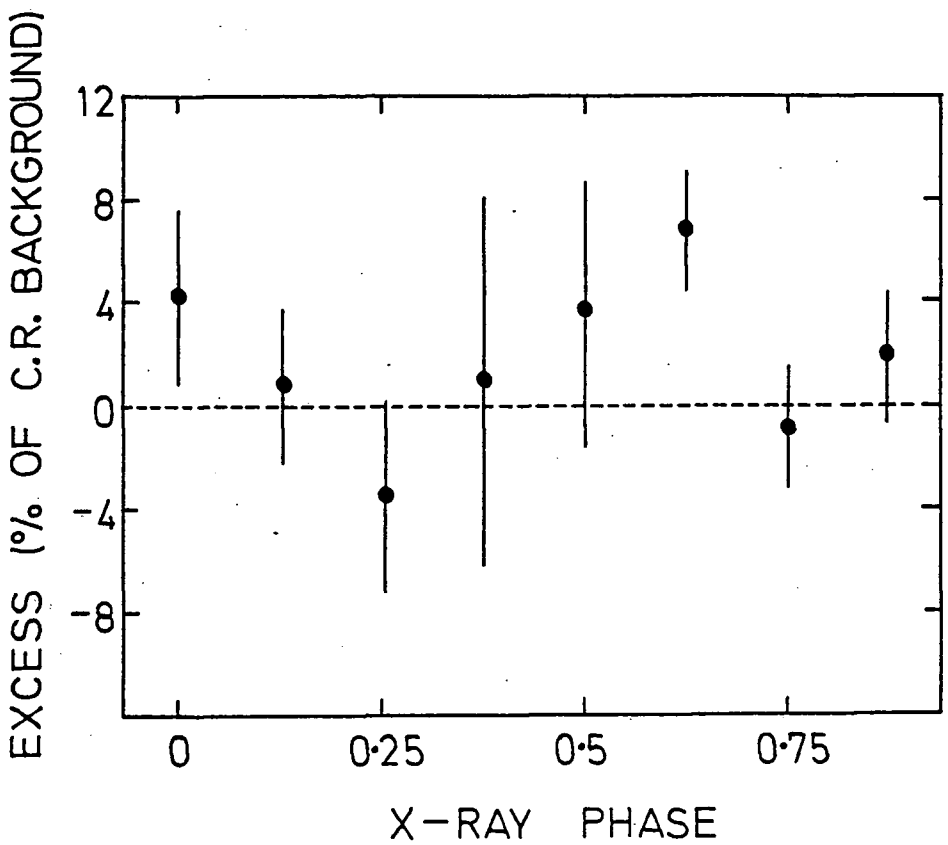
EXCESS (% OF C.R. BACKGROUND)
12
8
4
0
-4
-8
0
0·25
0·5
0·75
X-RAY PHASE

Figure 6.5

The overall % excess of Cerenkov events recorded in the low energy channel from Cygnus X-3 at various phases of the 4.8 hour cycle

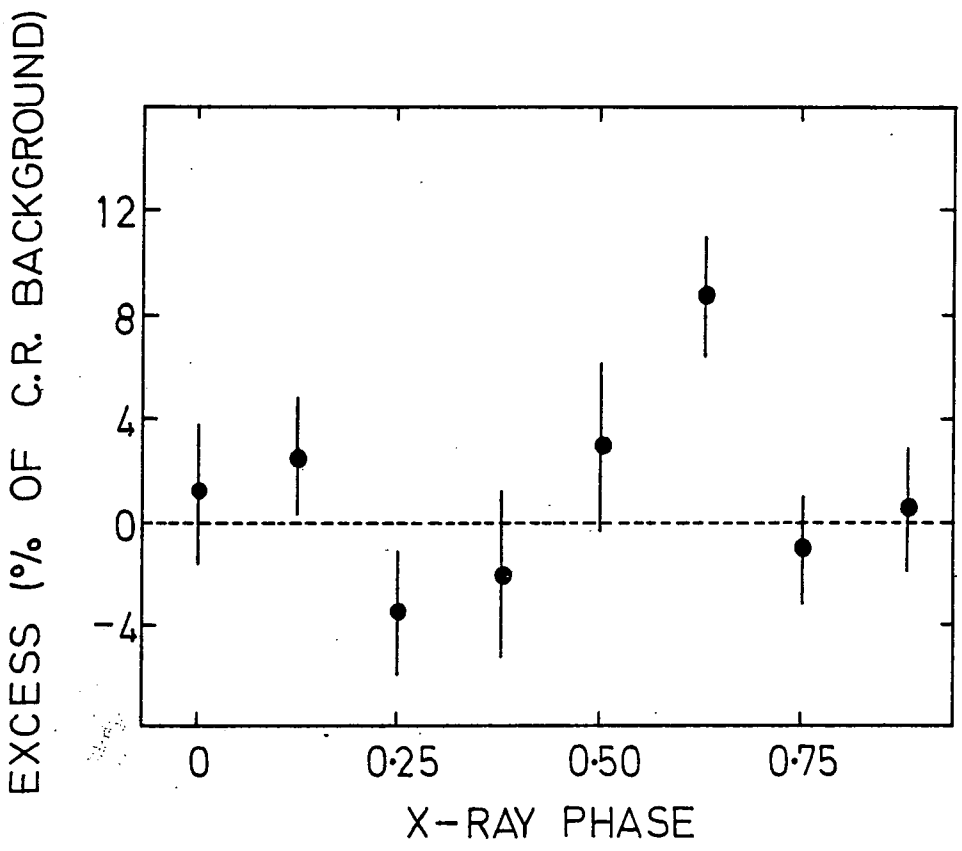
EXCESS (% OF C.R. BACKGROUND)
12
8
4
0
−4
0
0·25
0·50
0·75
X−RAY PHASE

Figure 6.6

The energy spectrum of Cygnus X-3 over the range 10^3 - 10^{19} eV

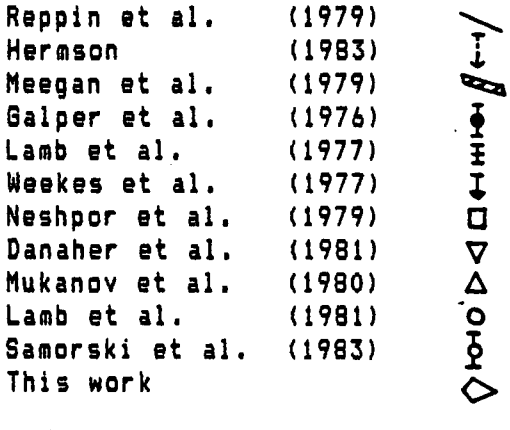

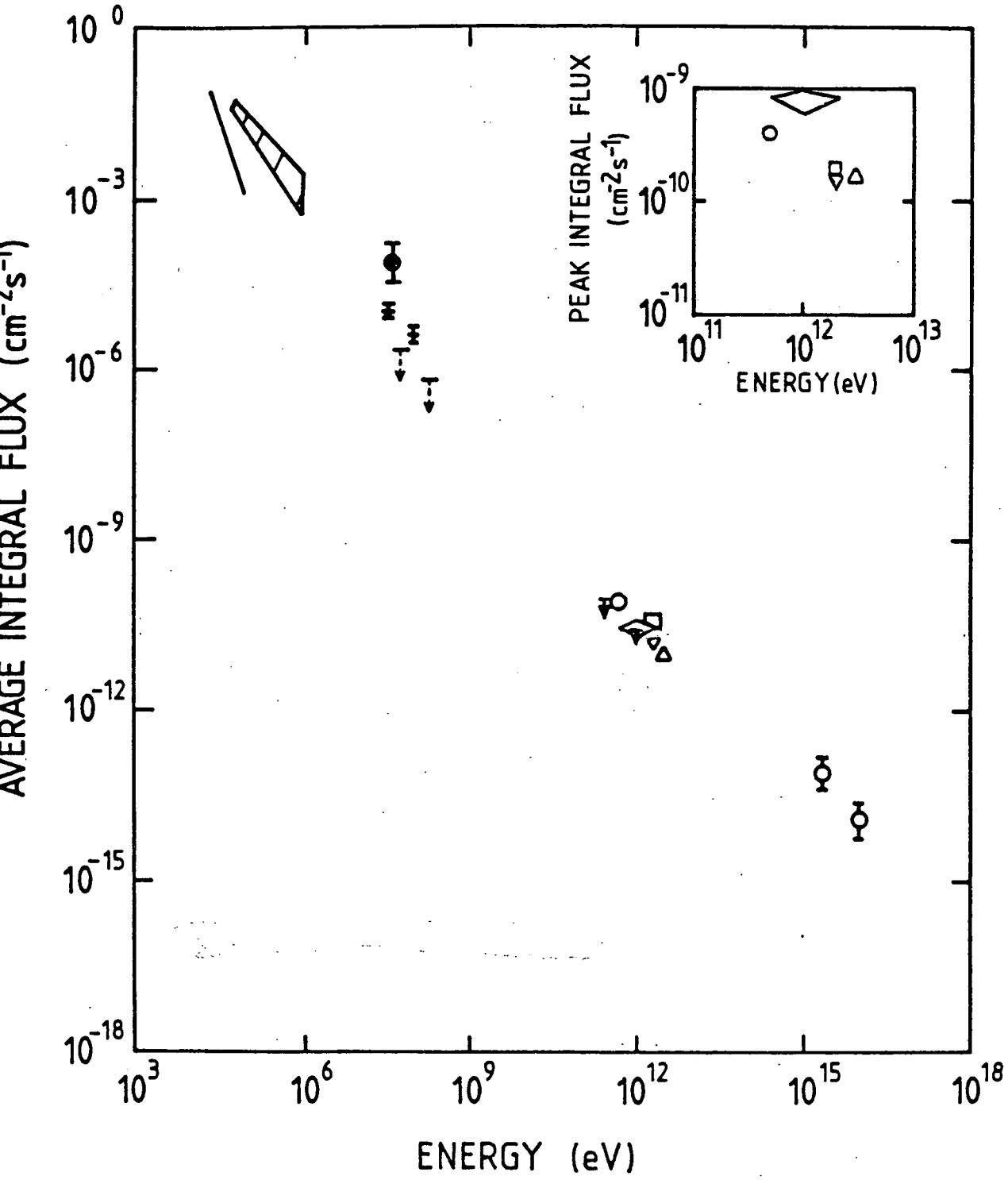
AVERAGE INTEGRAL FLUX (cm⁻²s⁻¹)
10 0
10⁻³
10⁻⁶
10⁻⁹
10⁻¹²
10⁻¹⁵
10⁻¹⁸
10³
10⁶
10⁹
10¹²
10¹⁵
10¹⁸
ENERGY (eV)
PEAK INTEGRAL FLUX (cm⁻²s⁻¹)
10⁻⁹
10⁻¹⁰
10⁻¹¹
10¹¹
10¹²
10¹³
ENERGY (eV)

the Cygnus X-3 1982 tracking data is that it necessarily assumes the emission to have a duration of 10 minutes and to be centred precisely at phase 0.625. If the emission occurs over a period not equal to 10 minutes, or is not centred on the assumed phase the flux value deduced by the method will be incorrect. We therefore decided to examine the 1982 tracking data (in which Cygnus X-3 had been kept in the centre of the field of view at all times) to investigate any structure in the emission at phase 0.625.

Summing the data from the 5 nights which individually showed a greater than 20% excess on the low energy channel, we obtain the count rate profile seen in Figure 6.7 for the 30 minutes about phase 0.625. The indication is that the emission does occur roughly within the 10 minute window about phase 0.625 but that individual outbursts tend to show structure on a timescale of only a few minutes. At times of such intense activity the gamma ray flux can amount to almost 50% of the cosmic ray background on the low energy channel, corresponding to an integral peak flux of about $5.0\ 10^{-9}$ cm^{-2} s^{-1} at E > 1000 GeV.

6.2d The 34.1 Day Periodicity

During the 1981/1982 seasons of observation of Cygnus X-3 a total of 28 acceptable passes at phase 0.625/0.655 were made with a low energy threshold telescope operating. Since an overall excess of 8.8% exists at this phase it is of interest to examine the individual excesses for evidence of any longer term variability of the object.

The most recent period suggested for the long term X-ray

Figure 6.7

The combined count rate profile of the 5 1982 tracking mode observations of Cygnus X-3 showing a greater than 20% excess at phase 0.625 of the 4.8 hour cycle

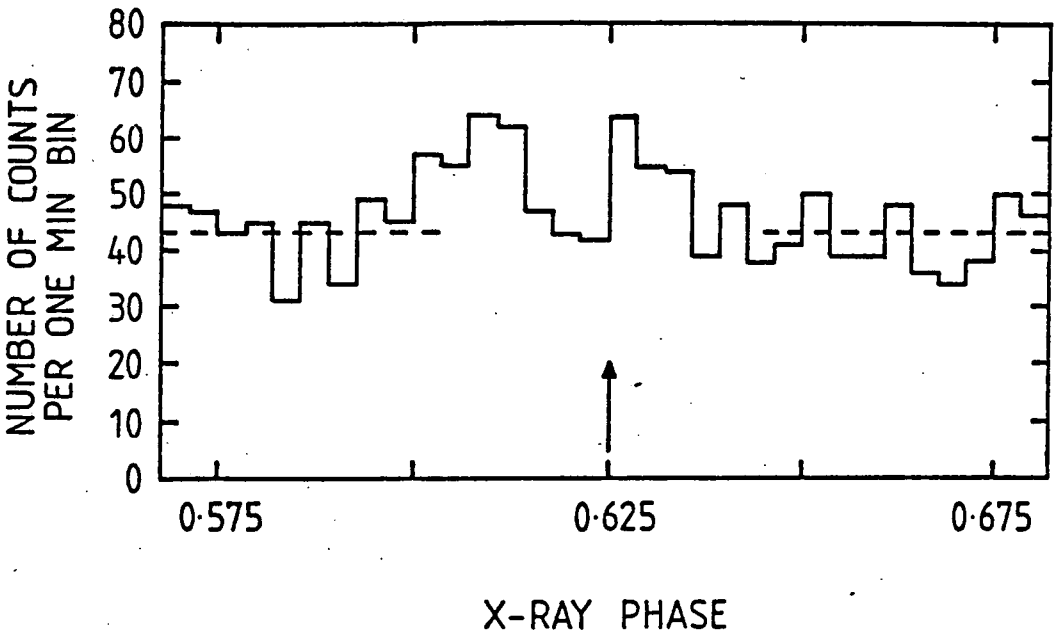
80
70
60
50
40
30
20
10
0
NUMBER OF COUNTS
PER ONE MIN BIN
0·575
0·625
0·675
X-RAY PHASE

variability of Cygnus X-3 is 34.1 days (Molteni et al., 1980). Defining zero phase to be the 34.1 day X-ray minimum (as deduced from the information given by Molteni), we have therefore assigned each individual scan an approximate 34.1 day phase ϕ_{34}, as is shown in Table 6.5. Plotting a scan's observed excess against its 34.1 day phase results in Figure 6.8 which suggests that the 8.8% overall emission may not occur continuously.

The X-ray maximum shown in Figure 6.8 has been carried forward from that given by Molteni for 1978 and is uncertain by about $\pm$ 0.16 in phase because of the quoted uncertainties in the exact period and absolute phase of the cycle.

In contrast a best-fit sine wave fitted to the gamma ray data :

$$\text{excess}(\%) = 11.\sin(\phi_{34} - 0.89) + 11$$

suggests that the gamma ray maximum occurs at about phase 0.14, and thus that if the X-ray and gamma ray cycles are to coincide a phase slippage from Molteni's ephemeris of at least 0.36 must have occurred since the time of the X-ray observations. Such a slippage is consistent with the true period of the modulation being about 33.8 $\pm$ 0.1 days, which does not conflict with Molteni's X-ray data recorded in 1977-1978. The mean flux of 11% indicated by the fit, when compared to the observed mean of 8.8%, suggests that on the whole our observations were made at slightly unfavourable 34 day phases. It is also suggested that at times the peak 0.625 phase output from Cygnus X-3 may fall to zero.

Date	Jul.Date	% Excess	ϕ_{34}
Aug 4 1981	2444821	22.1 ± 11.5	0.855
27	4844	0.8 ± 10.6	0.529
31	4848	14.2 ± 8.3	0.647
Sep 1	4849	5.7 ± 13.1	0.676
2	4850	14.3 ± 12.5	0.705
25	4873	40.9 ± 20.5	0.380
26	4874	5.7 ± 18.6	0.409
27	4875	16.2 ± 20.8	0.438
Oct 21	4899	17.0 ± 11.0	0.142
Jul 14 1982	5165	35.1 ± 20.1	0.943
16	5167	12.1 ± 18.2	0.001
17	5168	6.5 ± 19.7	0.031
18	5169	30.0 ± 19.4	0.060
20	5171	-8.2 ± 21.7	0.119
Aug 16	5198	20.1 ± 9.6	0.911
24	5206	30.1 ± 16.8	0.145
25	5207	3.5 ± 16.2	0.174
Oct 8	5251	13.5 ± 9.8	0.464
9	5252	6.7 ± 9.5	0.494
10	5253	7.7 ± 12.4	0.523
14	5257	9.0 ± 10.0	0.641
20	5263	7.7 ± 10.3	0.817
20	5263	20.0 ± 18.3	0.817
21	5264	0.4 ± 10.6	0.846
Nov 13	5287	9.9 ± 7.9	0.521
14	5288	1.5 ± 7.9	0.550
16	5290	-2.1 ± 7.2	0.609
19	5293	0.1 ± 6.5	0.696

Table 6.5

The 34.1 day phase ascribed to each 0.625/0.655 scan of Cygnus X-3

Figure 6.8

The % excesses in the 28 acceptable scans of Cygnus X-3 at phase 0.625 (for which the low energy channel was in operation), folded with the 34.1 day period suggested by Molteni et al. (1980)

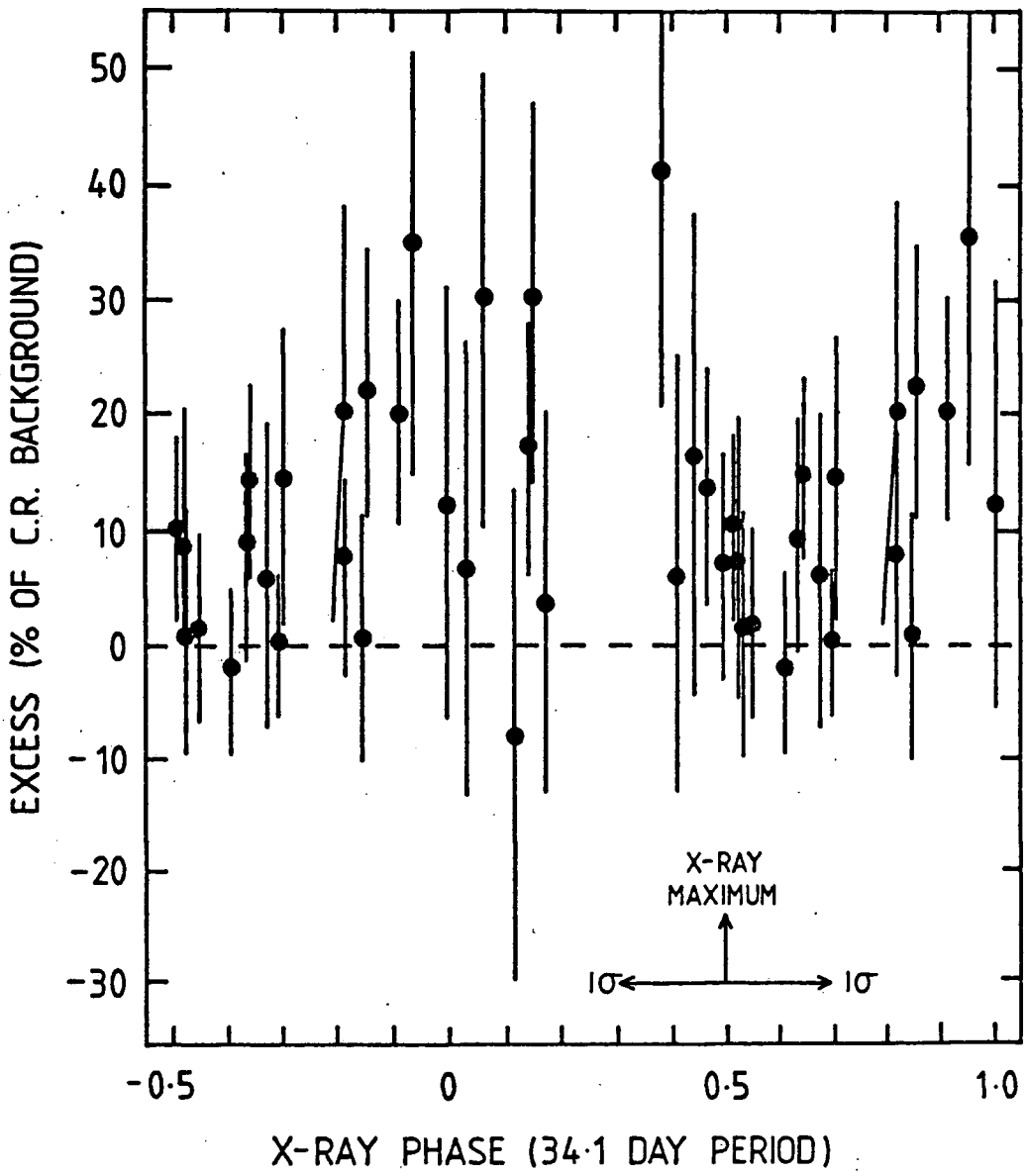
50
40
30
20
10
0
-10
-20
-30
EXCESS (% OF C.R. BACKGROUND)
X-RAY
MAXIMUM
1σ
1σ
-0·5
0
0·5
1·0
X-RAY PHASE (34·1 DAY PERIOD)

6.2e The Spectral Slope between 1000 and 3000 GeV

Consider the following independent ON/OFF ratios for the sum of all 28 acceptable scans made on Cygnus X-3 at phase 0.625/0.655 :

ON/OFF ratio (low energy channel) = 1.088 $\pm$ 0.022

ON/OFF ratio (all other events) = 0.988 $\pm$ 0.021

Clearly, the 4 standard deviation positive excess seen in the low energy channel does not reproduce at the higher energies. At first sight this would appear to indicate that the gamma ray spectrum from Cygnus X-3 at around 1000 GeV is much steeper than the spectrum of the cosmic ray proton background - which would not seem to be consistent with the recent claims of a positive detection of Cygnus X-3 at 10^{15} eV (Samorski and Stamm, 1983, and Lloyd-Evans et al., 1983) unless a dip exists in the spectrum just above 10^{12} eV. An alternative explanation is connected with the variation of the field of view of the array with the number of telescopes triggered by a shower. It is indicated from computer simulations of the response of the array (Macrae, private communication) that the aperture function of the array is significantly narrower for 2-telescope initiating showers than for those triggering only 1 telescope. While this effect makes 2-fold responses more interesting for observations in the tracking mode (see, for example, the Crab Pulsar results), it has the opposite effect for observations in the drift scan mode, since the object spends proportionally less of the total drift scan time in the

field of view. As a result the ON/OFF ratio (where 'ON' corresponds to a 10 minute interval) is greatly reduced. However, since much of the Cygnus X-3 data was taken in the tracking mode it is not clear to what extent this provides an explanation of the effect.

6.2f A Note on the Diffuse Galactic Gamma Radiation

Results obtained at Dugway in 1983 from drift scan observations of the galactic plane, made at the longitude of Cygnus X-3, suggested the presence of diffuse galactic gamma radiation at E > 1000 GeV with a peak strength, above the general background, of about 5% (Dowthwaite et al., 1985). In addition, the previously reported 'hole' from the direction of Cygnus X-3 (see, for example, Weekes et al., 1979, or Fomin et al., 1977) at 4.8 hour phases other than 0.625 was evident. Although the details of these results will be reported elswhere (Walmsley, Ph.d. thesis, in preparation) it became apparent that they may have implications for the interpretation of the 1981 Cygnus X-3 drift scan data, which precisely covered the region of the sky containing the hole.

In fact, if all the acceptable 1981 drift scans of Cygnus X-3 (excluding phases 0.625 and 0.125) are summed, the low energy channel shows a maximum likelihood deficit of events of 2.0% $\pm$ 1.6%. While not in itself significant, this effect correlates well with the 1983 results, and suggests several things :

(1) The general trend for points other than at phases 0.125 and 0.625/0.655 in Figure 6.2 to show slightly negative excesses was not coincidental.

(2) The peak 0.625 phase flux from Cygnus X-3 reported here may be slightly underestimated, and the significance level of the 1981 result may be greater than the 3.3 standard deviation value quoted. (3) The effect at phase 0.125/0.155 in Figure 6.2 may be significant at about the two standard deviation level.

6.2g Transient Bursts of emission from Cygnus X-3

Several groups have reported incidents of sporadic bursts of VHE gamma ray emission from Cygnus X-3 occuring usually at apparently random 4.8 hour phases and lasting for perhaps only a few minutes (see, for example, Weekes, 1982, or Neshpor et al., 1975). We have found several occurrences of similar effects in which the overall count rate increases by perhaps 25%, though all occurred during the 1981 tracking mode observations for which the AGC system had not been employed. This, combined with the fact that the effect often showed up on only one telescope caused us to have severe doubts about their origin and to surmise that they were possibly caused by rapid changes in the sky brightness (such as with a lightning strike) and/or electrical pickup in the equipment.

6.2h Search for Periodicity in the Cygnus X-3 Data

A search for periodicity, using the Rayleigh test described in Section 5.3f, has been conducted on the low energy channel events of the 10 minute ON-times of the 4 scans showing the strongest excesses at 4.8 hour phases 0.625 and 0.655. The test was made at each of the 6 10^5 independent trial periods between 1ms and 10s,

and thus a large number of degrees of freedom were expended. Since typical samples contained only about 100 events, with perhaps 20% possibly being pulsed gamma rays, any real periodicity could only show up at around the 10^{-3} level which, considering the number of trials, could not be considered statistically significant.

As yet, no conclusive evidence has been found to suggest that any particular period in the range specified has been repeatedly occurring at significant probability levels more often than would be expected. A full summary of this analysis will be reported separately (Dowthwaite, Ph.D. thesis, in preparation).

6.3 The Crab Pulsar, PSR 0531+21

6.3a The Search for Continuous Pulsed Emmision

Using the Crab Pulsar ephemeris for 1982 obtained from contemporary radio measurements at Jodrell Bank (Lyne, private communication), it was possible to assign an absolute phase to each event recorded by the array during the year. This was not possible for the data taken in 1981 since the ephemeris could not be extended back with sufficient accuracy.

As was discussed in Section 4.2b, the data taken in October 1982 was not found to be acceptable for analysis as the array had not been correctly tracking the object. In addition, the data taken in August and September 1982 was not able to be properly transformed to Coordinated Universal Time (UTC) as the clock slippage rate had not been constant during this period - so this data was also

rejected for this analysis.

After these stringent but necessary requirements had been met we were left with the month of November 1982 which contained 104994 events in about 70 hours of data, and constituted the majority of the data taken in the year. These observations consisted of 9 nights, each of about 7 hours duration, over a 10 day period during which time the clock had not been re-initialised. This is important as it rules out any uncertainty in the relative times of arrival of events in the data sample due to changes that may occur in the propagation delay of the WWV synchronisation signal. This data was analysed using an epoch folding technique, as discussed in Section 5.3f, to produce the light curve shown in Figure 6.9a, on which is marked the predicted position of the centre of the radio main and inter-pulses. For comparison, the average light curve over the period 1975-1980 for 50-3000 MeV gamma rays according to the COS-B experiment is shown in Figure 6.9b (Wills et al., 1982). From the results at 50 MeV there appear to be 3 regions of the light curve in which VHE gamma ray emission may possibly be observed :

(1) The 'main' pulse lying in the phase range 0.98 - 0.02.

(2) The 'interpulse' lying in the phase range 0.34 - 0.46.

(3) The 'bridging' region falling between the main and interpulses and covering the phase range 0.10 - 0.30.

The numbers of events falling in the above regions may be statistically compared (using the Maximum Likelihood test described in Section 5.2a) with the expected number, as derived from the phase range 0.50 - 0.94 for which no evidence of pulsed emission

Figure 6.9

The light curve of the Crab Pulsar

(a) As seen in this experiment at E > 1300 GeV
(b) As seen at 50-3000 MeV by the COS-B experiment (Wills et al., 1982)

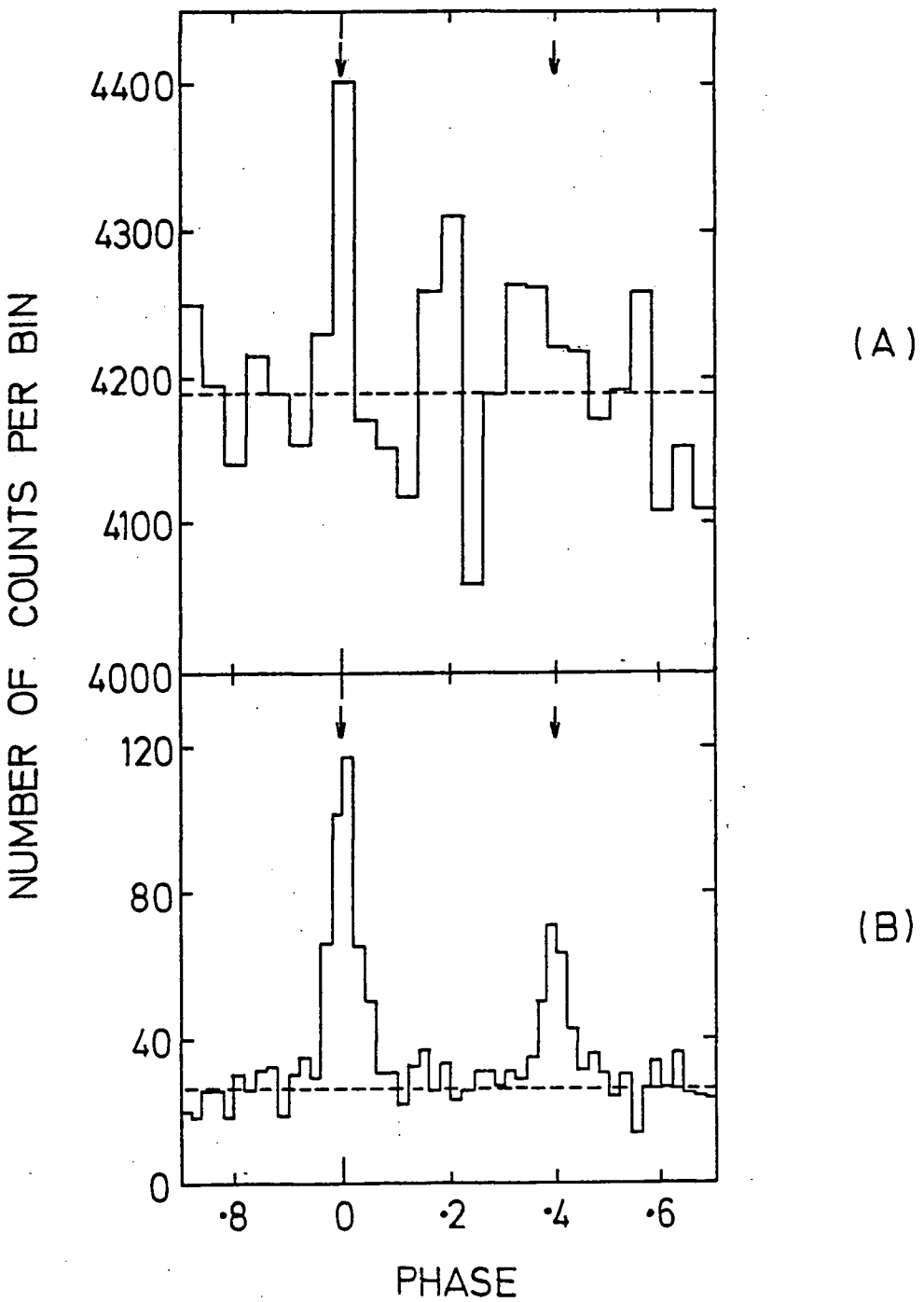
NUMBER OF COUNTS PER BIN
4400
4300
4200
4100
4000
120
80
40
0
·8
0
·2
·4
·6
PHASE
(A)
(B)

was found at 50 MeV. The results of this comparison are given in Table 6.6.

It can be seen that an excess of events exists at the position of the radio main pulse (number of events in main pulse bin 4402, expected number 4178.5 $\pm$ 68.8), having a strength of about 0.213 $\pm$ 0.066 % of the background level due to cosmic ray protons. The effect has a conservative probability of chance occurrence of about 6 10^{-4}, and constitutes an integral pulsed flux of about (1.3 $\pm$ 0.4) 10^{-11} cm^{-2} s^{-1} at E > 1300 GeV.

Positive excesses are also seen in both the interpulse and bridging regions of the light curve, though neither can be considered to be statistically significant. Certainly there is no strong evidence for the existence of a narrow interpulse at the expected position. The ratio of the apparent pulsed content in the interpulse to that in the main pulse is 0.73 $\pm$ 0.61, which is consistent with the values of about 0.4 seen by the COS-B group at 50 MeV energies since about 1977 (Wills et al., 1982).

It is of interest to examine the contents of the main pulse in Figure 6.9a for evidence of structure on a time scale shorter than the bin width (about 1.33 ms). Two further light curves were therefore formed having 100 and 250 bins - corresponding to bin widths of 0.33 and 0.13 ms respectively. These are shown in Figures 6.10b and 6.10c for the phase range 0.9 - 0.1, with Figure 6.10a being the corresponding section of the 25 bin light curve. It appears that the majority of the excess events contained in the main pulse of Figure 6.9a occur in the relatively narrow phase range between 0.98 - 0.992, which is slightly before the expected

Region	Phase Range	No.Events	Excess	Excess(%)
Background	0.50-0.94	45964	-	-
Main Pulse	0.98-0.02	4402	223.5± 68.8	0.213±0.066
Interpulse	0.34-0.46	12698	162.4±126.7	0.155±0.121
Bridge	0.10-0.30	20943	50.3±174.3	0.048±0.166

Table 6.6

A statistical comparison of the number of Cerenkov events falling in various regions of the Crab Pulsar light curve (obtained from observations in November 1982)

Figure 6.10

The light curve of the Crab Pulsar at
E > 1300 GeV between phases 0.9 - 0.1

(a) bin width 1.33 ms
(b) bin width 0.33 ms
(c) bin width 0.13 ms

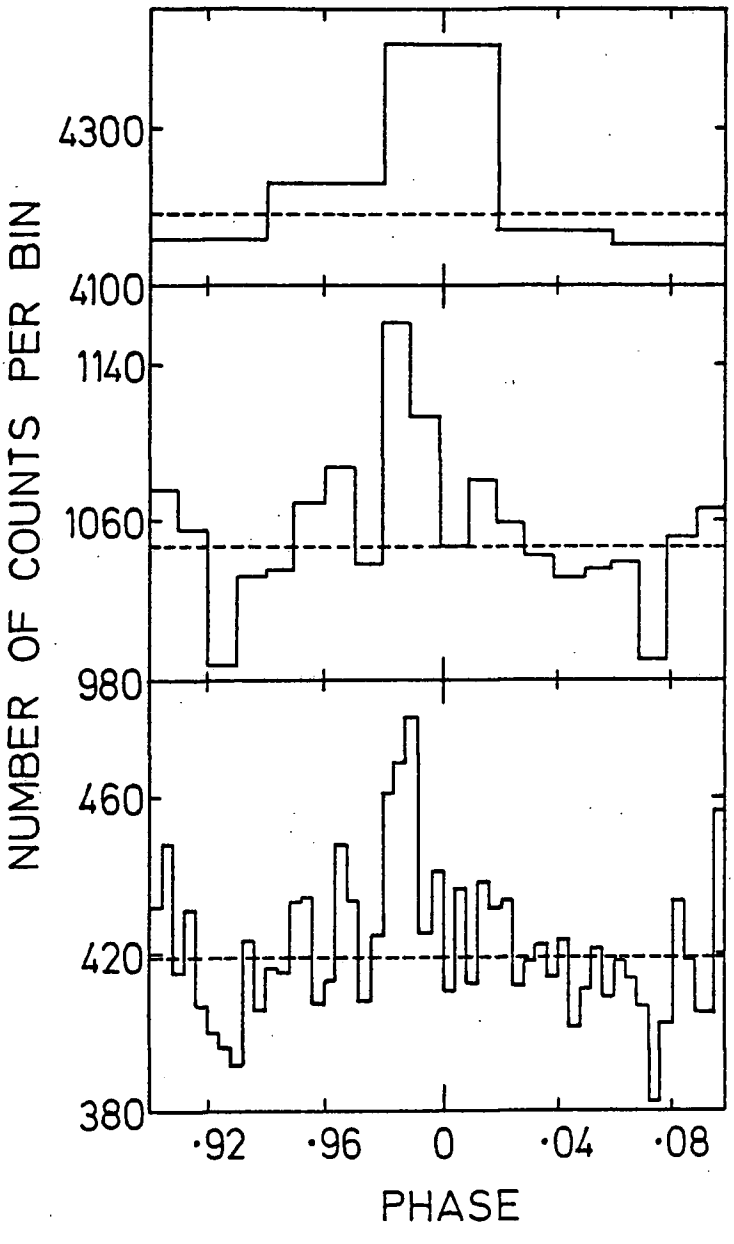
4300
4100
1140
1060
980
460
420
380
NUMBER OF COUNTS PER BIN
·92
·96
0
·04
·08
PHASE
(A)
(B)
(C)

radio main pulse position. Since the absolute timing uncertainty in the experiment was about $\pm$ 0.5 ms (inherent in all off-air timing systems) no significance can be drawn from this discrepency. The width of the main pulse in Figure 6.10c is about 0.4 ms, which is signficantly narrower than that seen at 50-3000 MeV. Furthermore, the estimated non-linearity of the oven-controlled crystal upon which the timing was based (about 5 10^{-10} s s^{-1} over the 10 days of the observation) could have the effect of smearing out a main pulse of even shorter duration to one having the duration observed. Thus a main pulse of duration $<$ 0.4 ms is not ruled out.

If this narrowing of the main pulse emission is confirmed it would appear to support the suggestion (McBreen et al., 1973) that a systematic reduction in the duration of the pulse occurs over the 4 decades of energy between 100 MeV and 1000 GeV.

It is of interest to investigate the individual light curves formed from the data taken on each of the nights for evidence of any variation in strength of the main pulse effect. The independent values for the excess at the main pulse (defined as the phase range 0.98-0.02) from each dataset are therefore shown in Figure 6.11, in which it is noted that a positive (but not necessarily significant) effect occurs on every night but one, ruling out the possibility that the whole of the effect arises, for example, from a single night's observation.

It has already been noted that the aperture function of the array appears to be narrower for those events initiating two-telescope responses than for those triggering only one

Figure 6.11

The % excess seen in the main pulse bin of the Crab Pulsar on individual nights in November 1982

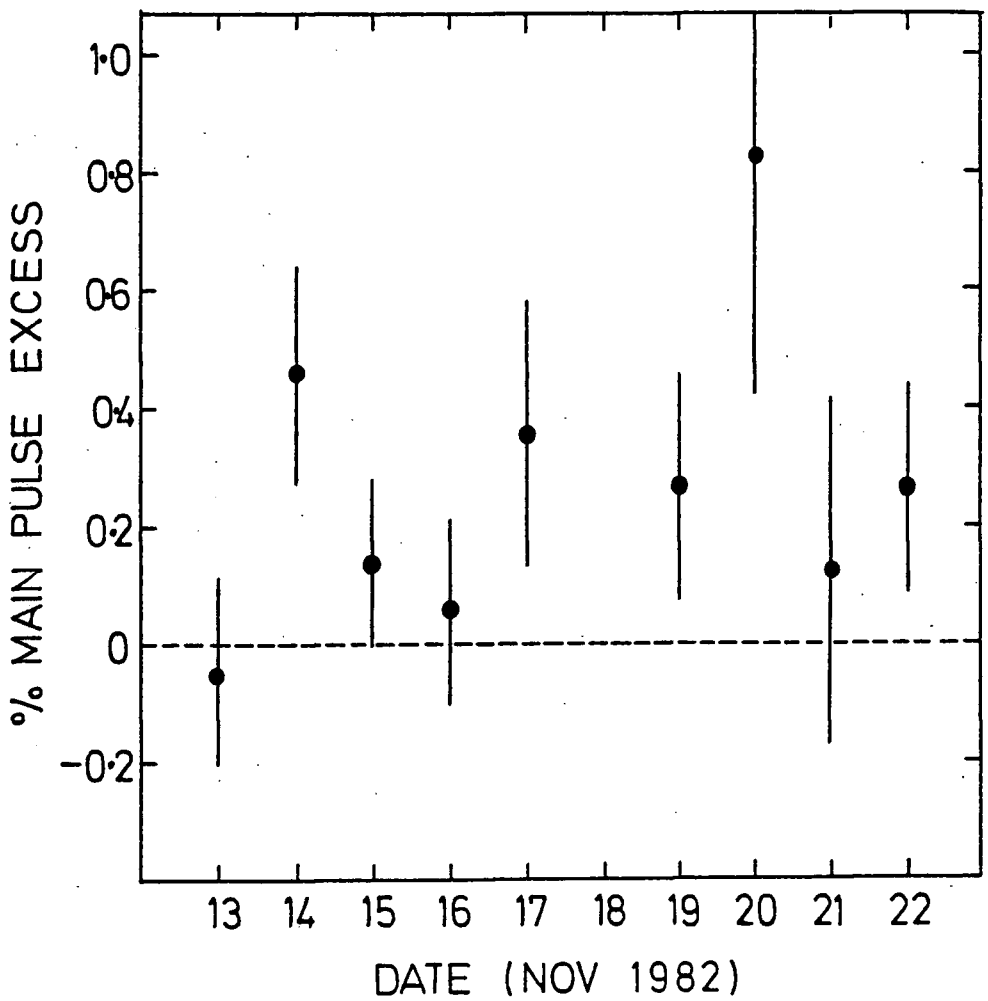
1·0
0·8
0·6
0·4
0·2
0
−0·2
% MAIN PULSE EXCESS
13
14
15
16
17
18
19
20
21
22
DATE (NOV 1982)

telescope. We therefore expect that the twofold responses will be proportionally richer in on-axis gamma ray candidates and will contain less off-axis background. To test this supposition we therefore formed the 2 independent light curves, shown in Figures 6.12a and 6.12b, consisting of one and twofold events respectively. The percentage pulsed component in the main pulse, while evident in both datasets, is seen to be a factor of 1.7 $\pm$ 1.0 higher in the data of Figure 6.12b than for those of Figure 6.12a. This indicates that the excess events have arisen preferentially from near the centre of the field of view, and thus from the direction of the pulsar. In connection with this an analysis of the deduced arrival directions of the 2 and 3-telescope initiating showers falling in the main pulse bin has been made and will be reported seperately (Walmsley, Ph.D. thesis, in preparation).

Considering the source to emit isotropically it can be shown, using the equations given in Section 5.5, that the time-averaged luminosity occurring in the main pulse above 1300 GeV is (4.7 $\pm$ 1.5) 10^{34} ergs s^{-1}, assuming a distance to the source of 2 Kpc and an integral spectral slope of -1.4. The spectrum of PSR 0531 in the range 1 - 10^4 GeV, shown in Figure 6.13, will be described further in Section 6.3d.

6.3b The Search for Transient Pulsed emission

In addition to the search for continous periodic pulsed emission from the Crab Pulsar the data taken in 1981 and August, September and November 1982 were analysed for evidence of any transient pulsed phenonema. Each night's data was arbitrarily split into

Figure 6.12

The light curve of the Crab Pulsar seen in the present experiment

(a) single telescope responses
(b) double telescope responses

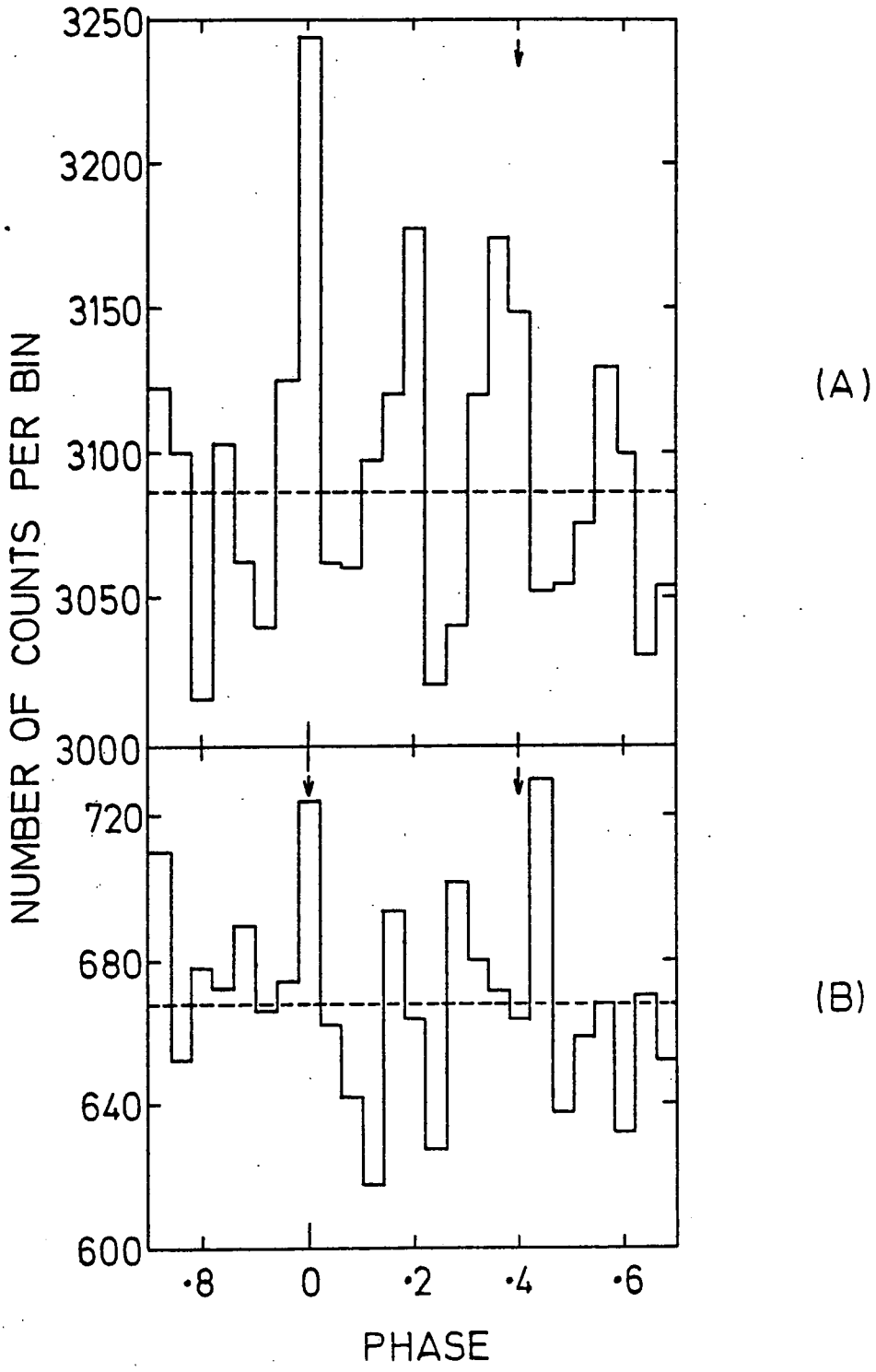
3250
3200
3150
3100
3050
3000
720
680
640
600
NUMBER OF COUNTS PER BIN
·8
0
·2
·4
·6
PHASE
(A)
(B)

Figure 6.13

The spectrum of pulsed emission from the Crab Pulsar over the range 1 - 10^4 GeV

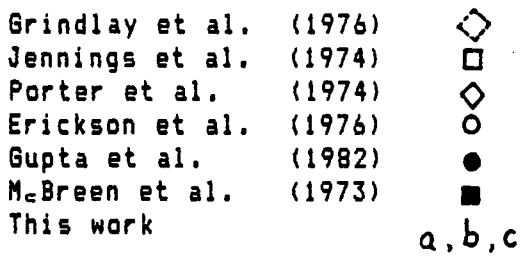

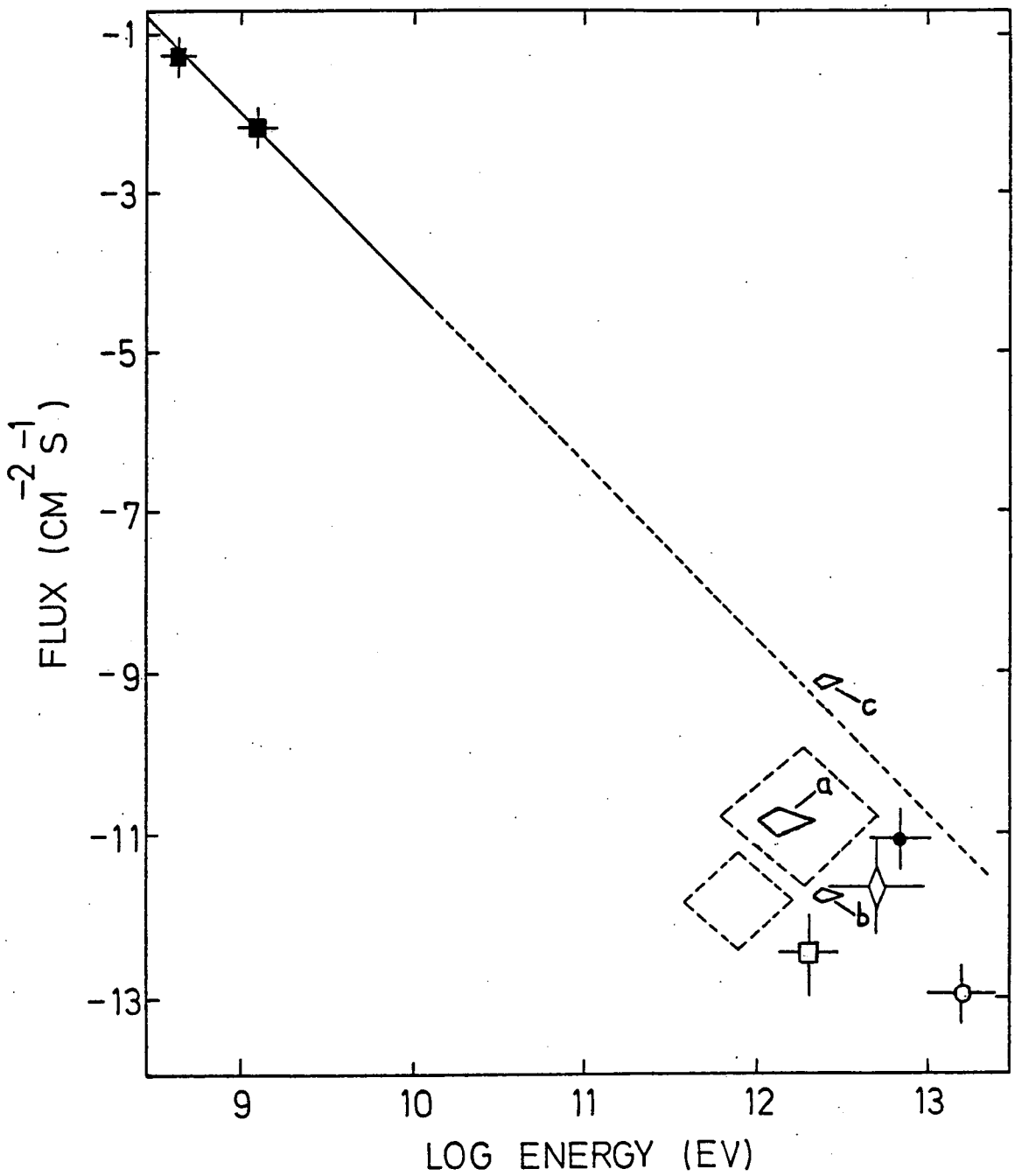
-1
-3
-5
-7
-9
-11
-13
FLUX (CM^{-2} S^{-1})
9
10
11
12
13
LOG ENERGY (EV)
a
b
c

independent data sections containing 200 events; this being a reasonable number required to detect a pulsed component of about 15% at about the 1% chance probability level. The data sections were then unfolded separately with the appropriate barycentre period and tested for evidence of non-uniformity in phase using the Rayleigh Test discussed in Section 5.3f.

We found one example of a data section having a significantly low chance probability of $< 10^{-4}$, which occurred on October 23 1981 at 0920 UT. To determine the exact position and duration of this apparent burst of periodic emission 2 further steps were taken:

(1) The number of events in a data section was relaxed in steps of 20, both downwards to 100 and upwards to 300.

(2) The data section was slid through each night in increments of 10%.

It was found that the burst on October 23 gave the lowest chance probability value when a section of 160 events was used, this corresponding to a time duration of about 15 minutes. Figure 6.14 shows the probability of lack of periodicity (assuming only 1 degree of freedom) in non-independent 160 event data sections on this night. It can be seen that in a 15 minute sample near the end of the night 34% $\pm$ 5% of the events were pulsed at the Crab Pulsar period, giving rise to a probability of lack of periodicity for the sample of about $9\ 10^{-9}$.

An upper limit to the number of degrees of freedom expended in the search is given by the total number of non-independent data sections tested in the course of the analysis. The number of independent data sections was about 700; if we increase this by a

Figure 6.14

The probability of lack of periodicity existing in non-independent 160 event data sections from the Crab Pulsar on October 23 1981

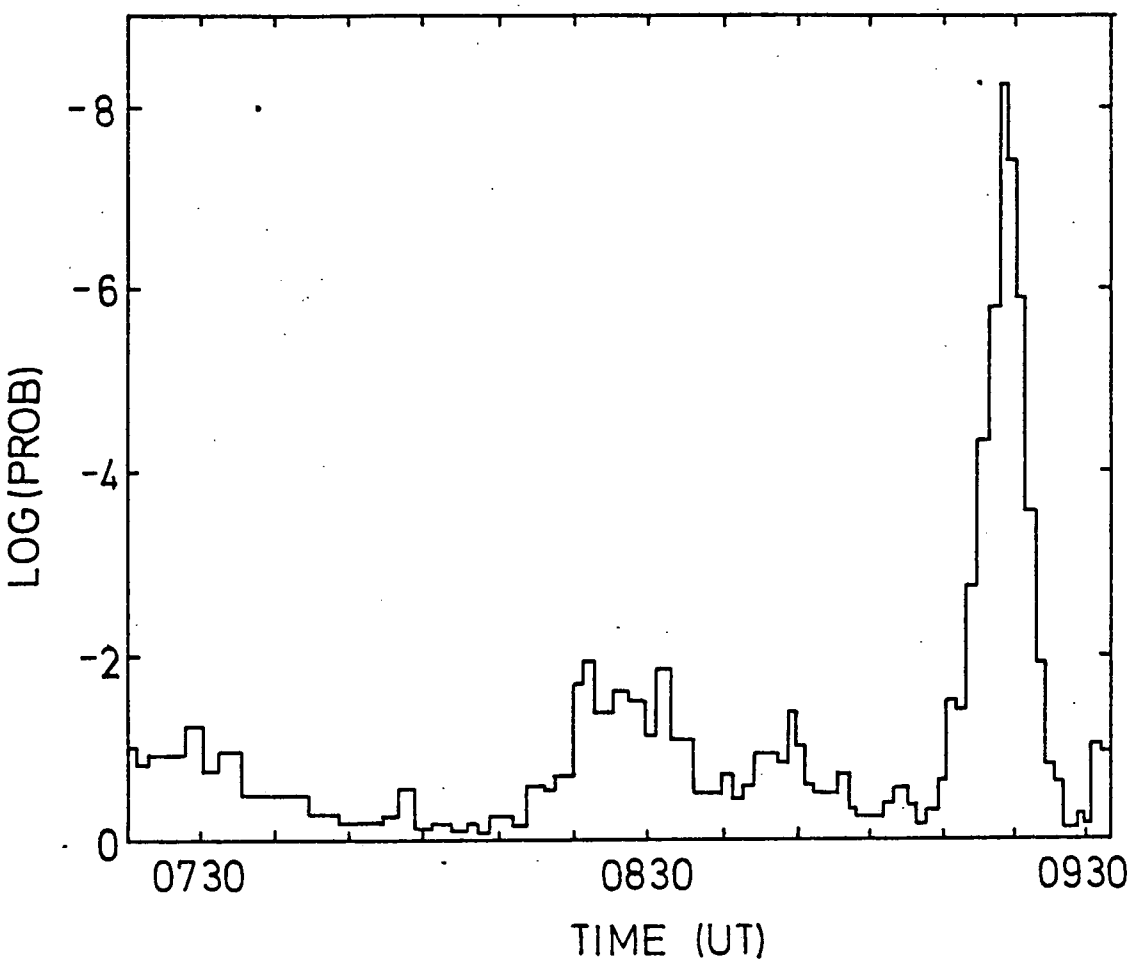
-8
-6
-4
-2
0
LOG(PROB)
0730
0830
0930
TIME (UT)

factor of 10 for using 10 different widths of data section, and a further factor of 10 for sliding the data sections in increments of 10%, the maximum possible number of degrees of freedom becomes 7 10^4. Thus, a conservative estimate of the overall chance probability of finding such a highly periodic data section is about 6 10^{-4}.

Other examples of transient effects showing similar properties to the October 23 1981 event were found throughout the whole of 1981 and 1982 data, though when the degrees of freedom were taken into account none were found to have a significantly small chance probability of occurrence. It is possible, however, that the strong transient reported here was not an isolated occurrence but an unusually strong example of an event normally below the detection threshold of the equipment.

Let us now examine the properties of the October 23 1981 burst in more detail.

6.3c Detailed Analysis of the Transient Event

The light curve for the events occuring during the burst period, illustrated in Figure 6.15, showed a single pulse of FWHM 6ms, rising to a maximum over a period of about 10 ms, and falling to zero again within about 3 ms.

Figures 6.16a and 6.16b show the two independent light curves derived from I-fold and II-fold initiating showers respectively occurring in the burst interval. It is seen that the periodic events showed the same characteristic increase in the proportion of II-fold responses as was observed with the continuous main pulse

Figure 6.15

The light curve of all events recorded by the array during the periodic outburst of October 23 1981

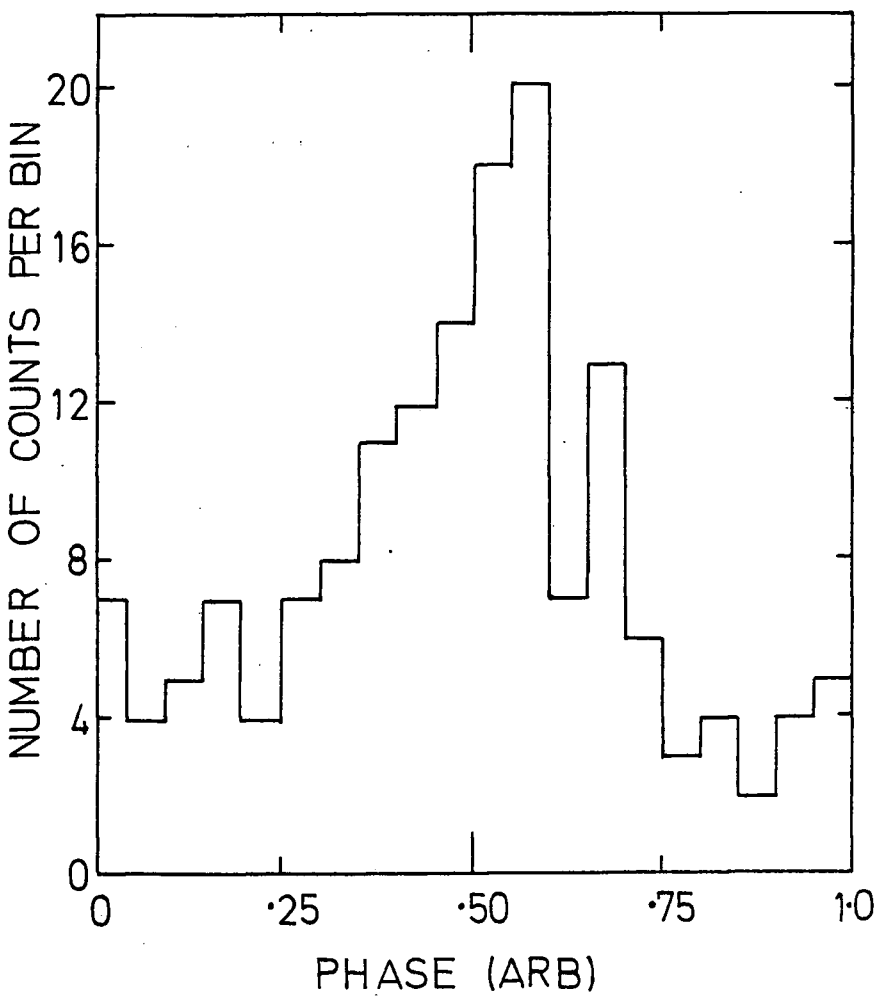
NUMBER OF COUNTS PER BIN
20
16
12
8
4
0
0
·25
·50
·75
1·0
PHASE (ARB)

Figure 6.16

The light curve of events recorded during the periodic outburst of October 23 1981 for

(a) single telescope responses
(b) double telescope responses

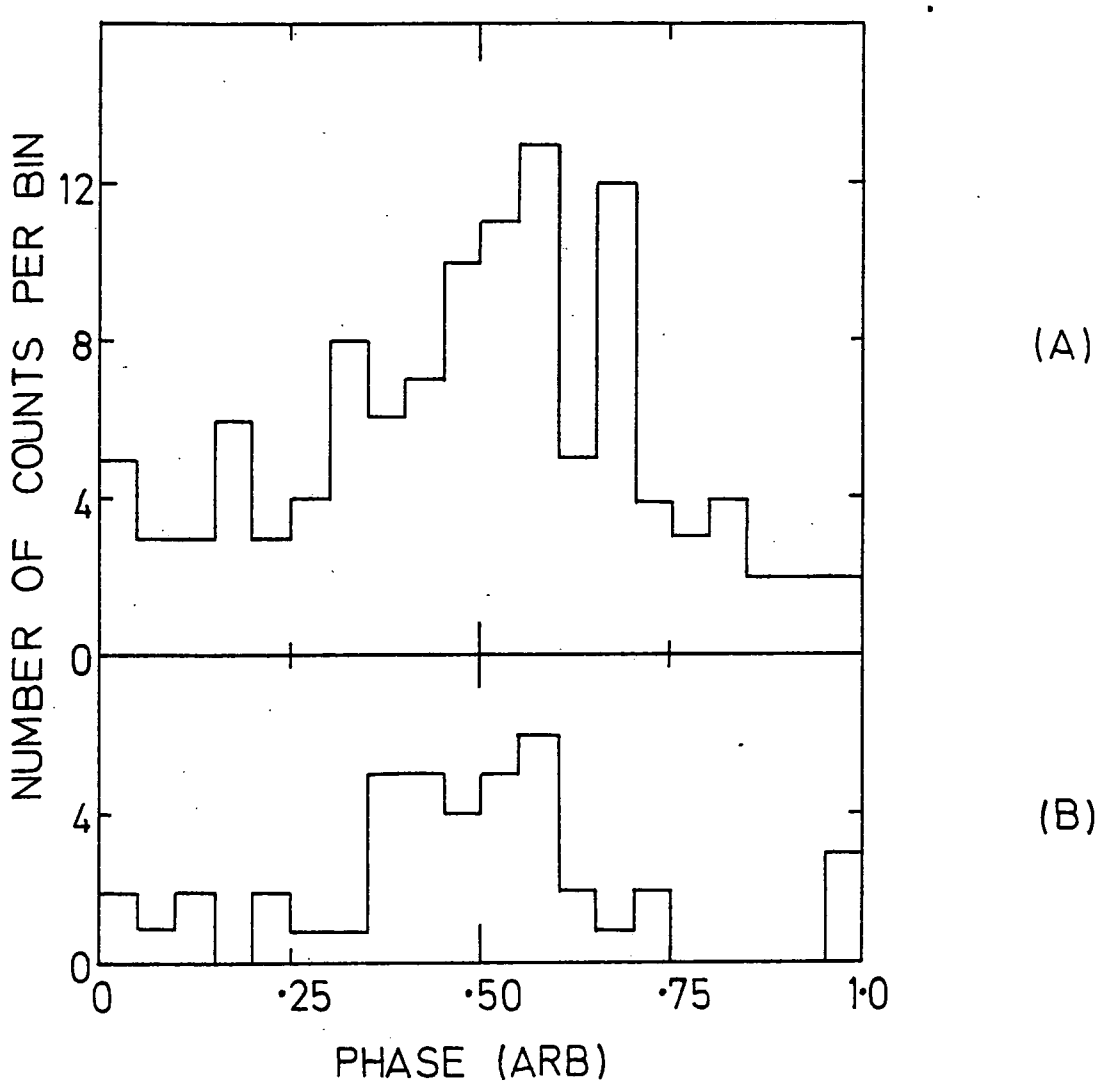
NUMBER OF COUNTS PER BIN
12
8
4
0
4
0
0
·25
·50
·75
1·0
PHASE (ARB)
(A)
(B)

emission; a pulsed component of about 33% for I-folds and about 44% for II-folds. Once again, this is seen as evidence for the periodic events arising preferentially from the source direction.

As has been pointed out earlier, absolute phase was not available for the measurements made in 1981; we could not therefore relate the phase of the burst with that of the sharp peak characteristic of the continuous emmision.

The presence of a 34% pulsed flux would be expected to show up on the overall count rate, the lack of AGC notwithstanding. In fact, the total number of showers recorded during the burst is higher, by about 18% $\pm$ 7%, than the number predicted from similar periods immediately before and after the event.

The housekeeping records, taken every minute during a run, were closely examined and gave no indication for any unusual behaviour of the atmospheric temperature, atmospheric pressure, phototube anode currents (related to sky brightness), or individual phototube counting rates for the period of activity.

At the peak of the outburst of October 23 1981 34% $\pm$ 5% of the events recorded by the array were periodic, corresponding to an integral pulsed flux of about $(8.7 \pm 1.2)\ 10^{-10}$ cm^{-2} s^{-1}, for a gamma ray threshold energy, estimated from the count rate of the array at the time of the outburst, of about 2400 GeV. Taking this event to be the only genuine pulsed gamma ray burst detected in the course of the 1981 and 1982 seasons of observations we arrive at a time-averaged pulsed flux, for emission in the form of short outbursts, of about $(1.7 \pm 0.2)\ 10^{-12}$ cm^{-2} s^{-1} at E $>$ 2400 GeV, for the period September 25 1981 - November 23 1982.

6.3d The Energy Spectrum of the Crab Pulsar

The integral energy spectrum over the range 1 - 10^4 GeV is shown in Figure 6.13. Shown on the figure are all previously quoted fluxes (Grindlay et al., 1976; Jennings et al., 1974; Porter et al., 1974; Erickson et al., 1976; Gupta et al., 1982; Mcbreen et al., 1973); previously quoted limits are not given. The present results are represented by three data points :

A : The continuous pulsed flux present in the main pulse at E > 1300 GeV.

B : The time averaged pulsed flux at E > 2400 GeV emitted in the form of a single transient event.

C : The pulsed flux at E > 2400 GeV at the peak of intensity of the October 23 1981 gamma ray transient.

Further discussion of this figure will be given in Chapter 7.

Chapter Seven

Conclusions and Suggestions for Future Work

7.1 Discussion of Results

7.1a Cygnus X-3

The results of the 1981 and 1982 seasons of observation of Cygnus X-3 can be summarised as follows :

(1) At the 4.1 SD chance probability level the object appears to show a 4.8 hour amplitude modulation of its gamma ray emission above 1000 GeV. The peak of the emission occurs at around phase 0.625 - in broad agreement both with the results at X-ray energies and other results at VHE gamma ray energies.

(2) The indication is that the individual outbursts of emission at phase 0.625 last for only a few minutes - in contrast to results at X-ray energies.

(3) The average integral flux at phase 0.625 comprises about 8.8 $\pm$ 2.1% of the cosmic ray background at E > 1000 GeV, corresponding to an integral photon flux of about (8.76 $\pm$ 2.13) 10^{-10} cm^{-2} s^{-1} and an average peak luminosity, assuming the source to emit isotropically at a distance of 10 Kpc and to have a differential spectral slope of -2.2, of (1.01 $\pm$ 0.23) 10^{38} ergs s^{-1}.

(4) The variation of the individual excesses seen at around phase 0.625 seems to support the existence of a further 34 day amplitude modulation of the object's emission. The peak emission, at the maximum of both cycles, is about 5 $10^{-9}$$cm^{-2}$ s^{-1} at E > 1000 GeV, which corresponds to a peak power output in excess of 5 10^{38} ergs s^{-1}.

(5) The mean fluxes quoted are in reasonable agreement with past results at similar energies, as shown in Figure 6.6.

The relative variation of the mean and peak flux values shown at around 1000 GeV arises because different groups have made differing estimates of the duration of the activity at around phase 0.625.

The detection of VHE gamma rays from Cygnus X-3 at the 4.1 SD level is seen not only as important confirmation of past results, but also as a useful validation of the sensitivity of the Dugway array. The production of evidence supporting the previously reported 34 day amplitude modulation (Molteni et al., 1980) shows a link between observations taken more than 7 decades apart in energy, and suggests that other objects may be found to show similar properties at VHE gamma ray and X-ray wavelengths. However, the sharpness of the emission at phase 0.625 of the 4.8 hour cycle, when compared to the near sinusoidal curve seen in X-rays (Elsner, et al., 1980), emphasises the possible fundamental difference in production mechanisms at the two energies.

Most of the models put forward to explain the observed properties of the Cygnus X-3 system incorporate a fast pulsar as the primary energy source. A recent example of such is that suggested by Vestrand and Eichler (1982) - illustrated schematically in Figure 7.1. According to this model Cygnus X-3 is composed of a fast pulsar in a 4.8 hour binary orbit with a stellar companion. The pulsar, it is supposed, emits a beam of very high energy cosmic ray particles which strikes the atmosphere of the companion star and, by a π° production process (see Section 1.3) or a thin bremsstrahlung process, causes the emission of VHE gamma rays. The observer would be expected to see this emission at two

Figure 7.1

A model for the Cygnus X-3 system,
according to Vestrand and Eichler (1982)

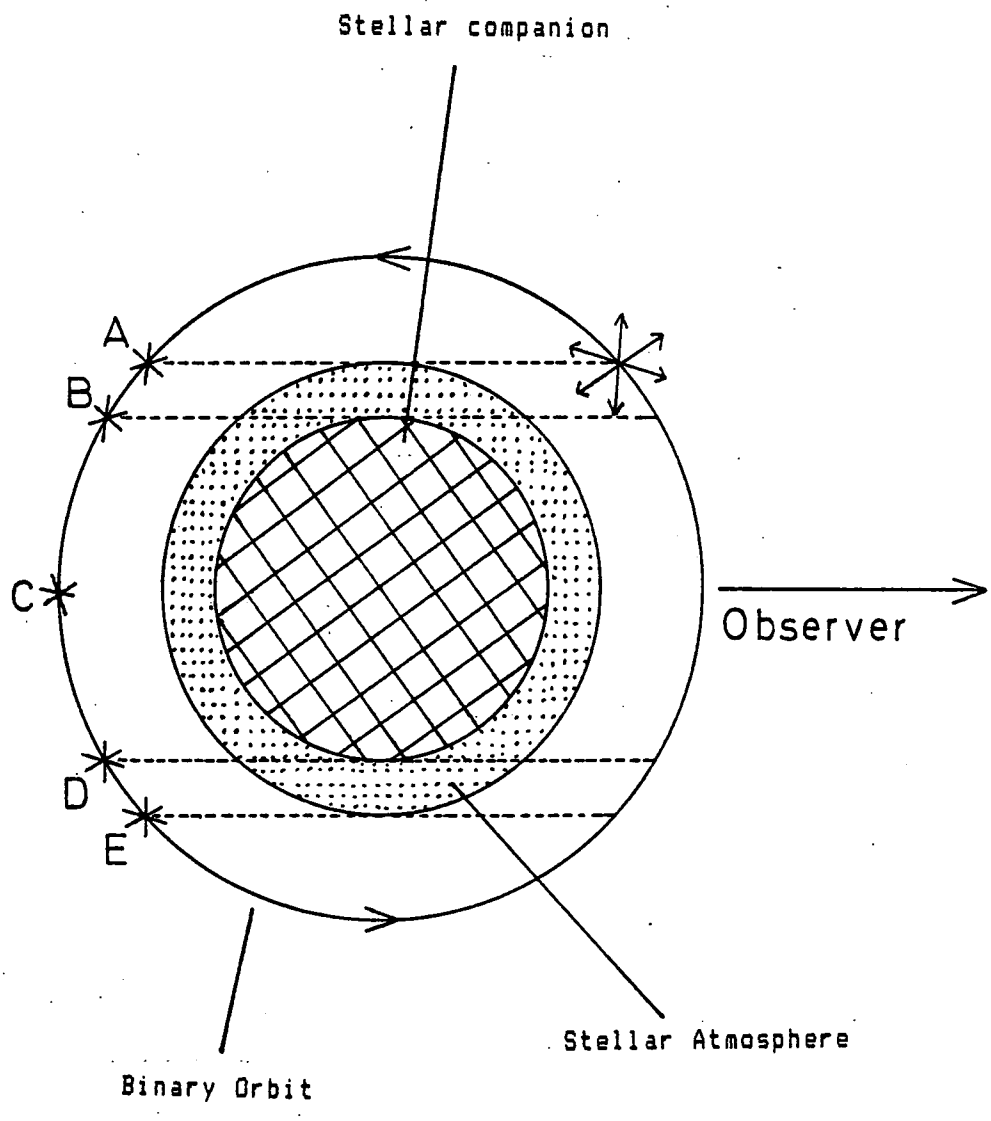
Stellar companion
A
B
C
D
E
Observer
Stellar Atmosphere
Binary Orbit

phases in the orbit of the pulsar; between points A and B, and points D and E. According to the authors the width of these pulses could easily be as short as the 0.05 of a cycle (corresponding to a duration of about 10-15 mins) reported by most observers at 1000 GeV. This, however, has been called into question by Grindlay (1982) who suggests that the cosmic ray beam may not be sufficiently well collimated, due to the scattering process (known as Alfven scattering) which affects energetic charged particles travelling through a region containing magnetic fields embedded in a partially ionised plasma (see, for example, Longair, 1981, page 333) as to produce such sharp features. In addition, other evidence (Elsner, 1980) suggests that the companion may be a helium star having too thin an atmosphere to support the model. A similar type of model has been presented by Hillas (1984) who claims that a mono-energetic beam of 10^{17} eV protons, emitted by the pulsar and causing an electron-photon cascade in the atmosphere of the stellar companion, could account for all emissions from the object above energies of about 1 GeV - including the recently reported emission at $E > 10^{15}$ eV (Samorski and Stamm, 1983, and Lloyd-Evans, et al., 1983). It is not clear, however, to what extent the model is able to explain the (unconfirmed) existence of the 34 day amplitude modulation of the X-ray and VHE gamma ray signal, nor the lack of detection of periodicity on a ms timescale in the X-ray data.

It has been suggested by Grindlay (1982) that since the X-ray properties of Cygnus X-3 have much in common with other low mass X-ray binaries the system may be powered by a matter accretion process. The model proposed, the geometry of which is illustrated

in Figure 7.2, is based upon that put forward to explain the properties of SS433, and involves a compact object (which may be a black hole) in a 4.8 hour orbit about a stellar companion. The spin axis of the companion star is supposed to be misaligned with the axis of the orbit, and to precess about it with a period of about 34 days. Accretion of matter from the companion star onto the compact object occurs giving rise to optical and X-ray photons which in turn, through the inverse Compton process with relativistic electrons (presumed to be generated in flares during episodes of enhanced mass transfer), give rise to VHE gamma rays. Enhanced accretion is expected to occur twice per orbit when the compact object crosses the line of nodes between the plane of the orbit and the equatorial plane of the companion star. The gamma ray emission in the direction of the observer would be further modulated with the precessional period of the companion as the relative orientation of the line of nodes changes and the apparent projected area of the accretion disk varies. Once again problems appear to exist with the model. For instance, it is not clear to what extent the observed emission at 10^{15} eV is explained.

While many of the properties of this enigmatic object have been well studied, it is clear that much work still needs to be done, at all wavelengths, before a full understanding can be achieved. Perhaps the most important breakthrough would be the discovery of a millisecond periodicity indicating the presence of a pulsar in the system. Since the object emits most of its energy at VHE gamma ray wavelengths this is a task for which workers in this field, for once, are perhaps at an advantage.

Figure 7.2

A model for the Cygnus X-3 system,
suggested by Grindlay (1982)

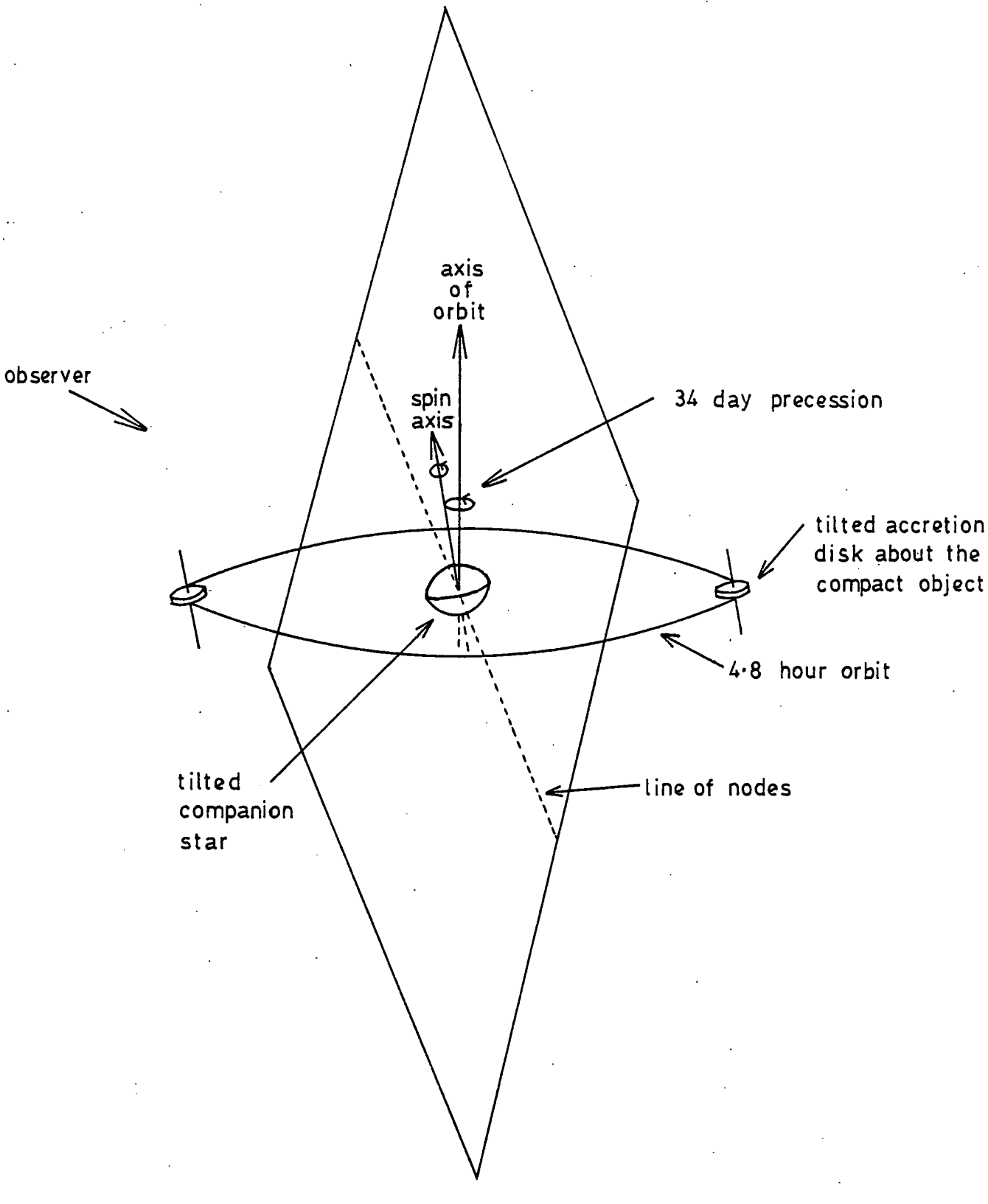
axis
of
orbit
observer
spin
axis
34 day precession
tilted accretion
disk about the
compact object
4·8 hour orbit
tilted
companion
star
line of nodes

7.1b The Crab Pulsar

The results of the 1981 and 1982 seasons of observations of PSR 0531 can be summarised as follows :

(1) The observations in November 1982 have provided evidence, significant at the 6 10^{-4} chance probability level, that the object emits continuous periodic emission, with the light curve having a narrow main pulse coincident with that seen at other wavelengths.

(2) The excess of events in the the main pulse constitute about (0.21 $\pm$ 0.06) % of the cosmic ray background, corresponding to an integral pulsed flux of about (1.3 $\pm$ 0.4) 10^{-11} cm^{-2} s^{-1} at E > 1300 GeV. The deduced luminosity of the object in the main pulse, assuming a distance of 2 Kpc and a differential spectral slope of -2.4, is about (4.7 $\pm$ 1.5) 10^{34} ergs s^{-1}.

(3) The duration of the main pulse activity can be shown to be < 0.4 ms, apparently confirming the previous suggestion (McBreen et al., 1973) that a gradual narrowing of the pulse may occur between the energies 100 MeV and 1000 GeV.

(4) A positive excess is also found at the expected position of the interpulse - though not at a significant chance probability level. The ratio of the apparent signal in the interpulse region to that in the main pulse (0.73 $\pm$ 0.61), however, is consistent with the more recent values found at 50 - 3000 MeV by the COS-B group (Wills et al., 1982).

(5) In addition to the continuous pulsed emission a strong pulsed transient was detected at 0920 UTC on October 23 1981. The

probability of chance occurrence of such an outburst in the total 1981 and 1982 data sample, after correction for the maximum possible number of degrees of freedom expended in searching for the effect, was $< 10^{-3}$. At the peak of the outburst gamma rays made up 34% of all Cerenkov showers detected and constituted a peak integral pulsed flux of $(8.7 \pm 1.2)\ 10^{-10}$ cm^{-2} s^{-1} at $E > 2400$ GeV, corresponding to a peak power output of about $(5.7 \pm 0.8)\ 10^{36}$ ergs s^{-1}, assuming a differential gamma ray spectral slope of -2.4 above 2400 GeV, and a distance of 2 Kpc.

(6) The approximate duration of the pulsed outburst, at a flux level strong enough to be detected, was about 15 minutes. During this time an overall count rate excess of 18% $\pm$ 7% was found to have occurred. The periodic events constituting the burst showed a rather broad single peaked light curve of width 6 ms, with a slowly rising front edge followed by a much sharper back edge. The absolute phase of the outburst, in relation to the main pulse, could not be determined since a suitable ephemeris for 1981 was not available.

(7) The events constituting both the transient and the continuous pulsed emission were found to contain a larger proportion of II-fold telescope responses than would be expected. This would indicate that in both cases the excess of events (the gamma ray candidates) arose preferentially from near the centre of the field of view of the system.

The energy spectrum of the Crab Pulsar between 1 - 10^4 GeV is shown in Figure 6.13; the various points given on the figure have

been described in Section 6.3d. It is clear from the figure that the majority of the emission at E > 1300 GeV occurs in the form of the continuous main pulse flux. Although the peak strength of the reported transient is several orders of magnitude greater than the time-averaged main pulse flux, outbursts of such intensity appear to occur only relatively rarely. The existing view that the spectrum must steepen in the region between the balloon-borne gas Cerenkov detector results (below 10 GeV) and those from ground based atmospheric Cerenkov experiments is confirmed. The presence of this 'break' in the spectrum implies that the object emits only about 10^{-4} of its total luminosity at energies above about 1000 GeV - in strong contrast to Cygnus X-3 where the energy carried by VHE gamma rays is dominant.

As noted by Grindlay (1982), it may be expected that the VHE gamma ray-optical photon interaction (see Section 1.4b) would cause the angular separation of the VHE gamma ray and radio/optical beams to be small - since the interaction cross-section would be at a minimum for parallel beams. This has the consequence that the VHE gamma ray emission, if occurring at the same phase as the optical peak, should have much the same shape. The present result, with the characteristic narrow peak in phase with the radio main pulse, supports this idea of close coupling between the VHE gamma ray and radio/optical emissions. Since pair-production absorption (see Section 1.4c) limits the emission of VHE gamma rays to regions at or very close to the distance of the light cylinder it is suggested (Ruderman, 1981) that this also is where the radio emission must originate from.

The observations reported above were the first for which an independent and contemporary radio ephemeris was available. It appears that unless such an accurate ephemeris can be used the weak periodic fluxes reported in this work would probably not be detectable. The indication is that the Crab Pulsar is a good 'standard candle' in the VHE gamma ray field, and that provided good timekeeping is kept there should be little difficulty in reproducing the present results.

7.2 Suggestions for Future Work

One thing that has become increasingly obvious from both this and other works is that sources of VHE gamma rays may show a high level of variability. Three of the four detected sources seem to show sporadic, unpredictable activity, while Cygnus X-3 is thought possibly to emit occasional intense outbursts at apparently random 4.8 hour phases. Given that there may be more, as yet undiscovered, sources of VHE gamma rays showing much the same behaviour, it is important to consider the form that future observations should take in order to have the best chance of detecting them. At present energy thresholds (with the correspondingly low counting rates) many hours of observation are necessary to detect even the 2 strong sources Cygnus X-3 and the Crab Pulsar. It is clear that a general search of the sky for new, highly variable, sources with the type of system currently used would not be productive. It is suggested that for future observations a much lower energy threshold telescope, which can

simultaneously monitor a large area of the sky, would be necessary.

Given the accepted performance of modern phototubes the energy threshold of a ground based VHE gamma ray telescope is essentially dependent upon its mirror collecting area; the larger the mirror area the lower the telescope's energy threshold. Apart from the multiple mirror system in use at JPL all gamma ray observatories have been dependent upon surplus searchlight mirrors, which are now in very short supply. It would be most advantageous to be able to construct mirrors of sufficient size and reflectivity, and of low enough cost, as to remove these supply obstacles to constructing telescopes with larger collecting areas. In pursuit of this a programme of mirror fabrication is currently being carried out at the University of Durham. Assuming that the problems connected with producing custom built mirrors can be overcome, telescopes with counting rates of several hundred counts per minute (for a system having the same field of view as the present equipment) will become possible. Such an increase in counting rate would lead to an improvement in sensitivity of about an order of magnitude. Alternatively, to deduce the same flux limits as are currently quoted on candidate sources would require far less time than at present, allowing many more objects to be meaningfully observed.

The second factor which limits the ability of present systems to detect new sources is the limited amount of sky they are able to monitor; the Dugway system, for example, has a field of view of only about 4 square degrees. One method of achieving an enlargement of the area of sky able to be observed is to place a 'bundle' of phototubes at the focus of the mirror system, with the outer rings

of tubes looking 'off-axis' and seeing different parts of the sky from that seen by the central tube. With careful alignment an individual tube could act in coincidence with a corresponding tube mounted paraxially on a second mirror. Each phototube would be independently using the full collecting area of the mirror system to see a different part of the sky. The benefits from such a system would be significant :

(1) A very large increase in the amount of sky able to be monitored at a single pass, with the resultant decrease in the length of time needed to survey the whole sky.

(2) The count rate occurring in a particular channel could be continuously compared with that of the adjacent channels. Thus, there would be no requirement to drift scan an object (with the resultant decrease in the fraction of time spent 'ON-source') to obtain an accurate estimate of the background counting rate.

The higher gamma ray/proton ratio seen in 2-fold telescope responses (see, for example, Section 6.3a) would indicate that the fields of view of the individual phototubes should be reduced somewhat from the value of 1.7° (defined in terms of the FWHM of the PSF) used in the present work. It is not clear yet, however, how much this reduction should be.

Whatever improvements in telescope design are achieved, several priorities exist in the VHE gamma ray field in the coming years :

(1) Continued monitoring of Cygnus X-3 and the Crab pulsar. These two objects are not only the most obvious 'standard

candles' in the field, but may also be representative of two of the different types of VHE gamma ray emitter : the fast pulsar whose energy source takes the form of a rapidly rotating neutron star, and the X-ray binary - possibly emitting VHE gamma rays via a mass accretion process.

(2) More detailed observations of the two southern hemisphere sources the Vela pulsar and Cen-A. The Vela pulsar, being similar in many ways to the Crab pulsar, is a good candidate for VHE gamma ray emission. Further observations of the active galaxy, Cen-A, are needed to confirm the previously reported positive result.

(3) A thorough series of observations of other radio pulsars should be undertaken - supported, if possible, by simultaneous radio measurements.

(4) A general survey of the sky for evidence of new sources of VHE gamma rays. If such a search were to have a positive outcome a new class of source - objects predominantly emitting VHE gamma rays - could open up a new field in astronomy.

Whatever the outcome of these and other lines of research it is clear that the future holds exciting possibilities, and that unexpected discoveries are likely to be made in the field in the years to come.

References

Ash, M.E., Shapiro, I.I., Smith, W.B., (1967), A.J., 72, 338.

Blackett, P.M.S., (1948), 'A possible contribution to the night sky due to Cerenkov radiation emitted by cosmic rays', report of a conference of the Gassiot committee of the Physical Society on the emission spectra of the night sky and aurorae, page 34.

Browning, R., Turver, K.E., (1977), Nuova Cimento, 38, 223.

Cerenkov, P.A., (1934), Dokl. Akad. Nauk. SSSR, 2, 451.

Craig, M. A.B., (1984), Ph.D. Thesis, University of Durham.

Danaher, S., Fegan, D.J., Porter, N.A., Weekes, T.C., (1981), Nature, 289, 568.

Dowthwaite, J.C., Ph.D. Thesis, in preparation, University of Durham.

Dowthwaite, J.C., Harrison, A.B., Kirkman, I.W., Macrae, J.H.K., Orford, K.J., Turver, K.E., Walmsley, M., (1985), Astron. Astrophys., 142, 55.

Eadie W., Drijard, D., James, F., Roos, M., Sadoulet, B., (1971), 'Statistical Methods in Experimental Physics', (Amsterdam: North Holland).

Elsner, R.F., Ghosh, P., Darbo, W., Weisskopf, M.C., Sutherland, P.G., Grindlay, J.E., (1980), Astrophys. J., 239, 335.

Erikson, R.A., Fickle, R.K., Lamb, R.C., (1976), Astrophys. J., 210, 539.

Fazio, G.G., (1967), Ann. Rev. Astron. Astrophys., 5, 481.

Fomin, V.P., Vladimirski, B.M., Stepanian, A.A., (1977), Proc. Int. Conf. Cosmic Rays (Plovdiv), 1, 12.

Frank, I.M., Tamm, Ig., (1937), Dokl. Akad. Nauk. SSSR, 14, 109.

Galbraith, W., Jelley, J.V., (1953), Nature, 171, 349.

Galbraith, W., Jelley, J.V., (1955), J. Atmos. Terr. Phys., 6, 250.

Galper, A.M., Kirillov-Ugiriumov, V.G., Kurochkin, A.V., Leikov, P.G., Luchkov, B.I., Yurkin, Yu.T., (1976), Pisma v Astron. Zh., 2, 524.

'Global Atlas of Relative Cloud Cover', 1967-1970, published by the US Department of Commerce and the USAF.

Gould, R.J., Schreder, G.P., (1966), Phys. Rev. Lett., 16, 252.

Gregory, P.C., (1972), Nature, 239, 439.

Grindlay, J.E., Helmken, H.F., Brown, R.H., Davis, J., Allen, L.R., (1975a), Proc. 14th Int. Conf. Cosmic Rays Munich, 1, 89.

Grindlay, J.E., Helmken, H.F., Hanbury Brown, R., Davis, J., Allen, L.R., (1975b), Ap. J. Lett., 197, L9.

Grindlay, J.E., Helmken, F.F., Weekes, T.C., (1976), Astrophys. J., 209,592.

Grindlay, J.E., (1982), Proc. Int. Workshop on High Energy Gamma Ray Astron. (TIFR. Bombay).

Gupta, S.K., Ramana Murthy, P.V., Sreekantan, B.V., Tonwar, S.C., Viswanath, P.R., (1982), Proc. Int. Workshop on Very High Energy Gamma Ray Astronomy (TIFR. Bombay), 279.

Hermson, W., (1980), Ph.D. Thesis, University of Leiden.

Hermson, W., (1983), Space Sci. Rev., 36, 61.

Hillas, A.M.,(1984), Nature, 312, 50.

Jelley, J.V., (1958), 'Cerenkov Radiation and its applications', Pergamon Press, London.

Jelley, J.V., Porter, N.A., (1963), Quart. J. Roy. Astron. Soc., 4, 275.

Jelley, J.V., (1967), Prog. Elem. particle and Cosmic Ray Phys., 9, 41.

Jelley, J.V., (1983), Photochemical. and Photobiological. Rev., 7, 275.

Jennings, D.M., White, G., Porter, N.A., O'Mongain, E., Fegan, D.J., White, J., (1974), Nuovo Cimento, 20, 71.

Kniffen, D.A., Fichtel, C.E., Hartman, R.C., Lamb, R.C., Thompson, D.J., (1977), 'Recent Advances in Gamma Ray Astronomy', ESA Frascati, 45.

Lamb, R.C., Fichtel, C.E., Hartman, R.C., Kniffen, D.A., Thompson, D.J., (1977), Astrophys. J., 212, L63.

Lamb, R.C., Godfrey, C.P., Wheaton, W.A., Tumer, T., (1981), Nature, 296, 543.

Leahy, D.A., Elsner, R.F., Weisskopf, M.C., (1983), Astrophys. J., 272, 256.

Lloyd-Evans, J., Coy, R.N., Lambert, A., Lapikens, J., Patel, M., Reid, R.J.O., Watson, A.A., (1983), Nature, 305, 784.

Longair, M.S., (1981), 'High Energy Astrophysics', Cambridge University Press.

Macrae, J.H.K., Ph.D. Thesis, in preparation, University of Durham.

Mardia, K.V., (1972), 'Statistics of Directional Data', Academic Press, London and New York.

Mason, K.O., Becklin, E.E., Blankenship, L., Brown, R.L., Elias, J., Hjellming, R.M., Matthews, S.K., Murdin, P.G., Neugebauer, G., Sanford, P.W., Willner, S.P., (1976), Astrophys. J., 207, L123.

McBreen, B., Ball, S.E., Campbell, M., Greisen, K., Koch, D., (1973), Ap. J., 184, 571.

Meegan, C.A., Fishman, G.J., Haymes, R.C., (1979), Astrophys. J. Lett., 234, L123.

Molteni, D., Rapisardi, M., Robba, N.R., Scarsi, L., (1980), Astron. Astrophys., 87, 88.

Morrison, P., (1958), Nuova Cimento, 7, 858.

Mukanov, D.B., Nesterova, N.M., Stepanian, A.A., Fomin, V.P., (1980), Izvestiya Krymskoi Astrofiz. Obs., 62, 98.

Neshpor, et al., (1975), Astr. and Sp. Sci., 61, 349.

Neshpor, Yu.I., Stepanian, A.A., Fomin, V.P., Gerasimov, S.A., Vladimirsky, B.M., Zyskin, Yu.L., (1979), Astrophys. Space Sci., 61, 349.

Nesterova, N.M., Chudakov, A.E., (1955), Zurn. Eksp. Teor. Fiz., 28, 384.

Ogelman, H., Ayasli, S., Hacinliyar, A., (1976), Proc. Gamma Ray Symposium, Goddard, 118.

Porter, N.A., Delaney, T., Weekes, T.C., (1974), Proc. 9th Eslab Symp. E.S.R.O., Frascati, 295.

Porter, N.A., Weekes, T.C., (1978), SAO Special Report, No. 381.

Protheroe, R.J., (1977), Ph.D. Thesis, University of Durham.

Reppin, C., Pietsch, W., Trumper, J., Voges, W., Staubert, R., (1979), Astrophys. J., 234, 329.

Ruderman, M.A., (1981), IAU Symp. 95, 'Pulsars', ed W. Sieber and R. Wielebinski (Dordrecht; Reidel), 156.

Samorski, M., Stamm, W., (1983), Astrophys. J. Lett., 268, L17.

Strong, A.W., (1982), Proc. Int. Workshop on High Energy Gamma Ray

Astronomy (TIFR. Bombay), 141.

Van der Klis, M., Bonnet-Bidaut, J.M., (1981), Astron. Astrophys., 95, L5.

Vestrand, W., Eichler, D., (1982), Astrophys. J., 251, 112.

Vladimirski, B.M., Stepanian, A.A., (1973), Proc. 13th Int. Conf. on Cosmic Rays (University of Denver), 1, 456.

Walmsley, M., Ph.D. Thesis, in preparation, University of Durham.

Weekes, T.C., Turver, K.E., (1977), Proc. 12th ESLAB symposium, Frascati.

Weekes, T.C., Helmken, H.F., (1977), Recent Advances in Gamma Ray Astro., ESASP-124, 39.

Weekes, T.C., Helmken, H.F., Grindlay, J.E., (1979), Proc. Int. Conf. Cosmic Rays (Kyoto), 1, 133.

Weekes, T.C., (1982), Proc. Int. Workshop on High Energy Gamma Ray Astron. (TIFR. Bombay).

Wills, R.C., Bennett, K., Bignami, G.F., Buccheri, R., Caraveo, P.A., Hermson, W., Kanbach, G., Masnou, J.L., Mayer-Hasselwander, H.A., Paul, J.A., Sacco, B., (1982), Nature, 296, 723.